Journal of Medicinal Chemistry

pubs.acs.org/jmc

Article

Design, Synthesis, Biological Evaluation, and Computational Studies of Novel Ureidopropanamides as Formyl Peptide Receptor 2 (FPR2) Agonists to Target the Resolution of Inflammation in Central Nervous System Disorders

Margherita Mastromarino, Maria Favia, Igor A. Schepetkin, Lylia N. Kirpotina, Ewa Trojan, Mauro Niso, Antonio Carrieri, Monika Leśkiewicz, Magdalena Regulska, Massimiliano Darida, Francesco Rossignolo, Stefano Fontana, Mark T. Quinn, Agnieszka Basta-Kaim, Marcello Leopoldo, and Enza Lacivita*

Cite This: https://doi.org/10.1021/acs.jmedchem.1c02203

Read Online

ACCESS | Metrics & More | Article Recommendations | Supporting Information

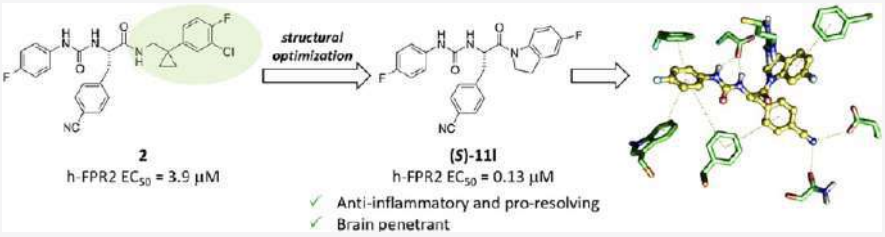

ABSTRACT: Formyl peptide receptor 2 (FPR2) agonists can boost the resolution of inflammation and can offer alternative approaches for the treatment of pathologies with underlying chronic neuroinflammation, including neurodegenerative disorders. Starting from the FPR2 agonist **2** previously identified in our laboratory and through fine-tuning of FPR2 potency and metabolic stability, we have identified a new series of ureidopropanamide derivatives endowed with a balanced combination of such properties. Computational studies provided insights into the key interactions of the new compounds for FPR2 activation. In mouse microglial N9 cells and in rat primary microglial cells stimulated with lipopolysaccharide, selected compounds inhibited the production of pro-inflammatory cytokines, counterbalanced the changes in mitochondrial function, and inhibited caspase-3 activity. Among the new agonists, (*S*)-**11l** stands out also for the ability to permeate the blood–brain barrier and to accumulate in the mouse brain *in vivo*, thus representing a valuable pharmacological tool for studies *in vivo*.

INTRODUCTION

Inflammation is a self-limited and protective process initiated by cells and tissues to protect the organism against pathogens or injuries by exogenous or endogenous agents and is finely orchestrated to resolve on its own with the final restoration of tissue homeostasis. If the inflammatory response becomes uncontrolled, it may cause tissue damage by perturbing homeostasis toward immune dysregulation.[1] When inflammation occurs within the central nervous system (CNS), it is referred to as neuroinflammation. When neuroinflammation becomes persistent or unresolved, it can be detrimental to neurological functions and lead to neurodegeneration.[2] In fact, although the underlying mechanisms are different, neuroinflammation is a common hallmark among neurodegenerative diseases.

The resolution phase of inflammation is mediated by specialized pro-resolving mediators (SPMs), including lipoxins, resolvins, protectins, and maresins, which trigger a series of molecular and cellular events, that lead to spontaneous regression of the inflammatory response.[3−5] During the past decade, the understanding of the resolution of inflammation has grown exponentially with the discovery of the intracellular pathways triggered by SPMs and their receptors,[6,7] leading to the concept of "resolution pharmacology" as a new research area focused on the development of new drugs acting as pro-resolving receptors.[8] This novel approach offers new opportunities to treat very different inflammatory-related pathologies, including cardiovascular disorders, chronic obstructive pulmonary disease (COPD), rheumatoid arthritis, and neurodegenerative diseases such as Alzheimer's disease, Parkinson's Disease, and multiple sclerosis.[9−12] It is now established that SPMs act *via* specific membrane receptors such as G-protein coupled receptors (GPCRs), and among these, *N*-formyl peptide receptor 2

Received: December 23, 2021

(FPR2) plays a pivotal role.[13] FPR2 is a member of the formyl peptide receptor family, which includes three receptor subtypes (FPR1, FPR2, and FPR3). FPRs play a critical role in the innate immune response because they interact with pathogen- and damage-associated molecular patterns.[14] FPR2 is highly expressed in several immune cells, including neutrophils, monocytes/macrophages, and microglia, as well as cells of diverse origins, including endothelium, epithelium, smooth muscle cells, and fibroblasts.[14] FPR2 can be activated by structurally diverse agonists, including endogenous lipids, proteins, and peptides, and small synthetic molecules.[9,13] Interestingly, FPR2 can mediate opposite physiological responses, depending on the agonists. For example, activation of FPR2 by serum amyloid A or β-amyloid triggers pro-inflammatory responses, whereas the activation by the pro-resolving mediators lipoxin A4, resolvin D1, or Annexin A1 induces anti-inflammatory or pro-resolving effects,[15,16] even though the nature of the LXA_4/FPR2 interaction is still a matter of ongoing debate.[17,18] This intriguing complexity of FPR2 pharmacology is slowly being clarified, considering that FPR2 can engage with distinct G proteins and thus activates different signaling cascades in a ligand- or cell target-specific manner.[19,20]

Preclinical studies show that the pro-resolving activation of FPR2 has therapeutic potential for treating several diseases, including myocardial ischemia−reperfusion, chronic obstructive pulmonary disease, cystic fibrosis, diabetic complications, sepsis, rheumatoid arthritis, cancer, and neurodegenerative diseases.[11,13] During the past decade, several research groups have focused their attention on the pro-resolving properties of the FPR2, and several synthetic small molecules have been studied in different *in vitro* and *in vivo* models of inflammatory diseases. For example, compound **43** and compound **17b** (Figure 1), belonging to the first generation of small molecule FPR2 agonists, showed different cardioprotective properties in an acute myocardial infarct model, which has been attributed to biased agonism with preferential activation of MAPK signaling over intracellular calcium elevation.[21,22] Bristol-Meyers Squibb recently disclosed the 4-phenylpyrrolidinone FPR2 agonist BMS-986235, which inhibited neutrophil chemotaxis and stimulated macrophage phagocytosis, providing functional improvements in a mouse model of heart failure.[23] Maciuszek et al. reported on a series of novel cyclopentane FPR2 agonists, such as compound **1** (Figure 1), with anti-inflammatory properties in *in vitro* models of cardiovascular inflammation.[24]

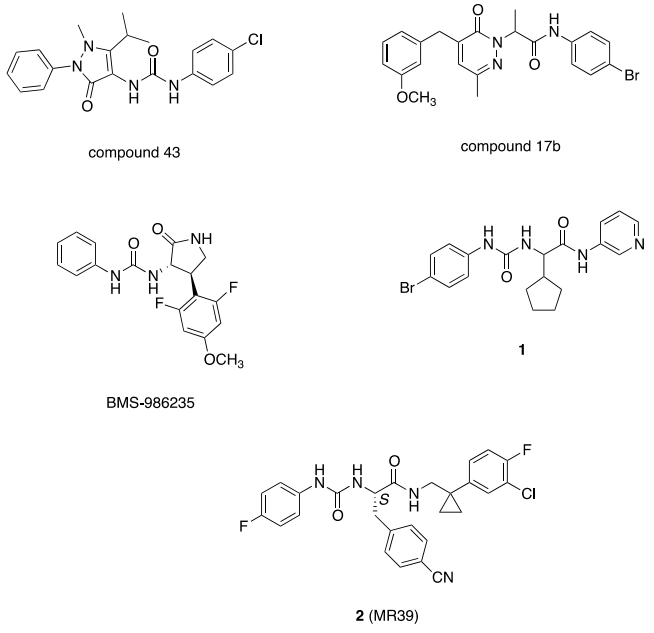

Figure 1. Selected examples of FPR2 small molecule agonists.

We contributed to the field by developing a series of ureidopropanamide-based FPR2 agonists with anti-inflammatory properties, exemplified by compound **2** (also known as MR39, Figure 1). Compound **2** activates FPR2 at submicromolar concentrations and displays anti-inflammatory properties as it reduces the release of the pro-inflammatory mediators interleukin (IL)-1β and tumor necrosis factor (TNF)-α in rat primary microglial cultures stimulated with lipopolysaccharide (LPS), an *in vitro* model of neuroinflammation.[25] In addition, compound **2** is characterized by promising *in vitro* pharmacokinetic properties, with good *in vitro* metabolic stability ($t_{1/2}$ = 48 min, rat microsomes) and good *in vitro* apparent permeability in brain microvascular endothelial cells (hCMEC/D3 cells, with an efflux ratio ER (BA/AB) of 2.6), predictive of brain penetration.[25] The anti-inflammatory effect of compound **2** was similar to that of lipoxin A4 (LXA4), as it was related to a significant reduction of the LPS-induced phosphorylation of ERK1/2, one of the proteins belonging to the MAPK family that is particularly involved in the production of pro-inflammatory mediators in microglial cells.[26] The neuroprotective and anti-inflammatory properties of compound **2** were confirmed in mouse hippocampal organotypic cultures (OHCs) stimulated with LPS. Pre-treatment with compound **2** abolished some of the LPS-induced changes in the expression of genes related to the pro- and anti-inflammatory microglial activation and attenuated the release of TNF-α and IL-1β. Moreover, compound **2** attenuated the LPS-evoked increase in the levels of the NLRP3 inflammasome, suggesting that the observed anti-inflammatory effects are related to the modulation of the NF-κB pathway. FPR2 mediates these effects because they were not observed in OHCs from FPR2 knock-out mice and were abolished by pre-treatment with the FPR2 antagonist WRW4 in OHCs from wild-type mice.[27] Compound **2** elicited similar anti-inflammatory and neuroprotective effects through FPR2 activation in OHCs stimulated with β-amyloid. In fact, compound **2** reduced cell death and the release of pro-inflammatory mediators (IL-1β, IL-6, and TNF-α) induced by β-amyloid and improved the release of anti-inflammatory mediators (IL-4 and TGF-β).[28] Finally, compound **2** improved neuronal survival and decreased microglial cell density and plaque load after systemic administration to the APP/PS1 mouse model of Alzheimer's disease, suggesting that activation of FPR2 may be a therapeutic strategy for Alzheimer's Disease.[28]

However, compound **2** produced anti-inflammatory and pro-resolving effects at micromolar concentrations, contrary to LXA4 and the epimer aspirin-triggered LXA4, which had such effects at the nanomolar range.[26] This can translate in high *in vivo* dosage and potential unwanted off-target side effects.

Thus, we embarked in a new medicinal chemistry campaign with the aim of further improving the FPR2 agonist potency of our ureidopropanamide derivatives without affecting their pharmacokinetic properties.

RESULTS AND DISCUSSION

Study Design. Compound **2** was identified in a structure−activity relationship study of the 3-(1*H*-indol-3-yl)-2-[3-(4-substituted-phenyl)ureido]propanamide scaffold.[25] We found

https://doi.org/10.1021/acs.jmedchem.1c02203
J. Med. Chem. XXXX, XXX, XXX−XXX

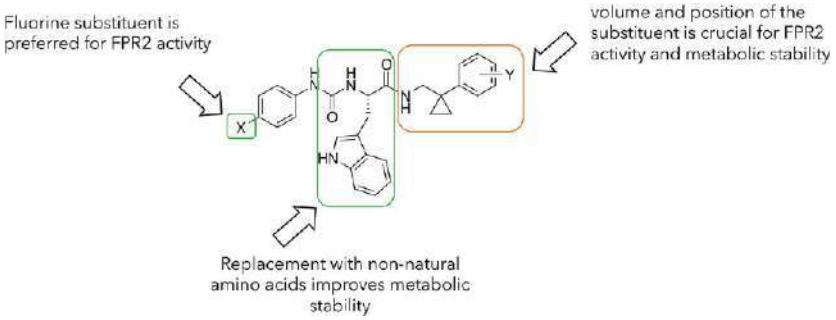

Figure 2. Design strategy for the target compounds.

that the presence of a fluorine substituent on the phenyl ureidic group was beneficial for FPR2 activity and that the indole ring of the central amino acid could be replaced by aromatic residues such as 4-CN-phenyl or 3-pyridyl, with a substantial improvement in microsomal stability. As for the phenylcyclopropylmethyl moiety linked to the amide function, we found that the volume and position of the substituent linked to the phenyl ring was crucial for FPR2 activity and metabolic stability (Figure 2). When bulky substituents were inserted in this part of the molecule, activity and stability were orthogonal, as bulky substituents improved metabolic stability while negatively impacting the agonist potency. This suggested that it is crucial to find the right balance in the dimension of the moiety linked to the amide function to combine high potency and good metabolic stability.[25] Thus, we replaced the phenylcyclopropyl moiety of compound **2** with other moieties with different dimensions. At first, we introduced aliphatic heterocyclic groups, such as e-caprolactam, piperidinyl, and pyrrolidinyl (compounds (*R*)- and (*S*)-**11a−c**, Table 1), already reported in other FPR2 agonists.[29] We also considered condensed heterocyclic groups, such as indolinyl, isoindolinyl, 1,2,3,4-tetrahydroquinolinyl, and 1,2,3,4-tetrahydroisoquinolinyl (compounds (*R*)- and (*S*)-**11d−f**, Table 1), to identify which substitutions best fit within the binding cavity. The data obtained from this first set of compounds confirmed that FPR2 activity and metabolic stability were orthogonal. Consequently, we further modified the most potent compounds (*R*)- and (*S*)-**11d,e** to improve metabolic stability. To this end, electron withdrawing groups (fluorine or aza group) were inserted on the aromatic rings of the "right hand" part of the molecule or the steric hindrance in proximity to the metabolically labile functions was increased by the introduction of *gem*-dimethyl groups (compounds (*R*)- and (*S*)-**11h-o**, Table 1).

Chemistry. The synthesis of the target compounds required the key amines **3a−o** (Figure 3), which were commercially available or synthesized according to the literature methods (see the Experimental Section), except for amine **3o**. This amine was prepared according to Scheme 1: 4-Fluorophenylacetonitrile (**4**) was alkylated with methyl iodide in the presence of NaH to obtain nitrile **5**, which was reduced with a borane dimethylsulfide complex to obtain amine **6**. The latter was condensed with trifluoroacetic acid to obtain amide **7**, which underwent a cyclization reaction with paraformaldehyde to form compound **8**. Hydrolysis of the latter under basic conditions resulted in amine **3o**. Synthesis of the target compounds is depicted in Scheme 2. The Boc-protected derivatives (*R*)- and (*S*)- **9a−c,f,j,n,o** were obtained by condensing amines **3a−c,f,j,n,o** with (*R*)-Boc- or (*S*)-Boc-4-CN-phenylalanine using *N*-*N*′-carbonyldiimidazole as a condensing agent, whereas the Boc-protected derivatives (*R*)- and (*S*)-**9d,e,g,k−m** were obtained by condensing amines **3d,e,g,k−m** with (*R*)-Boc- or (*S*)-Boc-4-CN-phenylalanine using PyBOP as the condensing agent in the presence of *N*-methylmorpholine. Subsequently, the Boc-protected derivatives (*R*)- and (*S*)-**9a−o** were deprotected with 3 N hydrochloric acid or with trifluoroacetic acid to obtain amines (*R*)- and (*S*)-**10a−o**, which were reacted with 4-fluorophenylisocyanate to obtain the target compounds (*R*)- and (*S*)-**11a−o**.

Functional Activity and Metabolic Stability of the Target Compounds. Agonist activity of the target compounds at FPR1 and FPR2 was assessed by measuring their ability to induce Ca^{2+} mobilization in HL-60 cells stably transfected with human FPR1 or FPR2 and was expressed as EC_{50} (Table 1). Moreover, considering that both receptors are known to undergo homologous desensitization after stimulation with agonists[14] and that this can result in a functional antagonism,[30] we also assessed the ability of the compounds to induce functional antagonism at FPR1 and FPR2 by measuring the inhibition of Ca^{2+} mobilization induced by subsequent treatment with FPR1 or FPR2 standard agonists (IC_{50}, Table 1).

The first structural modification performed on compound **2** was replacement of the phenylcyclopropylmethyl moiety with ε-caprolactam ((*R*)- and (*S*)-**11a**), with the cycloalkylamines piperidine ((*R*)- and (*S*)-**11b**) and pyrrolidine ((*R*)- and (*S*)-**11c**) and with the heterocycles isoindoline ((*R*)- and (*S*)-**11d**), indoline ((*R*)- and (*S*)-**11e**), 1,2,3,4-tetrahydroisoquinoline ((*R*)- and (*S*)-**11f**), and 1,2,3,4-tetrahydroquinoline ((*R*)- and (*S*)-**11g**). Considering the (*S*)-enantiomers of the cycloalkylamine derivatives, we found that the structural modifications were favorable. In particular, the ε-caprolactam derivative (*S*)-**11a** exhibited a 20-fold increase in potency as compared to **2**, the piperidinyl derivative (*S*)-**11b** was fourfold more potent than **2**, while the pyrrolidine derivative (*S*)-**11c** was equipotent to **2** (Table 1). Within this group of compounds, the (*S*)-enantiomers were more potent than the (*R*)-enantiomers. The same trend was observed within the heterocyclic derivatives (*R*)- and (*S*)-**11d**, (*R*)- and (*S*)-**11e**, (*R*)- and (*S*)-**11f**, and (*R*)- and (*S*)-**11g**, and more importantly, all of the (*S*)-enantiomers were at least 10-fold more potent than **2**, with (*S*)-**11e** being the most potent of the set (EC_{50} = 26 nM). These data univocally indicated that the size of the moiety linked to the amide function has great influence on agonist potency at FPR2, as well as the stereochemistry. As for selectivity over FPR1, these structural modifications led to an improvement. In fact, **2** was almost equipotent at both receptors, whereas the new compounds were at least fivefold selective toward FPR1.

The next step was to assess metabolic stability of the first set of compounds by measuring the percentages of recovery after 30

https://doi.org/10.1021/acs.jmedchem.1c02203
J. Med. Chem. XXXX, XXX, XXX−XXX

Table 1. Effect of the Compounds on Ca^{2+} Mobilization in FPR1- and FPR2-HL60 Transfected Cells (EC_{50}) and on Functional Antagonism at FPR1 and FPR2 (IC_{50}), Metabolic Stability, and Cytotoxicity in Murine N9 Cells

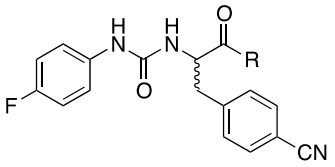

Compd.	R	Calcium Mobilization				Metabolic stability	Cytotoxicity N9 cells
		HL60-FPR2		HL60-FPR1		% after 30 min incubation	IC_{50}, μM
		EC_{50}, μM (efficacy, %)	IC_{50}, μM	EC_{50}, μM (efficacy, %)	IC_{50}, μM		
2	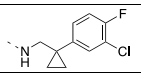	3.9[a]	N.T.	5.2[a]	N.T.	33[a]	3.26±0.4
(*R*)-**11a**	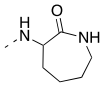	1.0 ± 0.3 (140)	3.8	4.2 ± 1.1 (110)	40.4	78	>100 (36)
(*S*)-**11a**		0.17 ± 0.025 (105)	0.35	0.78 ± 0.11 (120)	3.5	85	>100 (53)
(*R*)-**11b**		13.4 ± 3.3 (65)	49.3	18.2 ± 7.7 (75)	30.5	25	>100 (16)
(*S*)-**11b**		0.98 ± 0.45 (95)	12.0	6.8 ± 2.4 (90)	20.6	34	>100 (46)
(*R*)-**11c**		5.2 ± 2.2 (105)	16.5	26.4 ± 7.6 (75)	43.9	61	>100 (59)
(*S*)-**11c**		3.1 ± 1.1 (100)	6.4	15.3 ± 5.7 (80)	33.8	65	>100 (55)
(*R*)-**11d**	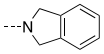	19.3 ± 3.1 (110)	N.A.	41.3 ± 5.6 (50)	N.A.[b]	15	12.1±0.9
(*S*)-**11d**		0.34 ± 0.05 (125)	4.4	2.2 ± 0.4 (95)	27.6	31	33.5±1.6
(*R*)-**11e**		5.6 ± 2.1 (115)	3.9	16.5 ± 6.3 (75)	N.A.	14	40.0±2.4
(*S*)-**11e**		0.026 ± 0.012 (140)	0.01	0.32 ± 0.11 (110)	17.6	22	58.3±6.3
(*R*)-**11f**	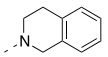	1.3 ± 0.35 (125)	3.5	6.8 ± 2.9 (90)	N.A	4	12.1±1.1
(*S*)-**11f**		0.24 ± 0.08 (135)	0.03	1.4 ± 0.37 (100)	14.5	6	12.6±0.9
(*R*)-**11g**		0.25 ± 0.12 (175)	0.012	0.44 ± 0.17 (115)	17.4	7	13.7±1.2
(*S*)-**11g**		0.27 ± 0.02 (120)	0.013	1.2 ± 0.4 (90)	24.2	10	14.7±2.1
(*R*)-**11h**		N.A.	N.A.	N.A.	N.A.	62	>100 (40)
(*S*)-**11h**		19.5 ± 2.0 (80)	30.1	N.A.	N.A.	67	>100 (9)
(*R*)-**11j**	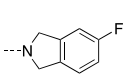	7.2 ± 2.4 (45)	N.A.	5.6 ± 2.7 (35)	N.A.	72	9.44±0.7
(*S*)-**11j**		1.7 ± 0.3 (70)	4.4	3.3 ± 1.4 (95)	N.A.	70	18.2±0.8
(*R*)-**11k**		6.9 ± 2.3 (45)	16.4	9.0 ± 3.1 (35)	N.A.	65	15.0±1.1
(*S*)-**11k**		2.3 ± 0.8 (55)	2.7	4.2 ± 1.6 (80)	N.A.	n.d.[c]	n.d.
(*R*)-**11i**	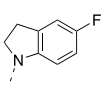	0.41 ± 0.13 (90)	3.4	1.8 ± 0.5 (80)	N.A.	58	23.8±3.2
(*S*)-**11i**		0.16 ± 0.07 (110)	0.21	4.8 ± 0.9 (120)	N.A.	19	29.4±3.4
(*R*)-**11l**	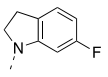	0.38± 0.16 (100)	0.085	2.9 ± 1.1 (80)	NA	28	29.5±2.6
(*S*)-**11l**		0.13±0.06 (100)	0.004	1.1 ± 0.21 (80)	NA	33	20.8±1.8
(*R*)-**11m**		1.1 ± 0.4 (100)	1.2	2.9 ± 0.3 (100)	NA	10	>100 (59)
(*S*)-**11m**		0.16 ± 0.07 (100)	0.14	2.5 ± 0.06 (90)	NA	14	>100 (59)
(*R*)-**11n**	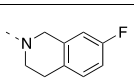	0.62 ± 0.27 (140)	0.24	2.6 ± 0.8 (85)	NA	14	97.3±7.2
(*S*)-**11n**		0.45 ± 0.11 (130)	0.26	1.5 ± 0.7 (90)	NA	8	9.86±0.6
(*S*)-**11o**	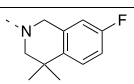	1.6 ± 0.4 (100)	0.6	6.9 ± 1.7 (110)	NA	34	4.28±0.3

https://doi.org/10.1021/acs.jmedchem.1c02203
J. Med. Chem. XXXX, XXX, XXX−XXX

Table 1. continued

[a]Data are taken from ref 25. [b]Not active. [c]Not determined.

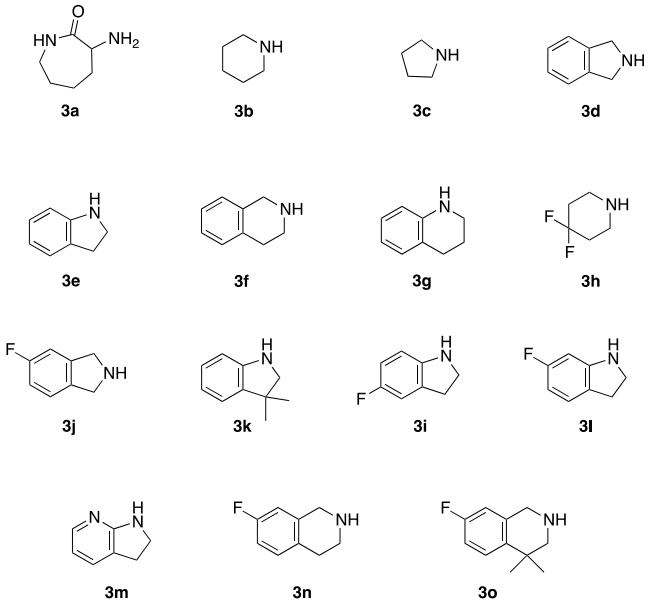

Figure 3. Structural formula of amines **3a**–**o**.

min of incubation with rat microsomes. We found that the cycloalkylamine derivatives (*R*)- and (*S*)-**11a**, (*R*)- and (*S*)-**11b**, and (*R*)- and (*S*)-**11c** were more stable than **2**, whereas the condensed heterocyclic derivatives were less stable than **2**. In fact, (*R*)- and (*S*)-**11d**, (*R*)- and (*S*)-**11e**, (*R*)- and (*S*)-**11f**, and (*R*)- and (*S*)-**11g** were 2–3-fold less stable than (*R*)- and (*S*)-**11b**, (*R*)- and (*S*)-**11c**, and **2**. These data highlight that FPR2 agonist potency and metabolic stability are orthogonal and forced us to design novel derivatives to combine high FPR2 potency and metabolic stability. To this aim, we decorated the aliphatic or condensed heterocyclic rings of compounds (*R*)- and (*S*)-**11b**, (*R*)- and (*S*)-**11d**, (*R*)- and (*S*)-**11e**, and (*R*)- and (*S*)-**11f** with fluoro, aza, or *gem*-dimethyl groups that might prevent oxidative metabolism.

Functionalization of the 4-position of (*R*)- and (*S*)-**11b** with *gem*-difluoro led to compounds (*R*)- and (*S*)-**11h**, which were inactive or 20-fold less potent than the non-substituted counterparts, respectively. On the other hand, this structural modification resulted in an improvement of metabolic stability.

The indoline derivatives (*R*)- and (*S*)-**11e** were the formal starting points of compounds (*R*)- and (*S*)-**11i**, (*R*)- and (*S*)-**11k**, (*R*)- and (*S*)-**11l**, and (*R*)- and (*S*)-**11m**. The introduction of a fluorine substituent in 5- or 6-position of the indoline ring resulted in an increase of FPR2 potency in the case of (*R*)-enantiomers ((*R*)-**11e** vs (*R*)-**11i** and (*R*)-**11l**) and a decrease of potency for the (*S*)-enantiomers ((*S*)-**11e** vs (*S*)-**11i** and (*S*)-**11l**). Regarding metabolic stability, the presence of the fluorine substituent was beneficial, except for (*S*)-**11i**, which was slightly less stable than (*S*)-**11e**. The introduction of an aza group in the indoline ring of (*R*)- and (*S*)-**11e** gave negative results with respect to both FPR2 potency and metabolic stability. Decoration of the 3-position of the indoline ring in with a *gem*-dimethyl group of (*R*)- and (*S*)-**11e** resulted in a decrease of FPR2 potency accompanied by an increase of stability in the case of (*R*)-**11k**. As for the 5-fluoroisoindoline derivatives (*R*)- and (*S*)-**11j**, formally derived from (*R*)- and (*S*)-**11d**, a similar trend was observed.

Considering derivatives (*R*)- and (*S*)-**11f** as starting points, decoration of the 1,2,3,4-tetrahydroisoquinoline ring with fluorine and *gem*-dimethyl substituents provided a small increase in FPR2 potency and a loss in metabolic stability ((*R*)- and (*S*)-**11n**). Substitution of (*S*)-**11e** with only the fluorine substituent gave (*S*)-**11o**, which was less potent than (*S*)-**11e** but more stable.

As for selectivity over FPR1, the performed structural modifications led to further improvement as compared to the corresponding compounds of the first set. In particular, compound (*S*)-**11i** was 30-fold more selective toward FPR1.

All compounds were also assessed for their ability to induce FPR1 and FPR2 desensitization. We found that all compounds were able to reduce Ca^{2+} mobilization induced by the reference agonist WKYMVM. In general, the IC_{50} values at FPR2 were in the same range of EC_{50} values, except for (*S*)-**11f** and (*R*)- and (*S*)-**11l**, which exhibited IC_{50} values in the nanomolar range, suggesting potent ability to desensitize FPR2. As for FPR1 desensitization, we found that only few compounds were able to reduce calcium mobilization induced by the reference FPR1 agonist *f*MLF, with IC_{50} values in the high micromolar range.

Collectively, these data indicate that the small structural changes introduced in the second set of compounds produced an increase in potency in the case of the (*R*)-enantiomers (except for (*R*)-**11h** and (*R*)-**11k**) and a decrease in potency in

Scheme 1. Synthesis of Amine 3o[a]

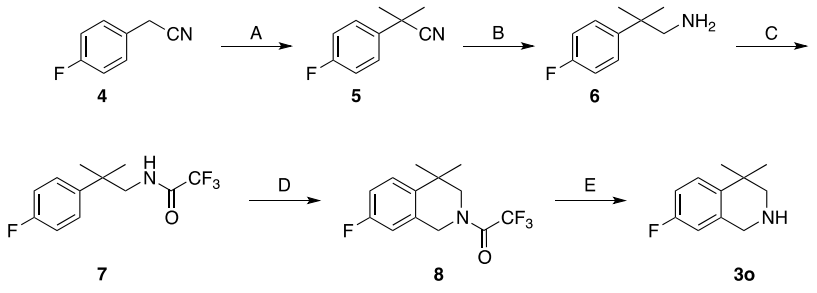

[a]Reagents and conditions: (A) sodium hydride, CH_3I, r.t., 2 days, 35% yield; (B) i: 10 M borane dimethylsulfide complex, ii: 3 N HCl, 38% yield; (C) trifluoroacetic anhydride, Et_3N, r.t., 30 min, 59% yield; (D) paraformaldehyde, CH_3COOH, H_2SO_4, r.t., overnight, 68% yield; (E) K_2CO_3, CH_3OH, reflux, 2 h, 59% yield.

https://doi.org/10.1021/acs.jmedchem.1c02203
J. Med. Chem. XXXX, XXX, XXX–XXX

Scheme 2. Synthesis of Target Compounds[a]

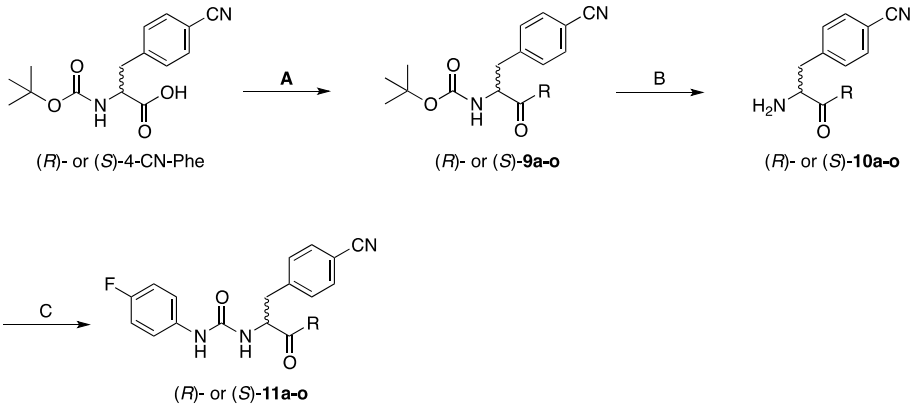

[a]Reagents and conditions: (A) amines **3a−o**, *N*-*N*′-carbonyldiimidazole or PyBOP, *N*-methylmorpholine, r.t.; overnight; 45−87% yield; (B) 3 N HCl or trifluoroacetic acid, r.t., quantitative yield; (C) 4-fluorophenylisocyanate, r.t., overnight, 10−80% yield.

the case of the (*S*)- enantiomers. As a result, no compound of the second set was more potent at FPR2 than their counterpart in the first set. Neverthless, various compounds exhibited EC_{50} at FPR2 in the submicromolar range. As far as metabolic stability is concerned, decoration of cycloalkylamines or heterocyclic rings with electron-withdrawing substituents resulted in the desired effect of increasing metabolic stability, with the exception of compounds (*S*)-**11i**, (*R*)-**11m**, and (*S*)-**11m** (as compared to their undecorated counterparts). Altogether, these data clearly indicated that to combine high FPR2 potency and stability to oxidative metabolism in these ureidopropanamide derivatives is not a trivial task. Nonetheless, fine tuning of the substitution pattern on the right hand of the molecule has provided compounds endowed with a favorable combination of FPR2 potency and metabolic stability.

Finally, based on our previous studies[31] showing that compounds with a recovery >20% predicted low clearance of compounds *in vivo*, we assessed the half-life ($t_{1/2}$) and intrinsic clearance (CL_{int}) of compounds (*S*)-**11e**, (*S*)-**11i**, (*S*)-**11l**, (*S*)-**11a**, (*S*)-**11d**, (*R*)-**11l**, (*R*)-**11a**, (*S*)-**11c**, (*S*)-**11j**, (*S*)-**11b**, and (*R*)-**11i**) (Table 2). Most of the compounds showed low

Table 2. Rat Liver Microsomes' Half-Life and Intrinsic Clearance of Selected Compounds

compd	half-life (min)	CL_{int} (μL/min/mg)
(*R*)-**11a**	120	5.5
(*S*)-**11a**	157	4.4
(*S*)-**11b**	50	13.9
(*S*)-**11c**	112	6.2
(*S*)-**11e**	21	33
(*S*)-**11d**	28	24.7
(*R*)-**11i**	108	6.4
(*S*)-**11i**	24	29
(*S*)-**11j**	169	4.1
(*R*)-**11l**	30	23.3
(*S*)-**11l**	44	15.8

clearance in rat liver micrsomes (CL_{int} < 13.2 μL/min/mg protein).[32] In particular, (*S*)-**11l**, (*S*)-**11a**, (*R*)-**11l**, (*R*)-**11a**, (*S*)-**11c**, (*S*)-**11j**, (*S*)-**11b**, and (*S*)-**11i** had $t_{1/2}$ values higher than **2** and, most importantly, these compounds exceed 15 min, which is reported as the lower limit for predicted low-clearance compounds *in vivo*.[33] Compounds (*S*)-**11a**, (*S*)-**11e**, (*S*)-**11i**, and (*S*)-**11l** featured the best combination of FPR2 agonist potency and metabolic stability and were, therefore, characterized further.

Molecular Modeling. The above discussed structural modifications were performed solely on the basis of FPR2 activity and metabolic stability data. During the completion of this study, a cryo-EM structure of the FPR2-G_i complex bound to the synthetic peptide WKYMVM was solved and published.[34] The overall molecular assembly presents the typical seven-transmembrane arrangement of GPCRs, with a wide ligand-binding pocket located in the upper third of the transmembrane spanning helices and open toward the extracellular milieu. The different types of positively and negatively charged aliphatic and aromatic amino acids delineate the chemical niches representing the anchoring spots for FPR2. Therefore, we decided to make use of this evidence to acquire fresh insights into the activity profile of the herein presented compounds.

As an initial test, we performed the docking of compound **43**, which fills the ligand cavity with a binding mode, whereby the 4-chloroureidophenyl moiety acts as a needle that is able to self-anchor the receptor surface, engaging strong aromatic stackings with Phe110, Trp254, and Phe257, and with the assistance of more than one hydrogen bond embracing Asp106 and Arg201. At the same time, the upper moiety of the ligand causes the phenyl ring to be packed between His102 and Phe178, and the isopropyl group to form van der Waals contacts with Leu81 and Val105 (Figure 4). Importantly, this binding pose involves those residues that mutagenesis experiments suggested as crucial for the activation of FPRs.[35,36]

A very similar interaction pattern was then achieved in the docking of (*S*)-**11e**, the compound having the lowest EC_{50} value within the set of the studied compounds. Similar types of interactions favor the ligand−receptor complex stabilization, as seen from the π-π stackings of the 4-fluorophenyl ring with Phe110, Trp254, and Ph257 and the polar interactions of the ureido fragment, respectively, with Asp106 and, assisted by a water molecule, Ser288 (Figure 4). From this type of binding, important clues emerge with respect to the importance of the chiral center: the indoline does indeed produce a charge transfer complex engaging the guanidinium terminal of Arg201, while the cyan substituent recruits a water molecule in its binding to Glu89. The configuration of (*R*)-**11e** produces not only reverse but, more importantly, a less efficient binding. A similar binding mode is found for the dockings of other properly selected

https://doi.org/10.1021/acs.jmedchem.1c02203
J. Med. Chem. XXXX, XXX, XXX−XXX

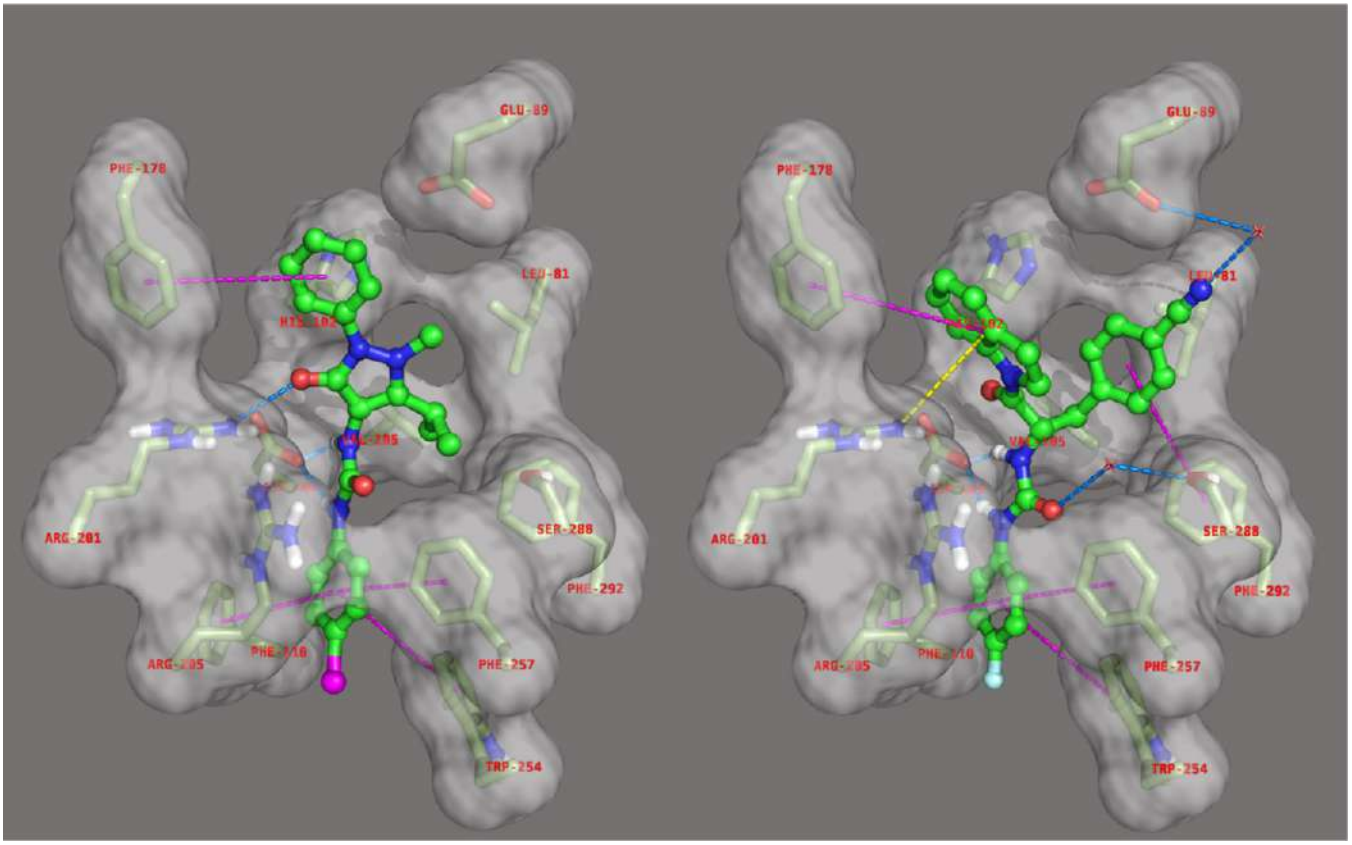

Figure 4. Binding mode of compounds **43** (left) and (*S*)-**11e** (right) to the FPR2 active site (PDB 6OMM). In the interaction pattern, scheme to hydrogen bonds, π-π stackings, and charge transfer are depicted in blue, magenta, and yellow, respectively, and water molecules as red crosses.

enantiomers, namely, (*R*)- and (*S*)-**11f** and (*R*)- and (*S*)-**11l** (Table 3, see Figures S2–S4).

Table 3. Summary of the Docking Results for the FPR2 Agonists

compounds	FEB[a]	ΔE[b]	EFF[c]	TAN[d]	POP[e]
compound **43**	−6.51	0.54	−0.241		434/1000
(*R*)-**11e**	−7-00	2.77	−0.219	0.648	26/1000
(*S*)-**11e**	−6.82	2.06	−0.213	0.715	125/1000
(*R*)-**11f**	−6.76	2.23	−0.205	0.820	90/1000
(*S*)-**11f**	−7.46	1.33	−0.226	0.679	169/1000
(*R*)-**11l**	−6.81	2.57	−0.213	0.869	30/1000
(*S*)-**11l**	−7.01	1.75	−0.212	0.474	171/1000

[a]FEB, free energy of binding. [b]DE, energy difference between the selected pose and the relative global minimum. [c]EFF, ligand efficacy. [d]TAN, Tanimoto similarity coefficient. [e]POP, cluster members population.

Overall, the three-dimensional structure of FPR2, together with the above presented dockings, might represent a valuable tool that could explain the observed activity for our tested compounds and suggest further chemical decorations to be applied to the molecular skeleton.

As an ex-post analysis, we also decided to run molecular dynamics (MD) simulations on **2** and (*S*)-**11e** in complex with FPR2 with the aim of explaining the increase in the EC_{50} values observed following the performed structural modifications. The dynamic trajectories were therefore produced using the relative docking poses of both **2** and (*S*)-**11e** as input.

At first glance, comparison of the aforementioned poses suggests differences in the three-dimensional properties of the two agonists. Indeed, the spatial arrangements of pharmacophoric moieties most likely affecting binding activities are divergent, as shown by the distances measured between 4-fluorophenylureid, 4-cyanophenyl, and the aromatic ring of the substituent linked to the chiral carbon atom (see Figure S5). In the case of (*S*)-**11e**, the smaller volume of indoline allows the achievement of a more widened bioactive conformation, whereas hindrance of the cyclopropyl substituted ring compels **2** to a more puckered pose. Hence, it might be proposed that persistence of this motif might be mandatory for prolongated, and thereafter tighter, interactions with the residues mainly responsible for receptor activation. This hypothesis was subsequently supported by interpretation of the simulation interaction diagrams drawn according to the frequencies of ligand–receptor interactions achieved in the two dynamic trajectories. As shown in Figure 5, the 4-fluorophenylureido portion of both compounds is able to promote noteworthy hydrophobic interactions with the inner part of the transmembrane helix bundle involving Leu109, Phe110, and Phe257, as the latter residue is part of the highly conserved aromatic cluster controlling activation in the majority of rhodopsin-like GPCRs.[37] In contrast, **2** is only 70% anchored to the receptor surface by means of polar interactions involving the ureido fragment, Asp106, His102, and water molecules, while for the same compound, the 4-cyanophenyl and cyclopropyl moieties make no significant contacts to other portions of the receptor.

Conversely, but much more interestingly, (*S*)-**11e** is almost 100% constantly engaged through several hydrogen bonds directly with Asp106, and with the assistance of water bridging

https://doi.org/10.1021/acs.jmedchem.1c02203
J. Med. Chem. XXXX, XXX, XXX−XXX

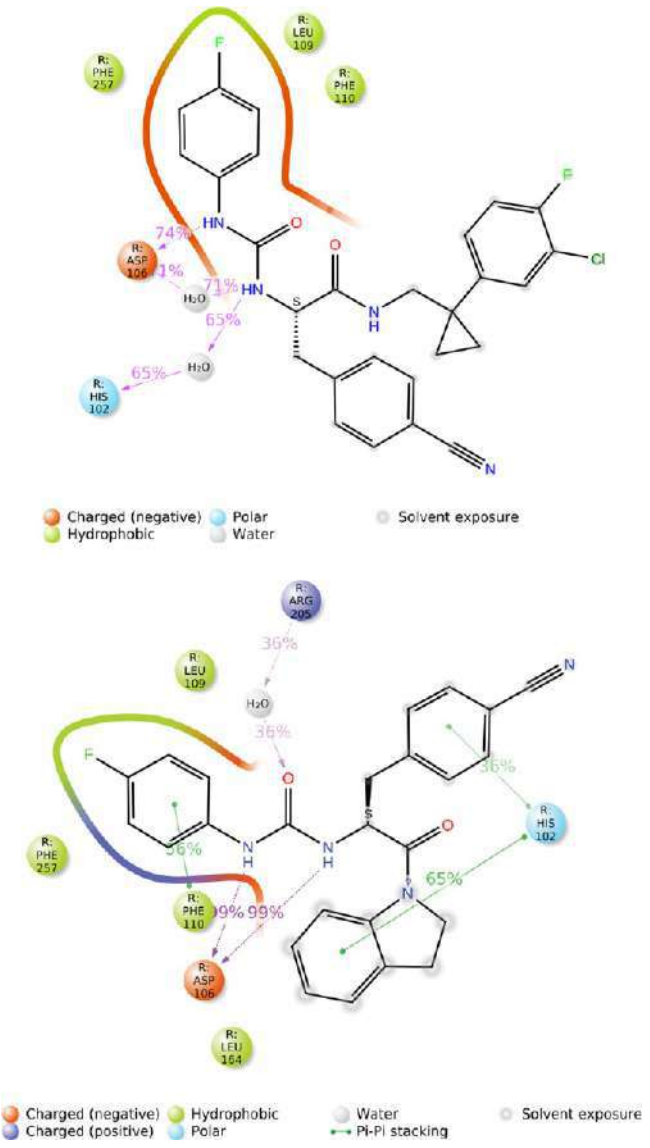

Figure 5. Simulation interactions diagrams (**2** upper and (*S*)-**11e** lower). The minimum contact strength was set to 35% of the trajectories' length.

molecules also with Arg205. The strongest difference applies to the indoline and 4-cyanophenyl rings, which are indeed able to recruit His102 with an efficient π-π stacking. Furthermore, timeline plots of the barycenter distances highlighted a remarkable divergence between the two receptor−ligand complexes, especially in the last 500 ns of the dynamic runs: the average distances were 11.10 ± 0.38 and 10.19 ± 0.26, with minimum and maximum values equal to 9.81 and 12.22, and 9.22 and 11.18 for **2** and (*S*)-**11e**, respectively (Figure 6).

Overall, these data suggest a more robust complementarity in the ligand−receptor fitting for (*S*)-**11e**, and this might, at least in part, explain the increased potency as the results of lowering molecular complexity and steric hindrance as compared to **2**.

Effect of the FPR2 Agonists on Cell Viability in Mouse Microglial N9 Cells. We assessed cytotoxicity of the target compounds by using the 3(4,5dimethylthiazol2yl)2,5diphenyl tetrazolium bromide (MTT) assay in mouse microglial N9 cells, an extensively used model of microglial cells. All of the new FPR2 agonists exhibited lower cytotoxicity than **2** in the MTT test (Table 1). In particular, compounds (*R*)- and (*S*)-**11a**, (*R*)- and (*S*)-**11b**, (*R*)- and (*S*)-**11c**, and (*R*)- and (*S*)-**11h** did not exert any cytotoxic effects, while the remaining compounds were cytotoxic only at micromolar concentrations, with EC_{50} values of about 1−2 orders of magnitude higher than the corresponding EC_{50} values at FPR2.

Next, we selected a subset of target compounds ((*S*)-**11a**, (*S*)-**11d**, (*S*)-**11f**, (*S*)-**11e**, (*S*)-**11g**, (*S*)-**11i**, and (*R*)- and (*S*)-**11l**), on the basis of FPR2 agonist potency and metabolic stability, to evaluate the effect on cell viability using the lactate dehydrogenase (LDH) test. The effect was assessed in N9 cells under basal conditions and after stimulation with LPS, a primary component of endotoxin from Gram-negative bacteria cell walls[38,39] that induces the activation of intracellular signaling pathways, resulting in the stimulation of pro-inflammatory factor production and cytotoxic effects.[40] The compound administration schedule (see the Experimental Section) was based on the observation that the highest FPR2 expression in N9 cells was achieved after 24 h stimulation with LPS.[39] The FPR2 agonists (*S*)-**11a**, (*S*)-**11d**, (*S*)-**11f**, (*S*)-**11e**, (*S*)-**11g**, (*S*)-**11i**, and (*R*)- and (*S*)-**11l** were tested at 0.5 and 5 mM, and **2** was included as internal reference (Figure 7).

Under resting conditions, the compounds did not exert any significant effect on cell viability, with the exception of compounds (*S*)-**11g** and (*R*)-**11l**. Stimulation of N9 cells with LPS (100 ng/mL) induced cell death by increasing LDH release. Interestingly, pre-treatment with the tested compounds (except for (*S*)-**11g**) effectively blocked LPS-induced cell death, suggesting that our FPR2 agonists have protective properties against LPS treatment in the LDH assay.[41]

Two different concentrations of indicated compounds (0.5 and 5 μM) were added to the culture medium 30 min before LPS treatment (100 ng/mL for 24 h), and then cell integrity was evaluated by LDH assay. Results are expressed as percentages of untreated cells. Data are displayed as mean ± SEM from at least three independent experiments performed in triplicate. Statistical significance was calculated by the Student's *t* test and defined as $^{\S}p < 0.05$, $^{\S\S}p < 0.01$, $^{\S\S\S\S}p < 0.0001$, significant values in comparison with untreated cells; and $^{*}p < 0.05$, $^{**}p < 0.01$, significant values in comparison with LPS-treated cells.

Effect of FPR2 Agonists on Pro-Inflammatory Mediator Production in N9 Cells. Based on the results on cell viability, we selected compounds (*S*)-**11a**, (*S*)-**11e**, (*S*)-**11i**, and (*S*)-**11l** to assess their effect on production of the pro-inflammatory mediators IL-1β and TNF-α (Figure 8). Inflammatory cytokines have physiological functions in the brain, including effects on neurite outgrowth, neurogenesis, neuronal survival, synaptic pruning during brain development, synaptic transmission, and synaptic plasticity.[42] However, overproduction and exaggerated release of cytokines is associated with neuronal dysfunction.

Compounds (*S*)-**11a**, (*S*)-**11e**, (*S*)-**11i**, and (*S*)-**11l** did not induce the release of IL-1β and TNF-α in N9 cells when evaluated over a dose range of 0.5 to 5 μM, whereas stimulation of the cells with LPS induced a significant upregulation of both IL-1β and TNF-α production. Interestingly, compounds (*S*)-**11a**, (*S*)-**11e**, (*S*)-**11i**, and (*S*)-**11l** were able to effectively decrease LPS-induced cytokines production, thus exhibiting anti-inflammatory properties. The effects elicited at 0.5 mM were reverted by the FPR2 antagonist WRW4, suggesting that they were FPR2-mediated.

Evaluation of the Anti-Inflammatory Properties of (*S*)-11e and (*S*)-11l in Rat Primary Microglial Cells. Based on the overall biological characterization, compounds (*S*)-**11e** and

https://doi.org/10.1021/acs.jmedchem.1c02203
J. Med. Chem. XXXX, XXX, XXX−XXX

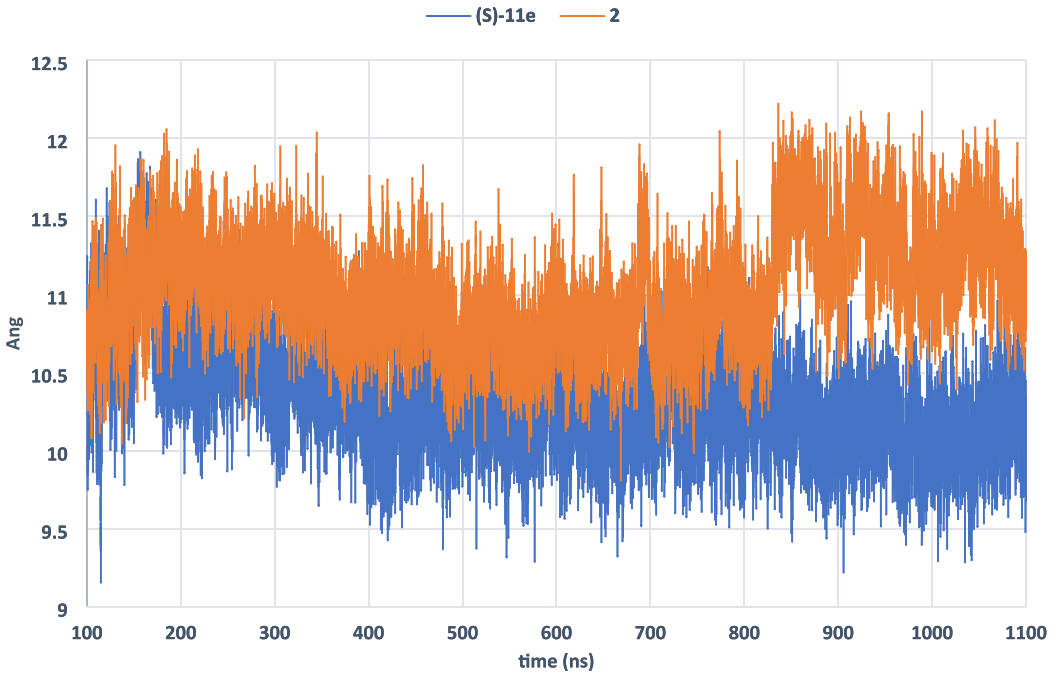

Figure 6. Timeline plots of the barycenter distances as measured in the receptor−ligand complexes.

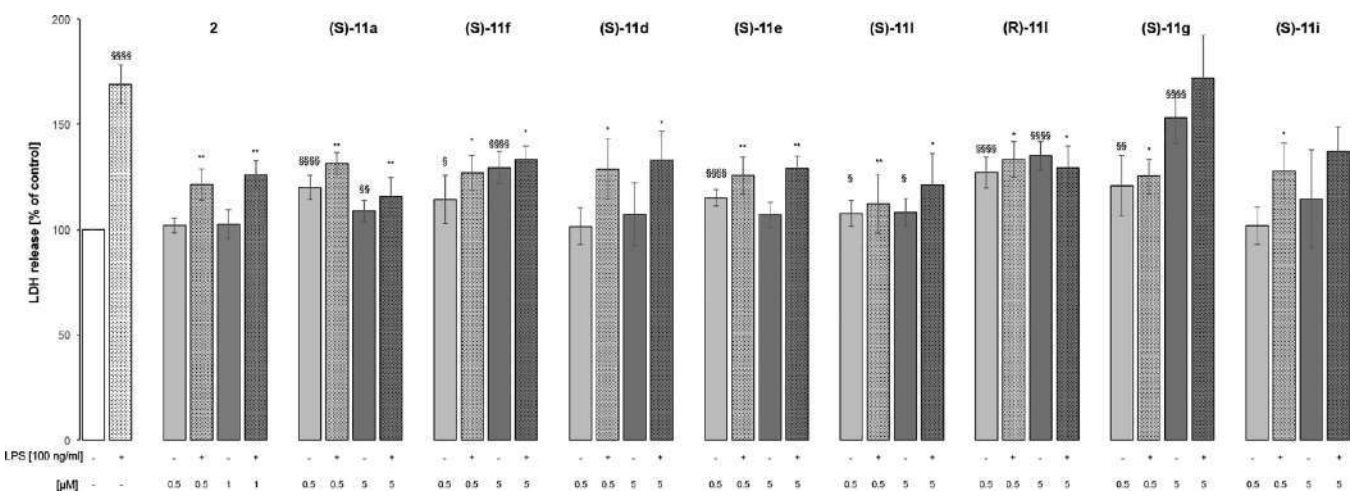

Figure 7. Effect of different FPR2 agonists on cell integrity in murine N9 cells.

(*S*)-**11l** were then selected for a more in-depth characterization of neuroprotective and anti-inflammatory properties in rat primary microglial cells. The neuroprotective properties were evaluated by assessing their effects on cell viability (LDH assay, Figure 9) and NO production (Figure 10) under resting conditions and after 24 h stimulation with LPS. NO is a cellular messenger that plays important roles in many physiological processes in the brain, like survival, differentiation of the neurons, synaptic activity, and neural plasticity.[43] However, excessive NO synthesis leads to neuronal cell death.

Both compounds did not induce any effect on cell viability or NO production under resting conditions, confirming that they have no pro-inflammatory effects. Stimulation of rat primary microglial cells with LPS (100 ng/mL) significantly increased both LDH release and NO production. Pre-treatment with (*S*)-**11e** (0.1 μM) and (*S*)-**11l** (0.1 μM) effectively blocked LPS-induced cell death and NO production. When the compounds were co-administered with the FPR2 antagonist WRW4 (10 μM), a tendency toward reducing the beneficial effects of the compounds was found, suggesting that the observed neuroprotective effects were, at least in part, FPR2-mediated.

The anti-inflammatory properties were evaluated by assessing the effect of compounds (*S*)-**11e** and (*S*)-**11l** on the production of the pro-inflammatory cytokines IL-1β, TNF-α, and IL-6 and of the anti-inflammatory cytokine IL-10 under resting condition and after 24 h stimulation with LPS. None of the compounds induced the release of pro-inflammatory cytokines under resting conditions, indicating no pro-inflammatory effects. Stimulation with LPS (100 ng/mL) significantly increased the levels of IL-1β, TNF-α, and IL-6. Pre-treatment with (*S*)-**11e** (0.1 μM) and (*S*)-**11l** (0.1 μM) effectively suppressed the effect of LPS stimulation. This effect was, at least in part, FPR2-mediated because it was reverted by co-administration of the antagonist WRW4 (10 μM). As for the anti-inflammatory cytokine IL-10, we did not observe statistically significant effects of either LPS

https://doi.org/10.1021/acs.jmedchem.1c02203
J. Med. Chem. XXXX, XXX, XXX−XXX

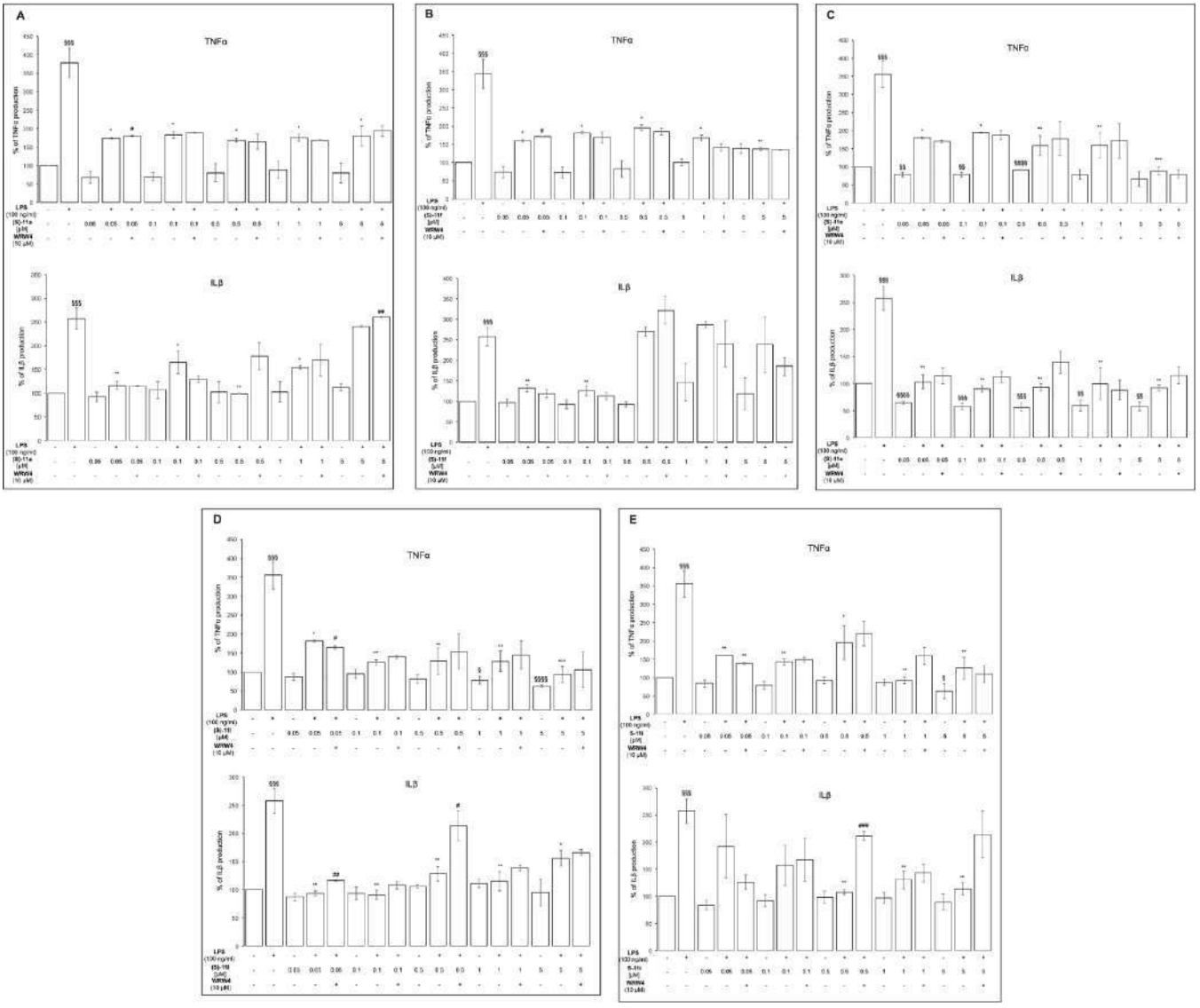

Figure 8. Effect of (*S*)-**11a** (A), (*S*)-**11f** (B), (*S*)-**11e** (C), (*S*)-**11l** (D), and (*S*)-**11i** (E) on the levels of pro-inflammatory cytokines TNF-α and IL-1β in murine N9 cells under resting conditions and after 24 h stimulation with LPS (100 ng/mL). Results are expressed as percentages of untreated cells. Data are displayed as mean ± SEM from at least three independent experiments performed in triplicate. Statistical significance was calculated by the Student's *t* test and defined as $^{\S}p < 0.05$, $^{\S\S}p < 0.01$, $^{\S\S\S}p < 0.001$, $^{\S\S\S\S}p < 0.0001$, significant values in comparison with untreated cells; $^{*}p < 0.05$, $^{**}p < 0.01$, $^{***}p < 0.001$, significant values in comparison with LPS-treated cells, $^{\#}p < 0.05$, $^{\#\#}p < 0.01$, $^{\#\#\#}p < 0.001$, significant values in comparison with LPS + agonist treated cells.

(100 ng/mL) or FPR2 agonist pre-treatment on IL-10 levels in rat primary microglial cells (Table 4).

Finally, to further explore the pro-resolving and neuroprotective potential of the new FPR2 agonists (*S*)-**11e** and (*S*)-**11l**, we evaluated their effects on mitochondrial membrane potential (Figure 11) and on inhibition of caspase 3 activity (Figure 12). The mitochondrial membrane potential ($\Delta\psi$m) is an index of mitochondria function, and changes in its value have been related to the production of pro-inflammatory factors, such as reactive oxygen species and pro-inflammatory cytokines. Recently, it has been reported that the SPM maresin 1 can increase mitochondrial membrane potential in animal models of sepsis and in *in vitro* models of cardiac dysfunction.[44,45] We found that stimulation of microglial cells with LPS (100 ng/mL) significantly reduced $\Delta\psi$m (Figure 11). Pre-treatment with (*S*)-**11e** or (*S*)-**11l** normalized the LPS-induced decrease in mitochondrial membrane potential after 24 h of LPS stimulation. However, this effect was not reverted by co-administration of the antagonist WRW4 (10 μM).

Caspase-3 is involved in apoptotic pathways, and its activation also leads to release of pro-inflammatory mediators in immune cells, including microglia cells. SPMs, including LXA4, can inhibit caspase-3 activation in several models of both peripheral and central inflammation.[46,47] We found that LPS stimulation significantly potentiated the activation of caspase-3 in rat primary microglial cells and that the pre-treatment with (*S*)-**11e** or (*S*)-**11l** (0.1 μM) significantly reduced this activation. Interestingly, the observed effects were reverted by co-administration of WRW4 (10 μM), suggesting that the effects were FPR2-mediated.

In conclusion, the evaluation of the new FPR2 agonists (*S*)-**11e** and (*S*)-**11l** in rat primary microglial cells stimulated with LPS provided additional evidence that both compounds have neuroprotective, anti-inflammatory, and pro-resolving effects.

https://doi.org/10.1021/acs.jmedchem.1c02203
J. Med. Chem. XXXX, XXX, XXX−XXX

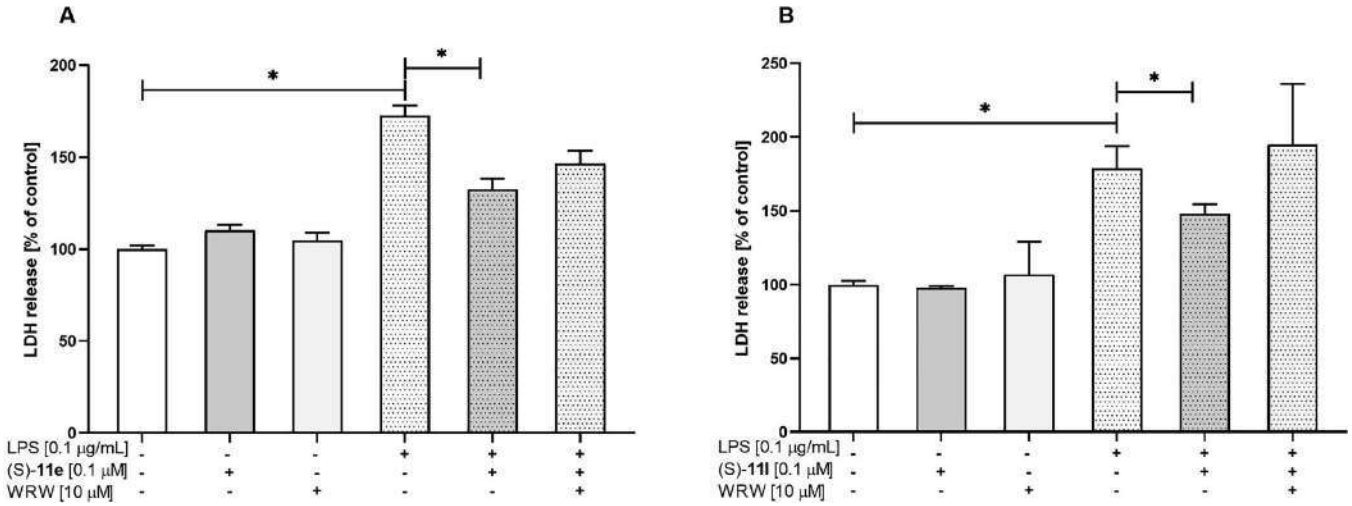

Figure 9. Effect of (*S*)-**11e** and (*S*)-**11l** on cell viability in rat primary microglial cells. LPS (100 ng/mL) induced a significant upregulation of LDH release ($p = 0.000017$ (A); $p = 0.000181$, (B)) in microglia cell cultures. Pre-treatment with (*S*)-**11e** (A) and (*S*)-**11l** (B) effectively blocked LPS-induced cell death ($p = 0.000738$; $p = 0.018249$, respectively).

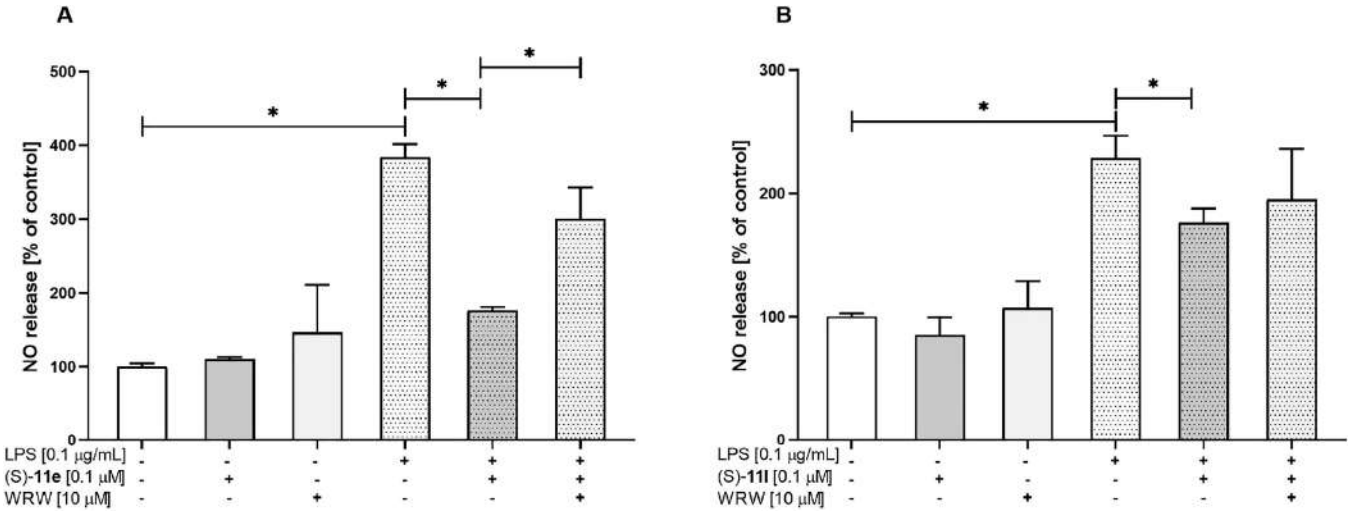

Figure 10. Effect of (*S*)-**11e** and (*S*)-**11l** on NO production in rat primary microglial cells. LPS (100 ng/mL) induced a significant upregulation of NO production ($p = 0.000325$ (A); $p = 0.00006$, (B)) in microglia cell cultures. Pre-treatment with (*S*)-**11e** (A) and (*S*)-**11l** (B) effectively blocked LPS-induced cell death ($p = 0.046393$; $p = 0.011956$, respectively).

Table 4. Effect of 24 h LPS Stimulation and FPR2 Agonists (*S*)-11e (0.1 μM) or (*S*)-11l (0.1 μM) Treatment on the Levels of Pro-Inflammatory (IL-1β, TNF-α, and IL-6) and Anti-Inflammatory (IL-10) Factors in Primary Microglial cells[a]

factors	control	(*S*)-**11e**	(*S*)-**11l**	WRW4	LPS	(*S*)-**11e** + LPS	(*S*)-**11l** + LPS	(*S*)-**11e** + LPS+ WRW4	(*S*)-**11l** + LPS+ WRW4
IL-1β	100 ± 13	95 ± 5.38	102 ± 6.2	103 ± 8.2	**259 ± 31***	**158 ± 11**$^{\#}$	**182 ± 27**$^{\#}$	95 ± 13	**264 ± 10**$^{\wedge}$
TNF-α	100 ± 1.5	101 ± 2.75	95 ± 5.6	121 ± 12.4	**1380 ± 78***	**1039 ± 19**$^{\#}$	**1131 ± 45**$^{\#}$	**1338 ± 4**$^{\wedge}$	1053 ± 110
IL-6	100 ± 2.16	94 ± 2.37	97 ± 6.8	108 ± 1.86	**142 ± 6 ***	**114 ± 7.12**$^{\#}$	**105 ± 3.14**$^{\#}$	120 ± 3.10	100 ± 7.07
IL-10	100 ± 3.9	97 ± 6	122 ± 3	103 ± 14	110 ± 4	111 ± 3	112 ± 6	93 ± 7	89 ± 2

[a]Control cultures were treated with the appropriate vehicle; the data are presented as the mean ± SEM percentage of the control (vehicle-treated cells) of independent experiments, $n = 2–5$, *$p < 0.05$ *vs* control, $^{\#}p < 0.05$ *vs* LPS group, $^{\wedge}p < 0.05$ *vs* FPR2 agonists + LPS.

Importantly, the beneficial effects were observed at nanomolar concentrations.

***In Vivo* Pharmacokinetics.** Finally, on the basis of the overall results and the in vitro metabolic stability, (*S*)-**11l** was selected for *in vivo* pharmacokinetics studies in the perspective of future analyses of *in vivo* drug efficacy in animal models of CNS disorders characterized by neuroinflammation. We tested two different routes of administration: intravenous (i.v.) injection at a dose level of 1 mg/kg ($n = 3$ for each time point) and intraperitoneal (i.p.) injection at a dose level of 10 mg/kg ($n = 3$ for each time point).

The peak plasma concentration of (*S*)-**11l** after i.v. injection was observed at the earliest time point (5 min after administration) with a C_{max} of 1380 ng/mL, and the compound was detectable until 4 h after injection ($C_{last} = 14.1$ ng/mL), with an AUC_{inf} of 613 ng·h/mL (Figure 13A). After i.p.

https://doi.org/10.1021/acs.jmedchem.1c02203
J. Med. Chem. XXXX, XXX, XXX−XXX

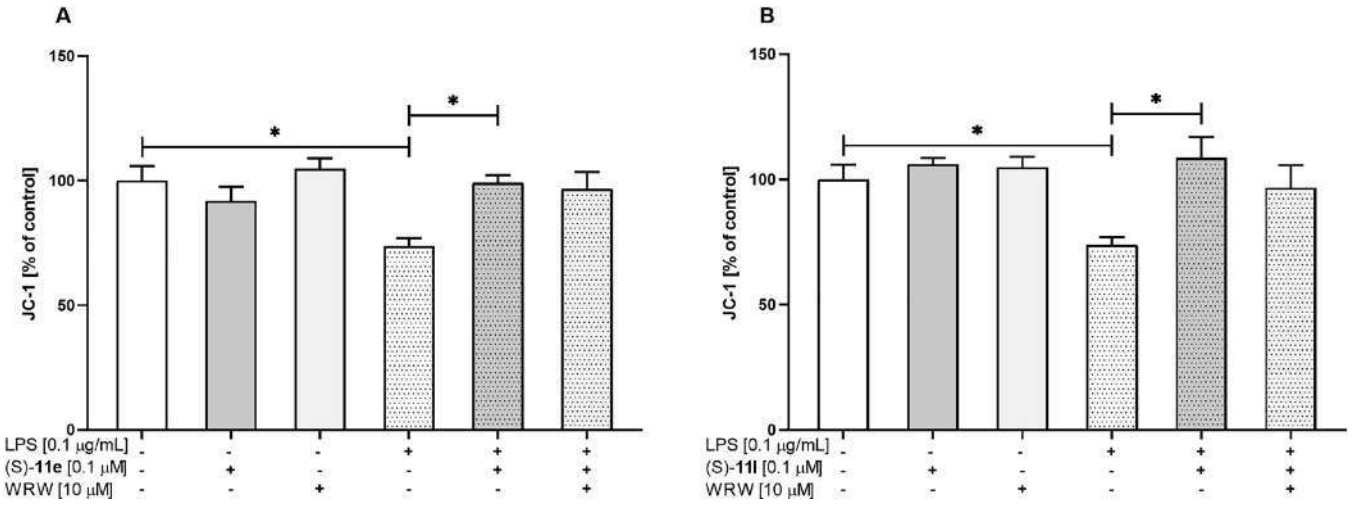

Figure 11. Effect of (*S*)-**11e** and (*S*)-**11l** on mitochondrial membrane potential in rat primary microglial cells. LPS (100 ng/mL) induced a significant reduction of $\Delta\psi$m (p = 0.018674) in microglia cell cultures. Pre-treatment with (*S*)-**11e** (A) and (*S*)-**11l** (B) effectively blocked LPS-induced cell death (p = 0.021179 and p = 0.002083, respectively).

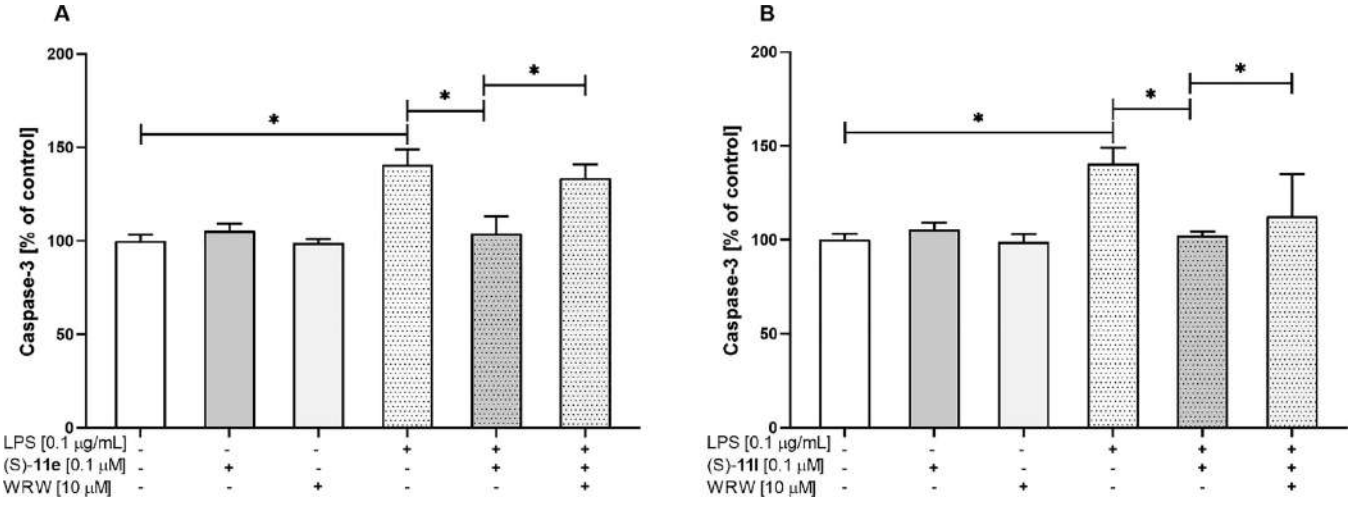

Figure 12. Effect of (*S*)-**11e** and (*S*)-**11l** on caspase-3 activity in rat primary microglial cells. LPS (100 ng/mL) induced a significant reduction of $\Delta\psi$m (p = 0.001770) in microglia cell cultures. Pre-treatment with (*S*)-**11e** (A) and (*S*)-**11l** (B) effectively blocked LPS-induced cell death (p = 0.002518 and p = 0.001929, respectively). The antagonist WRW4 blocked this effect (p = 0.000823 (A); p = 0.037092 (B)).

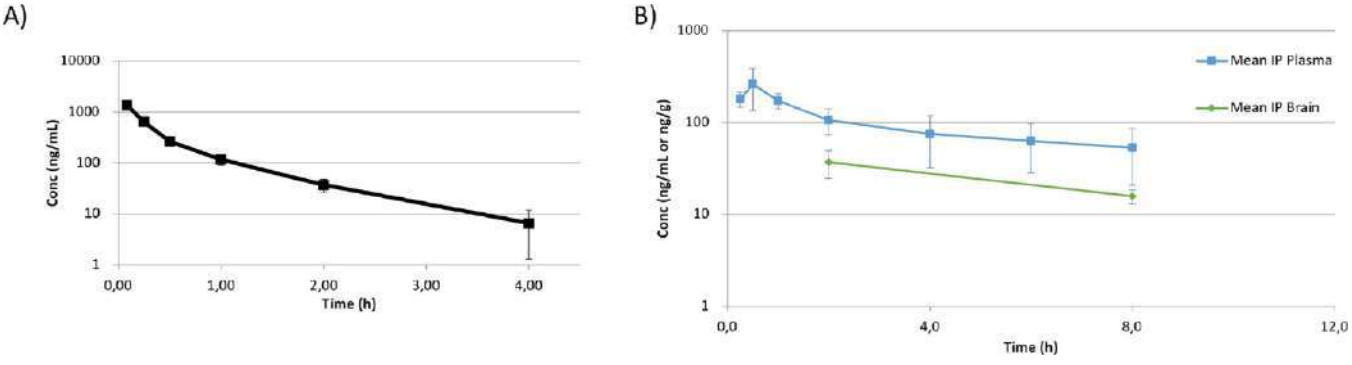

Figure 13. (A) Mean plasma concentration after i.v. injection of (*S*)-**11l** in mice (1 mg/Kg); (B) mean plasma and brain concentrations after i.p. injection of (*S*)-**11l** in mice (10 mg/kg).

administration, (*S*)-**11l** reached the systemic circulation relatively quickly, with a maximal plasma concentration 30 min after dosing with a C_{max} of 192 ng/mL, with an AUC_{inf} of 731 ng·h/mL, and the compound was detectable in plasma for 8 h after dosing (Figure 13B). We also sampled (*S*)-**11l** concentrations in brain after i.p. injection at 2 and 8 h. At 2 h after dosing, we found a brain concentration of 37 ng/g, with a brain-to-plasma ratio of 0.378, whereas at 8 h after dosing, a

https://doi.org/10.1021/acs.jmedchem.1c02203
J. Med. Chem. XXXX, XXX, XXX−XXX

brain concentration of 15.7 ng/g with a brain-to-plasma ratio of 0.205 was observed. These data indicated that (*S*)-**11l** is able to permeate the blood−brain barrier and to accumulate in the brain.

CONCLUSIONS

An increasing number of studies indicate that the resolution of inflammation is altered in several neurodegenerative disorders and that the activation of FPR2 by pro-resolving agonists can open new therapeutic perspectives in the treatment of neuroinflammation associated with these disorders. Thus, we aimed at identifying novel potent FPR2 pro-resolving agonists with pharmacokinetic properties suitable for *in vivo* studies, starting from the ureidopropanamide FPR2 agonist **2**. The structure−activity relationship study on the agonist **2** highlighted that the substituent linked to the amide function is a hot spot for FPR2 activity, which coincides with a soft spot for metabolic stability, with divergent structural requirements. However, the fine tuning of the shape and the volume of this part of the molecule provided potent FPR2 agonists with pharmacokinetic properties suitable for *in vivo* use. In addition, the newly synthesized compounds, characterized by a wide range of FPR2 potency, were valuable to challenge the topology of the FPR2 binding site revealed by a cryo-EM study of the FPR2−G_i complex bound to the peptide WKYMVM.

In order to achieve the broader goal of identifying FPR2 agonists with pro-resolving properties, a group of compounds featuring high potency and metabolic stability were characterized in a set of in vitro models on neuroinflammation. In mouse N9 microglial cells and in rat primary microglial cells, these compounds did not induce inflammatory responses in resting cells and were able to significantly reduce the production of pro-inflammatory cytokines induced by LPS, clearly indicating anti-inflammatory effects. In addition, compounds (*S*)-**11e** and (*S*)-**11l** were able to counterbalance the changes in mitochondrial function and to inhibit caspase-3 activity induced by LPS, in the same way as the endogenous SPMs. Collectively, the pharmacological characterization on different aspects of microglia activation has shown that our FPR2 agonists have anti-inflammatory and pro-resolving properties. Importantly, these effects are elicited at nanomolar concentrations, i.e., the same concentration range of the endogenous SPM LXA4.[26] Among the newly synthesized compounds, (*S*)-**11l** stands out also for the ability to permeate the blood−brain barrier and to accumulate in the mouse brain *in vivo*. We believe that the present study is a relevant contribution to the exploitation of the therapeutic potential of promoting the resolution of inflammation. It provides the scientific community with a valuable pharmacological tool for studies *in vivo*.

EXPERIMENTAL SECTION

Chemistry. Chemicals were purchased from Sigma-Aldrich and TCI Chemicals. Unless otherwise stated, all chemicals were used without further purification. Thin-layer chromatography (TLC) was performed using plates from Merck (silica gel 60 F254). Column chromatography was performed with 1:30 Merck silica gel 60 Å (63−200 μm) as the stationary phase. Flash chromatographic separations were performed on a Biotage SP1 purification system using flash cartridges pre-packed with KP-Sil 32−63 μm, 60 Å silica. The ^{1}H NMR spectra were recorded on a Varian Mercury-VX spectrometer (300 MHz) or on a 500-vnmrs500 Agilent spectrometer (500 MHz). All chemical shift values are reported in ppm (δ). Recording of the mass spectra (electron impact) was performed on an HP6890-5973 MSD gas chromatograph/mass spectrometer; only significant m/z peaks, with their percentage of relative intensity in parentheses, are reported. The high-resolution mass spectra (electrospray ionization, ESI-TOF) (HRMS) were recorded on an Agilent 6530 accurate mass Q-TOF (mass range, 50−3000 m/z; dry gas nitrogen, 10 mL/min; dry heater, 325 °C; capillary voltage, 4000 V, electrospray ion source in positive or negative ion mode). All spectra were in accordance with the assigned structures. Elemental analyses (C, H, and N) of the target compounds were performed on a Eurovector Euro EA 3000 analyzer. Analyses indicated by the symbols of the elements were within ±0.4% of the theoretical values. RP-HPLC analysis was performed on an Agilent 1260 Infinity Binary LC system equipped with a diode array detector using a Phenomenex Gemini C-18 column (250 × 4.6 mm, 5 μm particle size). All target compounds were eluted with CH_3OH/H_2O, 8:2, at a flow rate of 1 mL/min. The purity of the target compounds listed in Table 1 was assessed by RP-HPLC and combustion analysis. All compounds showed ≥95% purity.

The following compounds were prepared according to the literature methods: 5-fluoroisoindoline (**3j**),[48] 3,3-dimethylindoline (**3k**),[49] 5-fluoroindoline (**3i**),[50] 6-fluoroindoline (**3l**),[51] 7-azaindoline (**3m**),[52] and 7-fluoro-1,2,3,4-tetrahydroisoquinoline (**3n**).[53]

*2-(4-Fluorophenyl)-2-methylpropanenitrile (**5**).* To an ice-cooled suspension of NaH (1.25 g, 31.3 mmol) and iodomethane (2.2 mL, 35.3 mmol) in anhydrous DMF (15 mL), a solution of 4-fluorophenylacetonitrile (2.0 g, 14.8 mmol) in the same solvent (5.0 mL) was added dropwise. The mixture was stirred at room temperature for 2 days. The reaction mixture was poured onto ice-water and then extracted with EtOAc (3 × 30 mL). The collected organic layers were washed with brine, dried over Na_2SO_4, and evaporated in vacuo. The crude residue was purified by flash chromatography to obtain a colorless oil (0.84 g, 35% yield). ^{1}H NMR ($CDCl_3$, 300 MHz) δ: 1.74 (s, 6H), 7.12 (m, 2H), 7.28 (m, 2H). GC/MS m/z: 164 (M^+, +1, 5), 163 (M^+, 27), 148 (100), 121 (30).

*2-(4-Fluorophenyl)-2-methylpropan-1-amine (**6**).* To a cooled solution of benzylcyanide **5** (0.84 g, 5.2 mmol) in anhydrous THF (20 mL), a borane dimethylsulfide complex (10 M, 1.54 mL, 15.4 mmol) was added dropwise. The reaction mixture was refluxed overnight. After cooling, MeOH was cautiously added to destroy the borane excess, HCl (10 mL) was added dropwise, and the resulting mixture was refluxed for an additional 1 h. After evaporation of volatiles, the aqueous solution was alkalinized with 5% NaOH and extracted with CH_2Cl_2 (2 × 20 mL). The organic layers were collected, dried over Na_2SO_4, and concentrated under reduced pressure to obtain the desired compound as a pale-yellow oil, which was used in the next step without any further purification (0.32 g, 38% yield). ^{1}H NMR ($CDCl_3$, 300 MHz) δ: 1.40 (s, 6H), 1.89 (br s, 2H, D_2O exchanged), 2.90 (s, 2H), 7.12 (m, 2H), 7.42 (m, 2H). GC/MS m/z: 168 (M^+, +1, 1), 167 (M^+, 4), 137 (14), 109 (100).

*2,2,2-Trifluoro-N-(2-(4-fluorophenyl)-2-methylpropyl)acetamide (**7**).* To an ice-cooled solution of phenethylamine **6** (0.32 g, 1.9 mmol), triethylamine (0.3 mL, 2.11 mmol) in anhydrous CH_2Cl_2 (10 mL) and trifluoroacetic anhydride (0.54 mL, 3.8 mmol) were slowly added. The reaction mixture was allowed to reach room temperature and was stirred for 30 min. Next, H_2O was added, and the resulting mixture was extracted with EtOAc (3 × 20 mL). The collected organic layers were washed with brine solution, dried over Na_2SO_4, and concentrated in vacuo. The crude residue was purified by flash chromatography using a gradient elution from *n*-hexane/EtOAc, 7:3 (v/v), to *n*-hexane/EtOAc, 3:7 (v/v), to obtain the desired compound as a pale-yellow oil (0.30 g, 59% yield). ^{1}H NMR ($CDCl_3$, 300 MHz) δ: 1.40 (s, 6H), 3.45 (s, 2H), 7.03 (br t, 1H, NH), 7.16 (m, 2H), 7.44 (m, 2H). GC/MS m/z: 263 (M^+ 1), 137 (100), 109 (56).

*2,2,2-Trifluoro-1-(7-fluoro-4,4-dimethyl-3,4-dihydroisoquinolin-2(1H)-yl)ethanone (**8**).* To a mixture of acetic acid (1.5 mL) and sulfuric acid (2 mL), acetamide **7** (0.30 g, 1.1 mmol) and paraformaldehyde (0.06 g, 1.9 mmol) were added under N_2. The reaction mixture was stirred at room temperature for 20 h, and then it was poured into 50 mL of water and extracted with EtOAc (2 × 20 mL). The collected organic layers were washed first with a saturated aqueous solution of $NaHCO_3$ and then with brine, dried over Na_2SO_4, and concentrated under reduced pressure. The crude residue was purified

https://doi.org/10.1021/acs.jmedchem.1c02203
J. Med. Chem. XXXX, XXX, XXX−XXX

by column chromatography (CH_2Cl_2/EtOAc, 1:1 (v/v), as eluent) to obtain the target compound as a pale-yellow oil (0.21 g, 68% yield). ^{1}H NMR ($CDCl_3$, 300 MHz) δ: 1.26 (s, 3H), 1.28 (s, 3H), 3.45 (m, 2H), 4.45 (s, 2H), 6.69 (m, 1H), 6.97 (m, 1H), 7.32 (m, 1H, J = 8.31 Hz). GC/MS m/z: 276 (M^+, +1, 14), 275 (M^+, 100), 260 (60), 147 (54), 135 (48).

*7-Fluoro-4,4-dimethyl-1,2,3,4-tetrahydroisoquinoline (**3o**).* To a solution of amide **8** (0.21 g, 0.77 mmol) in CH_3OH (15 mL) and H_2O (1.5 mL), K_2CO_3 (0.06 g, 4.1 mmol) was added. The reaction mixture was refluxed for 2 h. Then, CH_3OH was evaporated, and the resulting aqueous layer was diluted with 5% NaOH (10 mL) and extracted with $CHCl_3$ (2 × 20 mL). The collected organic layers were dried over Na_2SO_4 and concentrated under reduced pressure. The crude residue was purified on a silica gel column (CH_2Cl_2/EtOAc, 1:1 as eluent) to obtain the desired compound as a colorless oil (0.08 g, 59% yield). ^{1}H NMR ($CDCl_3$, 300 MHz) δ: 1.25 (s, 3H), 1.26 (s, 3H), 1.90 (br s, 1H, D_2O exchanged), 2.80 (m, 2H), 3.81 (s, 2H), 6.69 (m, 1H), 6.97 (m, 1H), 7.32 (m, 1H, J = 8.31 Hz). HRMS (ESI$^+$) calcd for $[(C_{11}H_{14}FN) + H]^+$, 180.1183; found, 180.1182. ESI$^+$/MS/MS $[M + H]^+$ m/z: 109 (100).

General Procedure for the Synthesis of Boc-Derivatives 9a–c,f,j,n,o. *N′,N*-Carbonyldiimidazole (0.14 g, 0.88 mmol) was added to a solution of (*R*)- or (*S*)-Boc-4-CN-phenylalanine (0.23 g, 0.80 mmol) in anhydrous THF (10 mL), and the reaction mixture was stirred overnight at room temperature. Next, a solution of the appropriate amine (0.80 mmol) in the same solvent was added, and the reaction mixture was stirred for 24 h. The solvent was concentrated in vacuo, and the residue was partitioned between EtOAc (20 mL) and H_2O (20 mL). The organic layer was separated, and the aqueous phase was extracted with EtOAc (2 × 20 mL). The collected organic layers were dried over Na_2SO_4 and concentrated under reduced pressure. The crude residue was purified on a silica gel column as detailed below to obtain pure target compounds.

*(2R)-tert-Butyl (3-(4-Cyanophenyl)-1-oxo-1-((2-oxoazepan-3-yl)-amino)propan-2-yl)carbamate ((2R)-**9a**).* Eluted with $CHCl_3$/MeOH, 95:5. White solid, quantitative yield. ^{1}H NMR ($CDCl_3$, 300 MHz) δ: 1.36 (s, 9H), 1.68–1.87 (m, 4H), 1.87–2.00 (m, 2H), 3.04–3.13 (m, 1H), 3.15–3.23 (m, 3H), 4.41–4.45 (m, 2H), 5.10–5.29 (m, 1H), 6.17 (br s, 1H), 7.28–7.34 (m, 2H), 7.41 (br s, 1H), 7.55 (m, 2H). HRMS (ESI$^+$) calcd for $[(C_{21}H_{28}N_4O_4) + Na]^+$, 423.2003; found, 423.2004. ESI$^+$/MS/MS $[M + Na]^+$ m/z: 323 (100).

*(2S)-tert-Butyl (3-(4-Cyanophenyl)-1-oxo-1-((2-oxoazepan-3-yl)-amino)propan-2-yl)carbamate ((2S)-**9a**).* Eluted with $CHCl_3$/MeOH, 95:5. White solid, 56% yield. ^{1}H NMR ($CDCl_3$, 300 MHz) δ: 1.36 (s, 9H), 1.68–1.87 (m, 4H), 1.87–2.00 (m, 2H), 3.04–3.13 (m, 1H), 3.15–3.23 (m, 3H), 4.41–4.45 (m, 2H), 5.10–5.29 (m, 1H), 6.17 (br s, 1H), 7.28–7.34 (m, 2H), 7.41 (br s, 1H), 7.55 (m, 2H). HRMS (ESI$^+$) calcd for $[(C_{21}H_{28}N_4O_4) + Na]^+$, 423.2003; found, 423.2004. ESI$^+$/MS/MS $[M + Na]^+$ m/z: 323 (100).

*(R)-tert-Butyl (3-(4-Cyanophenyl)-1-oxo-1-(piperidin-1-yl)-propan-2-yl)carbamate ((R)-**9b**).* Eluted with *n*-hexane/EtOAc, 1:1. White solid, 63% yield. ^{1}H NMR ($CDCl_3$, 500 MHz) δ: 1.19–1.25 (m, 1H), 1.39 (s, 9H), 1.41–1.58 (m, 5H), 2.93 (dd, 1H, J = 5.8 and 13.2 Hz), 3.06 (dd, 1H, J = 7.3 and 13.2 Hz), 3.13–3.18 (m, 1H), 3.31–3.36 (m, 1H), 3.43–3.48 (m, 1H), 3.52–3.57 (m, 1H), 4.82–4.85 (m, 1H), 5.41 (br d, 1H, D_2O exchanged), 7.30 (d, 2H, J = 8.31 Hz), 7.57 (d, 2H, J = 8.31 Hz). HRMS (ESI$^+$) calcd for $[(C_{20}H_{27}N_3O_3) + Na]^+$, 380.1945; found, 380.1940. ESI$^+$/MS/MS $[M + Na]^+$ m/z: 280 (100).

*(S)-tert-Butyl (3-(4-Cyanophenyl)-1-oxo-1-(piperidin-1-yl)-propan-2-yl)carbamate ((S)-**9b**).* Eluted with *n*-hexane/EtOAc, 6:4. White solid, 74% yield. ^{1}H NMR ($CDCl_3$, 500 MHz) δ: 1.18–1.27 (m, 1H), 1.39 (s, 9H), 1.41–1.59 (m, 5H), 2.91–2.95 (dd, 1H, J = 6.4 and 13.1 Hz), 3.04–3.08 (dd, 1H, J = 7.3 and 13.2 Hz), 3.13–3.17 (m, 1H), 3.31–3.36 (m, 1H), 3.43–3.48 (m, 1H), 3.52–3.57 (m, 1H), 4.83–4.88 (m, 1H), 5.41 (br d, 1H, D_2O exchanged), 7.29 (d, 2H, J = 7.8 Hz), 7.57 (d, 2H, J = 7.8 Hz). HRMS (ESI$^+$) calcd for $[(C_{20}H_{27}N_3O_3) + Na]^+$, 380.1945; found, 380.1940. ESI$^+$/MS/MS $[M + Na]^+$ m/z: 280 (100).

*(R)-tert-Butyl (3-(4-Cyanophenyl)-1-oxo-1-(pyrrolidin-1-yl)-propan-2-yl)carbamate ((R)-**9c**).* Gradient elution from *n*-hexane/EtOAc, 6:4, to *n*-hexane/EtOAc, 1:9. White solid, 75% yield. ^{1}H NMR ($CDCl_3$, 300 MHz) δ: 1.39 (s, 9H), 1.54–1.87 (m, 4H), 2.81–2.88 (m, 1H), 2.94–3.10 (m, 2H), 3.27–3.36 (m, 1H), 3.42–3.48 (m, 2H), 4.58–4.63 (m, 1H), 5.36 (br d, 1H, D_2O exchanged), 7.31 (d, 2H, J = 8.2 Hz), 7.56 (d, 2H, J = 8.2 Hz). HRMS (ESI$^+$) calcd for $[(C_{19}H_{25}N_3O_3) + Na]^+$, 366.1788; found, 366.1788. ESI$^+$/MS/MS $[M + Na]^+$ m/z: 266 (100).

*(S)-tert-Butyl (3-(4-Cyanophenyl)-1-oxo-1-(pyrrolidin-1-yl)-propan-2-yl)carbamate ((S)-**9c**).* Gradient elution from *n*-hexane/EtOAc, 6:4, to *n*-hexane/EtOAc, 1:9. White solid, 36% yield. ^{1}H NMR ($CDCl_3$, 300 MHz) δ: 1.39 (s, 9H), 1.54–1.87 (m, 4H), 2.81–2.88 (m, 1H), 2.94–3.10 (m, 2H), 3.27–3.36 (m, 1H), 3.42–3.48 (m, 2H), 4.58–4.63 (m, 1H), 5.36 (br d, 1H, D_2O exchanged), 7.31 (d, 2H, J = 8.2 Hz), 7.56 (d, 2H, J = 8.2 Hz). HRMS (ESI$^+$) calcd for $[(C_{19}H_{25}N_3O_3) + Na]^+$, 366.1788; found, 366.1791. ESI$^+$/MS/MS $[M + Na]^+$ m/z: 266 (100).

*(R)-tert-Butyl (3-(4-Cyanophenyl)-1-(3,4-dihydroisoquinolin-2(1H)-yl)-1-oxopropan-2-yl)carbamate ((R)-**9f**).* Gradient elution from $CHCl_3$/EtOAc, 9:1, to $CHCl_3$/EtOAc, 8:2. Yellow solid, 90% yield. ^{1}H NMR ($CDCl_3$, 300 MHz) δ: 1.39 (s, 9H), 2.49–2.52 (m, 1H), 2.71–2.80 (m, 2H), 2.79–2.81 (m, 1H), 2.95–3.03 (m, 1H), 3.32–3.42 (m, 2H), 3.62–3.68 (m, 1H), 4.88–4.95 (m, 1H), 6.82 (app d, 1H, D_2O exchanged), 7.07–7.10 (m, 1H), 7.12–7.23 (m, 3H), 7.33 (d, 2H, J = 8.2 Hz), 7.48 (d, 2H, J = 8.2 Hz). HRMS (ESI$^+$) calcd for $[(C_{24}H_{27}N_3O_3) + Na]^+$, 428.1945; found, 428.1943. ESI$^+$/MS/MS $[M + Na]^+$ m/z: 328 (100), 158 (45), 64 (70).

*(S)-tert-Butyl (3-(4-Cyanophenyl)-1-(3,4-dihydroisoquinolin-2(1H)-yl)-1-oxopropan-2-yl)carbamate ((S)-**9f**).* Eluted with $CHCl_3$/EtOAc, 8.2. Yellow solid, 77% yield. ^{1}H NMR ($CDCl_3$, 300 MHz) δ: 1.37 (s, 9H), 2.49–2.52 (m, 1H), 2.71–2.80 (m, 2H), 2.79–2.81 (m, 1H), 2.95–3.03 (m, 1H), 3.32–3.42 (m, 2H), 3.62–3.68 (m, 1H), 4.88–4.95 (m, 1H), 6.82 (app d, 1H, D_2O exchanged), 7.07–7.10 (m, 1H), 7.12–7.23 (m, 3H), 7.33 (d, 2H, J = 8.2 Hz), 7.48 (d, 2H, J = 8.2 Hz). HRMS (ESI$^+$) calcd for $[(C_{24}H_{27}N_3O_3) + Na]^+$, 428.1945; found, 428.1948. ESI$^+$/MS/MS $[M + Na]^+$ m/z: 328 (100), 158 (30), 64 (70).

*(R)-tert-Butyl (3-(4-Cyanophenyl)-1-(5-fluoroisoindolin-2-yl)-1-oxopropan-2-yl)carbamate ((R)-**9j**).* Eluted with CH_2Cl_2/EtOAc, 1:1. White solid, 51% yield. ^{1}H NMR ($CDCl_3$, 500 MHz) δ: 1.39 (s, 9H), 3.02 (dd, 1H, J = 6.4 and 13.2 Hz), 3.14 (dd, 1H, J = 7.8 and 13.2 Hz), 4.33–4.37 (m, 1H), 4.58–4.65 (m, 1H), 4.72–4.82 (m, 2H), 4.90–4.96 (m, 1H), 5.31 (br s, 1H, NH), 6.95–7.10 (m, 2H), 7.10–7.16 (m, 1H), 7.35 (d, 2H, J = 8.3 Hz), 7.55 (d, 2H, J = 6.9 Hz). HRMS (ESI$^+$) calcd for $[(C_{23}H_{24}FN_3O_3) + Na]^+$, 432.1694; found, 432.1696. ESI$^+$/MS/MS $[M + Na]^+$ m/z: 332 (100).

*(S)-tert-Butyl (3-(4-Cyanophenyl)-1-(5-fluoroisoindolin-2-yl)-1-oxopropan-2-yl)carbamate ((S)-**9j**).* Eluted with CH_2Cl_2/EtOAc, 1:1. White solid, 28% yield. ^{1}H NMR ($CDCl_3$, 500 MHz) δ: 1.39 (s, 9H), 3.02 (dd, 1H, J = 6.4 and 13.2 Hz), 3.14 (dd, 1H, J = 7.8 and 13.2 Hz), 4.33–4.37 (m, 1H), 4.58–4.65 (m, 1H), 4.72–4.82 (m, 2H), 4.90–4.96 (m, 1H), 5.31 (br s, 1H, NH), 6.95–7.10 (m, 2H), 7.10–7.16 (m, 1H), 7.35 (d, 2H, J = 8.3 Hz), 7.55 (d, 2H, J = 6.9 Hz). HRMS (ESI$^+$) calcd for $[(C_{23}H_{24}FN_3O_3) + Na]^+$, 432.1694; found, 432.1696. ESI$^+$/MS/MS $[M + Na]^+$ m/z: 332 (100).

*(R)-tert-Butyl (3-(4-Cyanophenyl)-1-(7-fluoro-3,4-dihydroisoquinolin-2(1H)-yl)-1-oxopropan-2-yl)carbamate ((R)-**9n**).* Gradient elution from *n*-hexane/EtOAc, 7:3, to *n*-hexane/EtOAc, 6:4. White solid, 51% yield. ^{1}H NMR ($CDCl_3$, 300 MHz) δ: 1.30 (s, 9H), 2.65–2.78 (m, 2H), 2.95–3.15 (m, 2H), 3.32–3.47 (m, 1H), 4.02–4.19 (m, 1H), 4.52–4.71 (m, 2H), 4.87–4.96 (m, 1H), 5.38–5.44 (app t, 1H), 6.81–6.94 (m, 2H), 7.01–7.06 (m, 1H), 7.22–7.29 (m, 2H), 7.46–7.48 (m, 1H), 7.49–7.51 (m, 1H). HRMS (ESI$^+$) calcd for $[(C_{24}H_{26}FN_3O_3) + Na]^+$, 446.1850; found, 446.1850. ESI$^+$/MS/MS $[M + Na]^+$ m/z: 346 (100), 313 (40).

*(S)-tert-Butyl (3-(4-Cyanophenyl)-1-(7-fluoro-3,4-dihydroisoquinolin-2(1H)-yl)-1-oxopropan-2-yl)carbamate ((S)-**9n**).* Gradient elution from *n*-hexane/EtOAc, 7:3, to *n*-hexane/EtOAc, 6:4. White solid, 49% yield. ^{1}H NMR ($CDCl_3$, 300 MHz) δ: 1.30 (s, 9H), 2.65–2.78 (m, 2H), 2.95–3.15 (m, 2H), 3.32–3.47 (m, 1H), 4.02–4.19 (m, 1H), 4.52–4.71 (m, 2H), 4.87–4.96 (m, 1H), 5.38–5.44 (app t, 1H), 6.81–

https://doi.org/10.1021/acs.jmedchem.1c02203
J. Med. Chem. XXXX, XXX, XXX–XXX

6.94 (m, 2H), 7.01−7.06 (m, 1H), 7.22−7.29 (m, 2H), 7.46−7.48 (m, 1H), 7.49−7.51 (m, 1H). HRMS (ESI$^+$) calcd for [($C_{24}H_{26}FN_3O_3$) + Na]$^+$, 446.1850; found, 446.1850. ESI$^+$/MS/MS [M + Na]$^+$ *m/z*: 346 (100), 313 (40).

*(S)-tert-Butyl (3-(4-Cyanophenyl)-1-(7-fluoro-4,4-dimethyl-3,4-dihydroisoquinolin-2(1H)-yl)-1-oxopropan-2-yl)carbamate ((S)-**9o**).* Eluted with CH_2Cl_2/EtOAc, 1:1. Colorless oil, 57% yield. ^{1}H NMR ($CDCl_3$, 300 MHz) δ: 1.25 (s, 3H), 1.26 (s, 3H), 1.39 (s, 9H), 3.14 (dd, 1H, *J* = 7.8 and 13.2 Hz), 3.42−3.49 (m, 3H), 4.46 (s, 2H), 4.90−4.96 (m, 1H), 5.31 (br s, 1H, NH), 6.65−6.70 (m, 1H), 6.97−7.01 (m, 1H), 7.28−7.32 (m, 1H), 7.45 (d, 2H, *J* = 8.3 Hz), 7.55 (d, 2H, *J* = 8.3 Hz). HRMS (ESI$^+$) calcd for [($C_{26}H_{30}FN_3O_3$) + Na]$^+$, 474.2163; found, 474.2161. ESI$^+$/MS/MS [M + Na]$^+$ *m/z*: 332 (100).

General Procedure for the Synthesis of Boc-Derivatives 9d,e,g,k−m. A solution of (*R*)- or (*S*)-Boc-4-CN-phenylalanine (0.25 g, 0.86 mmol), amine (1.03 mmol), PyBOP (0.69 g, 1.29 mmol), and *N*-methylmorpholine (0.70 g, 6.88 mmol) in anhydrous DMF (10 mL) was stirred overnight at room temperature. Then, the mixture was diluted with H_2O (10 mL) and extracted with AcOEt (3 × 20 mL). The combined organic layers were washed with brine, dried over Na_2SO_4, and concentrated in vacuo. The crude residue was purified on a silica gel column as detailed below to obtain the pure target compounds.

*(R)-tert-Butyl (3-(4-Cyanophenyl)-1-(isoindolin-2-yl)-1-oxopropan-2-yl)carbamate ((R)-**9d**).* Gradient elution from *n*-hexane/EtOAc, 65:35, to *n*-hexane/EtOAc, 2:8. White solid, 71% yield. ^{1}H NMR ($CDCl_3$, 500 MHz) δ: 1.39 (s, 9H), 3.02 (dd, 1H, *J* = 6.3 and 13.2 Hz), 3.15 (dd, 1H, *J* = 7.8 and 13.2 Hz), 4.38 (d, 1H, *J* = 13.2 Hz), 4.66 (d, 1H, *J* = 15.7 Hz), 4.74−4.78 (m, 1H), 4.82 (d, 1H, *J* = 15.7 Hz), 4.95 (d, 1H, *J* = 13.2 Hz), 5.34 (br d, 1H, D_2O exchanged), 7.17−7.18 (app d, 1H), 7.27−7.31 (m, 3H), 7.35 (d, 2H, *J* = 8.32 Hz), 7.55 (d, 2H, *J* = 8.32 Hz). HRMS (ESI$^+$) calcd for [($C_{23}H_{25}N_3O_3$) + Na]$^+$, 414.1788; found, 414.1791. ESI$^+$/MS/MS [M + Na]$^+$ *m/z*: 314 (100).

*(S)-tert-Butyl (3-(4-Cyanophenyl)-1-(isoindolin-2-yl)-1-oxopropan-2-yl)carbamate ((S)-**9d**).* Gradient elution from *n*-hexane/EtOAc, 65:35, to *n*-hexane/EtOAc, 2:8. White solid, 76% yield. ^{1}H NMR ($CDCl_3$, 500 MHz) δ: 1.39 (s, 9H), 3.02 (dd, 1H, *J* = 6.3 and 13.2 Hz), 3.15 (dd, 1H, *J* = 7.8 and 13.2 Hz), 4.38 (d, 1H, *J* = 13.2 Hz), 4.66 (d, 1H, *J* = 15.7 Hz), 4.74−4.78 (m, 1H), 4.82 (d, 1H, *J* = 15.7 Hz), 4.95 (d, 1H, *J* = 13.2 Hz), 5.34 (br d, 1H, D_2O exchanged), 7.17−7.18 (app d, 1H), 7.27−7.31 (m, 3H), 7.35 (d, 2H, *J* = 8.32 Hz), 7.55 (d, 2H, *J* = 8.32 Hz). HRMS (ESI$^+$) calcd for [($C_{23}H_{25}N_3O_3$) + Na]$^+$, 414.1788; found, 414.1795. ESI$^+$/MS/MS [M + Na]$^+$ *m/z*: 314 (100).

*(R)-tert-Butyl (3-(4-Cyanophenyl)-1-(indolin-1-yl)-1-oxopropan-2-yl)carbamate ((R)-**9e**).* Eluted with *n*-hexane/EtOAc, 8:2. White solid, 50% yield. ^{1}H NMR ($CDCl_3$, 500 MHz) δ: 1.40 (s, 9H), 3.00−3.05 (m, 2H), 3.12−3.22 (m, 1H), 3.61−3.68 (m, 1H), 4.17−4.22 (m, 1H), 4.77−4.80 (m, 1H), 5.36−5.40 (m, 1H), 7.06 (t, 1H, *J* = 7.3 Hz), 7.17−7.22 (m, 2H), 7.34 (d, 2H, *J* = 7.8 Hz), 7.47 (br d, 1H, D_2O exchanged), 7.55 (d, 2H, *J* = 7.8 Hz), 8.17 (d, 1H, *J* = 7.8 Hz). HRMS (ESI$^+$) calcd for [($C_{23}H_{25}N_3O_3$) + Na]$^+$, 414.1788; found, 414.1792. ESI$^+$/MS/MS [M + Na]$^+$ *m/z*: 314 (100).

*(S)-tert-Butyl (3-(4-Cyanophenyl)-1-(indolin-1-yl)-1-oxopropan-2-yl)carbamate ((S)-**9e**).* Eluted with *n*-hexane/EtOAc, 8:2. White solid, 42% yield. ^{1}H NMR ($CDCl_3$, 500 MHz) δ: 1.40 (s, 9H), 3.00−3.05 (m, 2H), 3.12−3.22 (m, 1H), 3.61−3.68 (m, 1H), 4.17−4.22 (m, 1H), 4.77−4.80 (m, 1H), 5.36−5.40 (m, 1H), 7.06 (t, 1H, *J* = 7.3 Hz), 7.17−7.22 (m, 2H), 7.34 (d, 2H, *J* = 7.8 Hz), 7.47 (br d, 1H, D_2O exchanged), 7.55 (d, 2H, *J* = 7.8 Hz), 8.17 (d, 1H, *J* = 7.8 Hz). HRMS (ESI$^+$) calcd for [($C_{23}H_{25}N_3O_3$) + Na]$^+$, 414.1788; found, 414.1790. ESI$^+$/MS/MS [M + Na]$^+$ *m/z*: 314 (100).

*(R)-tert-Butyl (3-(4-Cyanophenyl)-1-(3,4-dihydroquinolin-1(2H)-yl)-1-oxopropan-2-yl)carbamate ((S)-**9g**).* Eluted with *n*-hexane/EtOAc, 8:2. Colorless oil, 13% yield. ^{1}H NMR ($CDCl_3$, 500 MHz) δ: 1.39 (s, 9H), 1.65−1.72 (m, 2H), 2.72−2.78 (m, 2H), 3.23−3.31 (m, 1H), 3.34−3.39 (m, 2H), 3.52−3.56 (m, 1H), 4.84 (app q, 1H), 5.26 (br d, 1H), 6.89−6.93 (m, 2H), 7.32−7.38 (m, 2H), 7.30 (d, 2H, *J* = 7.3 Hz), 7.58 (d, 2H, *J* = 7.3 Hz). HRMS (ESI$^+$) calcd for [($C_{24}H_{27}N_3O_3$) + Na]$^+$, 428.1945; found, 428.1965. ESI$^+$/MS/MS [M + Na]$^+$ *m/z*: 340 (100).

*(S)-tert-Butyl (3-(4-Cyanophenyl)-1-(3,4-dihydroquinolin-1(2H)-yl)-1-oxopropan-2-yl)carbamate ((S)-**9g**).* Eluted with *n*-hexane/EtOAc, 8:2. Colorless oil, 19% yield. ^{1}H NMR ($CDCl_3$, 500 MHz) δ: 1.39 (s, 9H), 1.65−1.72 (m, 2H), 2.72−2.78 (m, 2H), 3.23−3.31 (m, 1H), 3.34−3.39 (m, 2H), 3.52−3.56 (m, 1H), 4.84 (app q, 1H), 5.26 (br d, 1H), 6.89−6.93 (m, 2H), 7.32−7.38 (m, 2H), 7.30 (d, 2H, *J* = 7.3 Hz), 7.58 (d, 2H, *J* = 7.3 Hz). HRMS (ESI$^+$) calcd for [($C_{24}H_{27}N_3O_3$) + Na]$^+$, 428.1945; found, 428.1965. ESI$^+$/MS/MS [M + Na]$^+$ *m/z*: 340 (100).

*(R)-tert-Butyl (3-(4-Cyanophenyl)-1-(4,4-difluoropiperidin-1-yl)-1-oxopropan-2-yl)carbamate ((R)-**9h**).* Eluted in gradient from *n*-hexane/EtOAc, 8:2, to *n*-hexane/EtOAc, 1:1. White solid, 86% yield. ^{1}H NMR ($CDCl_3$, 500 MHz) δ: 1.39 (s, 9H), 1.58−1.65 (m, 1H), 1.86−1.91 (m, 3H), 2.96 (dd, 1H, *J* = 6.4 and 13.2 Hz), 3.09 (dd, 1H, *J* = 7.8 and 13.2 Hz), 3.25−3.29 (m, 1H), 3.43−3.49 (m, 1H), 3.58−3.61(m, 1H), 3.88−3.91 (m, 1H), 4.84 (app q, 1H), 5.26 (br d, 1H), 7.30 (d, 2H, *J* = 7.3 Hz), 7.58 (d, 2H, *J* = 7.3 Hz). HRMS (ESI$^+$) calcd for [($C_{20}H_{25}F_2N_3O_3$) + Na]$^+$, 416.1756; found, 416.1757. ESI$^+$/MS/MS [M + Na]$^+$ *m/z*: 340 (100).

*(S)-tert-Butyl (3-(4-Cyanophenyl)-1-(4,4-difluoropiperidin-1-yl)-1-oxopropan-2-yl)carbamate ((S)-**9h**).* Eluted with CH_2Cl_2/EtOAc, 8:2. White solid, 72% yield. ^{1}H NMR ($CDCl_3$, 500 MHz) δ: 1.39 (s, 9H), 1.58−1.65 (m, 1H), 1.86−1.91 (m, 3H), 2.96 (dd, 1H, *J* = 6.4 and 13.2 Hz), 3.09 (dd, 1H, *J* = 7.8 and 13.2 Hz), 3.25−3.29 (m, 1H), 3.43−3.49 (m, 1H), 3.58−3.61(m, 1H), 3.88−3.91 (m, 1H), 4.84 (app q, 1H), 5.26 (br d, 1H), 7.30 (d, 2H, *J* = 7.3 Hz), 7.58 (d, 2H, *J* = 7.3 Hz). HRMS (ESI$^+$) calcd for [($C_{20}H_{25}F_2N_3O_3$) + Na]$^+$, 416.1756; found, 416.1757. ESI$^+$/MS/MS [M + Na]$^+$ *m/z*: 340 (100).

*(R)-tert-Butyl (3-(4-Cyanophenyl)-1-(3,3-dimethylindolin-1-yl)-1-oxopropan-2-yl)carbamate ((R)-**9k**).* Gradient elution from *n*-hexane/EtOAc, 8:2, to *n*-hexane/EtOAc, 1:1. White solid, 49% yield. ^{1}H NMR ($CDCl_3$, 300 MHz) δ: 1.10 (s, 3H), 1.29 (s, 3H), 1.40 (s, 9H), 3.06 (dd, 1H, *J* = 6.4 and 12.8 Hz), 3.15−3.19 (m, 1H), 3.91 (d, 1H, *J* = 9.9 Hz), 5.38−5.41 (m, 1H), 5.40 (br s, 1H, NH), 7.02−7.12 (m, 2H), 7.19−7.25 (m, 2H), 7.33 (d, 2H, *J* = 8.2 Hz), 7.54 (d, 2H, *J* = 8.2 Hz), 8.14 (d, 1H, *J* = 8.2 Hz). HRMS (ESI$^+$) calcd for [($C_{25}H_{29}N_3O_3$) + Na]$^+$, 442.2101; found, 442.2104. ESI$^+$/MS/MS [M + Na]$^+$ *m/z*: 342 (100).

*(S)-tert-Butyl (3-(4-Cyanophenyl)-1-(3,3-dimethylindolin-1-yl)-1-oxopropan-2-yl)carbamate ((S)-**9k**).* Eluted with *n*-hexane/EtOAc, 8:2. White solid, 15% yield. ^{1}H NMR ($CDCl_3$, 300 MHz) δ: 1.10 (s, 3H), 1.29 (s, 3H), 1.40 (s, 9H), 3.06 (dd, 1H, *J* = 6.4 and 12.8 Hz), 3.15−3.19 (m, 1H), 3.91 (d, 1H, *J* = 9.9 Hz), 5.38−5.41 (m, 1H), 5.40 (br s, 1H, NH), 7.02−7.12 (m, 2H), 7.19−7.25 (m, 2H), 7.33 (d, 2H, *J* = 8.2 Hz), 7.54 (d, 2H, *J* = 8.2 Hz), 8.14 (d, 1H, *J* = 8.2 Hz). HRMS (ESI$^+$) calcd for [($C_{25}H_{29}N_3O_3$) + Na]$^+$, 442.2101; found, 442.2104. ESI$^+$/MS/MS [M + Na]$^+$ *m/z*: 342 (100).

*(R)-tert-Butyl (3-(4-Cyanophenyl)-1-(5-fluoroindolin-1-yl)-1-oxopropan-2-yl)carbamate ((R)-**9i**).* Gradient elution from *n*-hexane/EtOAc, 8:2, to *n*-hexane/EtOAc, 1:1. White solid, 63% yield. ^{1}H NMR ($CDCl_3$, 500 MHz) δ: 1.39 (s, 9H), 2.98−3.05 (m, 2H), 3.10−3.20 (m, 2H), 3.62−3.67 (m, 1H), 4.19−4.23 (m, 1H), 4.75−4.79 (m, 1H), 5.34 (br s, 1H), 6.87−6.91 (m, 2H), 7.33 (d, 2H, *J* = 7.8 Hz), 7.55 (d, 2H, *J* = 7.3 Hz), 8.13−8.15 (m, 1H). HRMS (ESI$^+$) calcd for [($C_{23}H_{24}FN_3O_3$) + Na]$^+$, 432.1694; found, 432.1690. ESI$^+$/MS/MS [M + Na]$^+$ *m/z*: 332 (100).

*(S)-tert-Butyl (3-(4-Cyanophenyl)-1-(5-fluoroindolin-1-yl)-1-oxopropan-2-yl)carbamate ((S)-**9i**).* Eluted with CH_2Cl_2/EtOAc, 8:2. White solid, 96% yield. ^{1}H NMR ($CDCl_3$, 500 MHz) δ: 1.39 (s, 9H), 2.98−3.05 (m, 2H), 3.10−3.20 (m, 2H), 3.62−3.67 (m, 1H), 4.19−4.23 (m, 1H), 4.75−4.79 (m, 1H), 5.34 (br s, 1H), 6.87−6.91 (m, 2H), 7.33 (d, 2H, *J* = 7.8 Hz), 7.55 (d, 2H, *J* = 7.3 Hz), 8.13−8.15 (m, 1H). HRMS (ESI$^+$) calcd for [($C_{23}H_{24}FN_3O_3$) + Na]$^+$, 432.1694; found, 432.1690. ESI$^+$/MS/MS [M + Na]$^+$ *m/z*: 332 (100).

*(R)-tert-Butyl (3-(4-Cyanophenyl)-1-(6-fluoroindolin-1-yl)-1-oxopropan-2-yl)carbamate ((R)-**9l**).* Gradient elution from *n*-hexane/EtOAc, 7:3, to *n*-hexane/EtOAc, 3:7. Yellow solid, 32% yield. ^{1}H NMR ($CDCl_3$, 300 MHz) δ: 1.39 (s, 9H), 2.89−3.20 (m, 4H), 3.58−3.68 (m, 1H), 4.21−4.28 (m, 1H), 4.72−4.77 (m, 1H), 5.36 (br d, 1H), 6.71−6.77 (m, 1H), 7.05−7.10 (m, 1H), 7.53 (d, 2H, *J* = 8.2 Hz), 7.56 (d, 2H, *J* = 8.2 Hz), 7.91−7.95 (dd, 1H, *J* = 2.3 and 10.5 Hz). HRMS (ESI$^+$) calcd for [($C_{23}H_{24}FN_3O_3$) + Na]$^+$, 432.1694; found, 432.1693. ESI$^+$/MS/MS [M + Na]$^+$ *m/z*: 332 (100).

https://doi.org/10.1021/acs.jmedchem.1c02203
J. Med. Chem. XXXX, XXX, XXX−XXX

*(S)-tert-Butyl (3-(4-Cyanophenyl)-1-(6-fluoroindolin-1-yl)-1-oxopropan-2-yl)carbamate ((S)-**9l**).* Eluted with *n*-hexane/EtOAc, 1:1. Yellow solid, 37% yield. ^{1}H NMR ($CDCl_3$, 300 MHz) δ: 1.39 (s, 9H), 2.89−3.20 (m, 4H), 3.58−3.68 (m, 1H), 4.21−4.28 (m, 1H), 4.72−4.77 (m, 1H), 5.36 (br d, 1H), 6.71−6.77 (m, 1H), 7.05−7.10 (m, 1H), 7.53 (d, 2H, J = 8.2 Hz), 7.56 (d, 2H, J = 8.2 Hz), 7.91−7.95 (dd, 1H, J = 2.3 and 10.5 Hz). HRMS (ESI$^+$) calcd for $[(C_{23}H_{24}FN_3O_3) + Na]^+$, 432.1694; found, 432.1693. ESI$^+$/MS/MS $[M + Na]^+$ *m/z*: 332 (100).

*(R)-tert-Butyl (3-(4-Cyanophenyl)-1-(2,3-dihydro-1H-pyrrolo[2,3-b]pyridin-1-yl)-1-oxopropan-2-yl)carbamate ((R)-**9m**).* Eluted with *n*-hexane/EtOAc, 6:4. White solid, 69% yield. ^{1}H NMR ($CDCl_3$, 300 MHz) δ: 1.31 (s, 9H), 2.73−2.80 (m, 1H), 3.07−3.19 (m, 2H), 3.33−3.37 (m, 1H), 4.00−4.10 (m, 1H), 4.12−4.24 (m, 1H), 5.40−5.43 (m, 1H), 6.26−6.29 (br t, 1H), 6.93−6.97 (m, 1H), 7.46 (d, 2H, J = 7.9 Hz), 7.49−7.52 (m, 1H), 7.56 (d, 2H, J = 7.9 Hz), 8.21 (d, 1H, J = 5.3 Hz). HRMS (ESI$^+$) calcd for $[(C_{22}H_{24}N_4O_3) + Na]^+$, 415.1741; found, 415.1741. ESI$^+$/MS/MS $[M + Na]^+$ *m/z*: 315 (60), 199 (100).

*(S)-tert-Butyl (3-(4-Cyanophenyl)-1-(2,3-dihydro-1H-pyrrolo[2,3-b]pyridin-1-yl)-1-oxopropan-2-yl)carbamate ((S)-**9m**).* Eluted with *n*-hexane/EtOAc, 1:1. White solid, 67% yield. ^{1}H NMR ($CDCl_3$, 300 MHz) δ: 1.31 (s, 9H), 2.73−2.80 (m, 1H), 3.07−3.19 (m, 2H), 3.33−3.37 (m, 1H), 4.00−4.10 (m, 1H), 4.12−4.24 (m, 1H), 5.40−5.43 (m, 1H), 6.26−6.29 (br t, 1H), 6.93−6.97 (m, 1H), 7.46 (d, 2H, J = 7.9 Hz), 7.49−7.52 (m, 1H), 7.56 (d, 2H, J = 7.9 Hz), 8.21 (d, 1H, J = 5.3 Hz). HRMS (ESI$^+$) calcd for $[(C_{22}H_{24}N_4O_3) + Na]^+$, 415.1741; found, 415.1741. ESI$^+$/MS/MS $[M + Na]^+$ *m/z*: 315 (60), 199 (100).

General Procedure for the Synthesis of Amino Derivatives (*R*)- and (*S*)-10a−c,f. A mixture of Boc-protected derivative (*R*)- or (*S*)-**9a−c,g** (0.36 mmol), 1,4-dioxane (7 mL), and 3 N HCl (3.5 mL) was stirred overnight at room temperature. Then, the solvent was removed under pressure, and the aqueous solution was alkalinized with 5% NaOH to pH 12 and extracted with EtOAc (3 × 20 mL). The combined organic layers were dried over Na_2SO_4, filtered, and concentrated under reduced pressure to obtain the desired pure compounds.

*(2R)-2-Amino-3-(4-cyanophenyl)-N-(2-oxoazepan-3-yl)-propanamide ((2R)-**10a**).* Yellow solid, 58% yield. ^{1}H NMR ($CDCl_3$, 300 MHz) δ: 1.38−1.53 (m, 2H), 1.81 (br s, 2H, D_2O exchanged), 1.87−2.09 (m, 4H), 2.81−2.91 (m, 1H), 3.19−3.29 (m, H), 3.63−3.72 (m, 1H), 4.46−4.50 (m, 1H), 6.11−6.18 (m, 1H), 7.34 (d, 2H, J = 8.2 Hz), 7.59 (d, 2H, J = 8.2 Hz), 8.07−8.15 (m, 1H). HRMS (ESI$^+$) calcd for $[(C_{16}H_{20}N_4O_2) + Na]^+$, 323.1478; found, 323.1482. ESI$^+$/MS/MS $[M + Na]^+$ *m/z*: 207 (100), 151 (60).

*(2S)-2-Amino-3-(4-cyanophenyl)-N-(2-oxoazepan-3-yl)-propanamide ((2S)-**10a**).* Colorless oil, 69% yield. ^{1}H NMR ($CDCl_3$, 300 MHz) δ: 1.38−1.53 (m, 2H), 1.81 (br s, 2H, D_2O exchanged), 1.87−2.09 (m, 4H), 2.81−2.91 (m, 1H), 3.19−3.29 (m, H), 3.63−3.72 (m, 1H), 4.46−4.50 (m, 1H), 6.11−6.18 (m, 1H), 7.34 (d, 2H, J = 8.2 Hz), 7.59 (d, 2H, J = 8.2 Hz), 8.07−8.15 (m, 1H). HRMS (ESI$^+$) calcd for $[(C_{16}H_{20}N_4O_2) + Na]^+$, 323.1478; found, 323.1480. ESI$^+$/MS/MS $[M + Na]^+$ *m/z*: 207 (100), 151 (60).

*(R)-4-(2-Amino-3-oxo-3-(piperidin-1-yl)propyl)benzonitrile ((R)-**10b**).* Yellow oil, quantitative yield. ^{1}H NMR ($CDCl_3$, 500 MHz) δ: 1.19−1.25 (m, 1H), 1.42−1.58 (m, 5H), 1.91 (br s, 2H, D_2O exchanged), 2.93 (dd, 1H, J = 5.9 and 13.2 Hz), 3.06 (dd, 1H, J = 7.3 and 13.2 Hz), 3.13−3.18 (m, 1H), 3.31−3.36 (m, 1H), 3.43−3.48 (m, 1H), 3.52−3.57 (m, 1H), 4.83−4.88 (m, 1H), 7.30 (d, 2H, J = 8.3 Hz), 7.57 (d, 2H, J = 8.3 Hz). HRMS (ESI$^+$) calcd for $[(C_{15}H_{19}N_3O) + H]^+$, 258.1606; found, 258.1599. ESI$^+$/MS/MS $[M + H]^+$ *m/z*: 145 (80), 128 (100).

*(S)-4-(2-Amino-3-oxo-3-(piperidin-1-yl)propyl)benzonitrile ((S)-**10b**).* Yellow oil, 90% yield. ^{1}H NMR ($CDCl_3$, 500 MHz) δ: 1.19−1.25 (m, 1H), 1.42−1.58 (m, 5H), 1.91 (br s, 2H, D_2O exchanged), 2.93 (dd, 1H, J = 5.9 and 13.2 Hz), 3.06 (dd, 1H, J = 7.3 and 13.2 Hz), 3.13−3.18 (m, 1H), 3.31−3.36 (m, 1H), 3.43−3.48 (m, 1H), 3.52−3.57 (m, 1H), 4.83−4.88 (m, 1H), 7.30 (d, 2H, J = 8.3 Hz), 7.57 (d, 2H, J = 8.3 Hz). HRMS (ESI$^+$) calcd for $[(C_{15}H_{19}N_3O) + H]^+$, 258.1606; found, 258.1589. ESI$^+$/MS/MS $[M + H]^+$ *m/z*: 145 (75), 128 (100).

*(R)-4-(2-Amino-3-oxo-3-(pyrrolidin-1-yl)propyl)benzonitrile ((R)-**10c**).* Yellow oil, 85% yield. ^{1}H NMR ($CDCl_3$, 300 MHz) δ: 1.70−1.88 (m, 4H), 1.91 (br s, 2H, D_2O exchanged), 2.83−2.93 (m, 2H), 3.01 (dd, 1H, J = 7.0 and 13.5), 3.31−3.51 (m, 3H), 3.71−3.76 (m, 1H), 7.32 (d, 2H, J = 8.2 Hz), 7.57 (d, 2H, J = 8.2 Hz). HRMS (ESI$^+$) calcd for $[(C_{14}H_{17}N_3O) + H]^+$, 244.1450; found, 244.1440. ESI$^+$/MS/MS $[M + Na]^+$ *m/z*: 145 (65), 128 (100).

*(S)-4-(2-Amino-3-oxo-3-(pyrrolidin-1-yl)propyl)benzonitrile ((S)-**10c**).* Yellow oil, quantitative yield. ^{1}H NMR ($CDCl_3$, 300 MHz) δ: 1.70−1.88 (m, 4H), 1.91 (br s, 2H, D_2O exchanged), 2.83−2.93 (m, 2H), 3.01 (dd, 1H, J = 7.0 and 13.5), 3.31−3.51 (m, 3H), 3.71−3.76 (m, 1H), 7.32 (d, 2H, J = 8.2 Hz), 7.57 (d, 2H, J = 8.2 Hz). ESI$^+$/MS *m/z*: 244 $[M + H]^+$. ESI$^+$/MS/MS *m/z*: 145 (60), 128 (100), 72 (73). HRMS (ESI$^+$) calcd for $[(C_{14}H_{17}N_3O) + H]^+$, 244.1450; found, 244.1442. ESI$^+$/MS/MS $[M + Na]^+$ *m/z*: 145 (60), 128 (100).

*(R)-4-(2-Amino-3-(3,4-dihydroisoquinolin-2(1H)-yl)-3-oxopropyl)benzonitrile ((R)-**10f**).* White solid, 84% yield. ^{1}H NMR ($CDCl_3$, 300 MHz) δ: 2.03 (br s, 2H, D_2O exchanged), 2.50−2.75 (m, 1H), 2.75−2.89 (m, 1H), 2.83−3.01 (m, 2H), 3.35−3.50 (m, 1H), 3.58−3.73 (m, 1H), 4.07−4.18 (m, 2H), 4.82−4.95 (m, 1H), 6.82−6.84 (m, 1H), 7.07−7.23 (m, 2H), 7.30−7.48 (m, 3H), 7.51 (d, 2H, J = 7.6 Hz). HRMS (ESI$^+$) calcd for $[(C_{19}H_{19}N_3O) + Na]^+$, 328.1420; found, 328.1421. ESI$^+$/MS/MS $[M + Na]^+$ *m/z*: 138 (68), 109 (100).

*(S)-4-(2-Amino-3-(3,4-dihydroisoquinolin-2(1H)-yl)-3-oxopropyl)benzonitrile ((S)-**10f**).* Colorless oil, 92% yield. ^{1}H NMR ($CDCl_3$, 300 MHz) δ: 2.03 (br s, 2H, D_2O exchanged), 2.50−2.75 (m, 1H), 2.75−2.89 (m, 1H), 2.83−3.01 (m, 2H), 3.35−3.50 (m, 1H), 3.58−3.73 (m, 1H), 4.07−4.18 (m, 2H), 4.82−4.95 (m, 1H), 6.82−6.84 (m, 1H), 7.07−7.23 (m, 2H), 7.30−7.48 (m, 3H), 7.51 (d, 2H, J = 7.6 Hz). HRMS (ESI$^+$) calcd for $[(C_{19}H_{19}N_3O) + Na]^+$, 328.1420; found, 328.1425. ESI$^+$/MS/MS $[M + Na]^+$ *m/z*: 138 (80), 109 (100).

General Procedure for the Synthesis of Amines (*R*)- and (*S*)-10d,e,g−−o. Trifluoroacetic acid (1.60 mL) was added to a solution of Boc-protected derivative (*R*)- or (*S*)-**9d,f,g−o** (0.628 mmol) in CH_2Cl_2. The reaction mixture was stirred at room temperature for 5 h and then alkalinized with aqueous 5% NaOH to pH 12. The separated aqueous phase was extracted with CH_2Cl_2 (3 × 20 mL). The combined organic layers were dried over Na_2SO_4, filtered, and concentrated under reduced pressure to obtain the desired pure compound.

*(R)-4-(2-Amino-3-(isoindolin-2-yl)-3-oxopropyl)benzonitrile ((R)-**10d**).* White solid, quantitative yield. ^{1}H NMR ($CDCl_3$, 500 MHz) δ: 2.04 (br s, 2H, D_2O exchanged), 3.03 (dd, 1H, J = 6.4 and 13.2 Hz), 3.16 (dd, 1H, J = 7.8 and 13.2 Hz), 4.38 (d, 1H, J = 13.2 Hz), 4.66 (d, 1H, J = 15.6 Hz), 4.74−4.79 (m, 1H), 4.82 (d, 1H, J = 15.6 Hz), 4.95 (d, 1H, J = 13.2 Hz), 7.17−7.18 (app d, 1H), 7.27−7.31 (m, 3H), 7.35 (d, 2H, J = 8.3 Hz), 7.55 (d, 2H, J = 8.3 Hz). HRMS (ESI$^+$) calcd for $[(C_{18}H_{17}N_3O) + H]^+$, 292,1450; found, 292.1442. ESI$^+$/MS/MS $[M + H]^+$ *m/z*: 237 (100).

*(S)-4-(2Amino-3-(isoindolin-2-yl)-3-oxopropyl)benzonitrile ((S)-**10d**).* White solid, 80% yield. ^{1}H NMR ($CDCl_3$, 500 MHz) δ: 2.02 (br s, 2H, D_2O exchanged), 3.03 (dd, 1H, J = 6.4 and 13.2 Hz), 3.16 (dd, 1H, J = 7.8 and 13.2 Hz), 4.38 (d, 1H, J = 13.2 Hz), 4.66 (d, 1H, J = 15.6 Hz), 4.74−4.79 (m, 1H), 4.82 (d, 1H, J = 15.6 Hz), 4.95 (d, 1H, J = 13.2 Hz), 7.17−7.18 (app d, 1H), 7.27−7.31 (m, 3H), 7.35 (d, 2H, J = 8.3 Hz), 7.55 (d, 2H, J = 8.3 Hz). HRMS (ESI$^+$) calcd for $[(C_{18}H_{17}N_3O) + Na]^+$, 314.1264; found, 314.1263. ESI$^+$/MS/MS $[M + Na]^+$ *m/z*: 91 (100).

*(R)-4-(2-Amino-3-(indolin-1-yl)-3-oxopropyl)benzonitrile ((R)-**10e**).* White solid, 32% yield. ^{1}H NMR ($CDCl_3$, 500 MHz) δ: 1.98 (br s, 2H, D_2O exchanged), 2.95−3.02 (m, 2H), 3.08−3.18 (m, 2H), 3.60−3.65 (m, 1H), 3.91 (br t, 1H), 4.08−4.14 (m, 1H), 7.05 (t, 1H, J = 4.0 Hz), 7.16−7.22 (m, 2H), 7.36 (d, 2H, J = 7.8 Hz), 7.56 (d, 2H, J = 7.8 Hz), 8.22 (d, 1H, J = 7.8 Hz). HRMS (ESI$^+$) calcd for $[(C_{18}H_{17}N_3O) + H]^+$, 291.1372: found, 292.1445. ESI$^+$/MS/MS $[M + H]^+$ *m/z*: 237 (100).

*(S)-4-(2-Amino-3-(indolin-1-yl)-3-oxopropyl)benzonitrile ((S)-**10e**).* White solid, 38% yield. ^{1}H NMR ($CDCl_3$, 500 MHz) δ: 2.08 (br s, 2H, D_2O exchanged), 2.93−3.04 (m, 2H), 3.07−3.19 (m, 2H), 3.58−3.67 (m, 1H), 3.92 (br t, 1H), 4.07−4.16 (m, 1H), 7.02−7.07 (m, 1H), 7.16−7.23 (m, 2H), 7.35 (d, 2H, J = 8.2 Hz), 7.56 (d, 2H, J = 8.2 Hz), 8.22 (d, 1H, J = 8.2 Hz). HRMS (ESI$^+$) calcd for $[(C_{18}H_{17}N_3O) + H]^+$, 291.1372; found, 292.1442. ESI$^+$/MS/MS $[M + H]^+$ *m/z*: 237 (100).

https://doi.org/10.1021/acs.jmedchem.1c02203
J. Med. Chem. XXXX, XXX, XXX−XXX

*(R)-4-(2-Amino-3-(3,4-dihydroquinolin-1(2H)-yl)-3-oxopropyl)-benzonitrile ((R)-**10g**).* Yellow oil, 70% yield. ^{1}H NMR ($CDCl_3$, 300 MHz): 1.67 (br s, 2H, D_2O exchanged), 1.72−1.78 (m, 2H), 2.73−2.78 (m, 2H), 3.24−3.32 (m, 2H), 3.38−3.51 (m, 1H), 3.58−3.64 (m, 1H), 3.95−4.07 (m, 1H), 6.93 (dd, 2H, J = 2.3 and 7.4 Hz), 7.28−7.32 (m, 1H), 7.38 (t, 1H, J = 7.4 Hz), 7.40 (d, 2H, J = 8.20 Hz), 7.53 (d, 2H, J = 8.20 Hz). HRMS (ESI$^+$) calcd for $[(C_{19}H_{19}N_3O) + H]^+$, 306.1601; found, 306.1597. ESI$^+$/MS/MS $[M + H]^+$ m/z: 134 (100), 106 (40).

*(S)-4-(2-Amino-3-(3,4-dihydroquinolin-1(2H)-yl)-3-oxopropyl)-benzonitrile ((S)-**10g**).* Yellow oil, 36% yield. ^{1}H NMR ($CDCl_3$, 300 MHz) δ: 1.67 (br s, 2H, D_2O exchanged), 1.72−1.78 (m, 2H), 2.73−2.78 (m, 2H), 3.24−3.32 (m, 2H), 3.38−3.51 (m, 1H), 3.58−3.64 (m, 1H), 3.95−4.07 (m, 1H), 6.93 (dd, 2H, J = 2.3 and 7.4 Hz), 7.28−7.32 (m, 1H), 7.38 (t, 1H, J = 7.4 Hz), 7.40 (d, 2H, J = 8.20 Hz), 7.53 (d, 2H, J = 8.20 Hz). HRMS (ESI$^+$) calcd for $[(C_{19}H_{19}N_3O) + H]^+$, 306.1601; found, 306.1597. ESI$^+$/MS/MS $[M + H]^+$ m/z: 134 (100), 106 (40).

*(R)-4-(2-Amino-3-(4,4-difluoropiperidin-1-yl)-3-oxopropyl)-benzonitrile ((R)-**10h**).* Yellow oil, 84% yield. ^{1}H NMR ($CDCl_3$, 500 MHz) δ: 1.60 (br s, 2H, D_2O exchanged), 1.85−1.96 (m, 4H), 2.85 (dd, 1H, J = 7.3 and 13.7 Hz), 3.05 (dd, 1H, J = 6.9 and 13.7 Hz), 3.32−3.39 (m, 1H), 3.52−3.59 (m, 2H), 3.79−3.84 (m, 1H), 3.83 (t, 1H, J = 6.8 Hz), 7. 31 (d, 2H, J = 7.8 Hz), 7.59 (d, 2H, J = 7.8 Hz). HRMS (ESI$^+$) calcd for $[(C_{15}H_{17}F_2N_3O) + H]^+$, 294.1412; found, 294.1411. ESI$^+$/MS/MS $[M + H]^+$ m/z: 145 (100).

*(S)-4-(2-Amino-3-(4,4-difluoropiperidin-1-yl)-3-oxopropyl)-benzonitrile ((S)-**10h**).* Yellow oil, 68% yield. ^{1}H NMR ($CDCl_3$, 500 MHz) δ: 1.60 (br s, 2H, D_2O exchanged), 1.85−1.96 (m, 4H), 2.85 (dd, 1H, J = 7.3 and 13.7 Hz), 3.05 (dd, 1H, J = 6.9 and 13.7 Hz), 3.32−3.39 (m, 1H), 3.52−3.59 (m, 2H), 3.79−3.84 (m, 1H), 3.83 (t, 1H, J = 6.8 Hz), 7.31 (d, 2H, J = 7.8 Hz), 7.59 (d, 2H, J = 7.8 Hz). HRMS (ESI$^+$) calcd for $[(C_{15}H_{17}F_2N_3O) + H]^+$, 294.1412; found, 294.1411. ESI$^+$/MS/MS $[M + H]^+$ m/z: 145 (100).

*(R)-4-(2-Amino-3-(5-fluoroisoindolin-2-yl)-3-oxopropyl)-benzonitrile ((R)-**10j**).* Yellow solid, 62% yield. ^{1}H NMR ($CDCl_3$, 500 MHz) δ: 1.65 (br s, 2H, D_2O exchanged), 2.90 (dd, 1H, J = 7.3 and 12.7 Hz), 3.09 (dd, 1H, J = 6.4 and 13.2 Hz), 3.79−3.82 (m, 1H), 4.35−4.41 (m, 1H), 4.65−4.70 (m, 1H), 4.72−4.90 (m, 2H), 6.90−7.02 (m, 1H), 7.12−7.15 (m, 1H), 7.21−7.24 (m, 1H), 7.36 (d, 2H, J = 7.4 Hz), 7.57 (d, 2H, J = 8.3 Hz). (ESI$^+$) calcd for $[(C_{18}H_{16}FN_3O) + Na]^+$, 332.1170; found, 332.1167. ESI$^+$/MS/MS $[M + Na]^+$ m/z: 206 (50), 81 (100).

*(S)-4-(2-Amino-3-(5-fluoroisoindolin-2-yl)-3-oxopropyl)-benzonitrile ((S)-**10j**).* Yellow solid, quantitative yield. ^{1}H NMR ($CDCl_3$, 500 MHz) δ: 1.65 (br s, 2H, D_2O exchanged), 2.90 (dd, 1H, J = 7.3 and 12.7 Hz), 3.09 (dd, 1H, J = 6.4 and 13.2 Hz), 3.79−3.82 (m, 1H), 4.35−4.41 (m, 1H), 4.65−4.70 (m, 1H), 4.72−4.90 (m, 2H), 6.90−7.02 (m, 1H), 7.12−7.15 (m, 1H), 7.21−7.24 (m, 1H), 7.36 (d, 2H, J = 7.4 Hz), 7.57 (d, 2H, J = 8.3 Hz). HRMS (ESI$^+$) calcd for $[(C_{18}H_{16}FN_3O) + Na]^+$, 332.1170; found, 332.1167. ESI$^+$/MS/MS $[M + Na]^+$ m/z: 206 (50), 81 (100).

*(R)-4-(2-Amino-3-(3,3-dimethylindolin-1-yl)-3-oxopropyl)-benzonitrile ((R)-**10k**).* White solid, 84% yield. ^{1}H NMR ($CDCl_3$, 300 MHz) δ: 1.14 (s, 3H), 1.31 (s, 3H), 1.72 (br s, 2H, D_2O exchanged), 2.93 (dd, 1H, J = 7.0 and 13.5 Hz), 3.11 (dd, 1H, J = 7.0 and 13.5 Hz), 3.33−3.36 (m, 1H), 3.79−3.86 (m, 2H), 7.06−7.13 (m, 2H), 7.20−7.24 (m, 1H), 7.35 (d, 2H, J = 8.2 Hz), 7.57 (d, 2H, J = 8.2 Hz), 8.21 (d, 1H, J = 7.6 Hz). HRMS (ESI$^+$) calcd for $[(C_{20}H_{21}N_3O) + H]^+$, 320.1757; found, 320.1756. ESI$^+$/MS/MS $[M + H]^+$ m/z: 148 (100), 128 (400).

*(S)-4-(2-Amino-3-(3,3-dimethylindolin-1-yl)-3-oxopropyl)-benzonitrile ((S)-**10k**).* Yellow solid, 78% yield. ^{1}H NMR ($CDCl_3$, 300 MHz) δ: 1.14 (s, 3H), 1.32 (s, 3H), 1.65 (br s, 2H, D_2O exchanged), 2.93 (dd, 1H, J = 6.9 and 13.2 Hz), 3.12 (dd, 1H, J = 6.9 and 13.2 Hz), 3.35 (d, 1H, J = 9.3 Hz), 3.81−3.85 (m, 2H), 7.07−7.13 (m, 2H), 7.21−7.24 (m, 1H), 7.35 (d, 2H, J = 8.2 Hz), 7.57 (d, 2H, J = 8.2 Hz), 8.21 (d, 1H, J = 7.6 Hz). ESI$^+$/MS m/z: 320 $[M + H]^+$. ESI$^+$/MS/MS m/z: 148 (100), 145 (88), 128 (47). HRMS (ESI$^+$) calcd for $[(C_{20}H_{21}N_3O) + H]^+$, 320.1757; found, 320.1756. ESI$^+$/MS/MS $[M + H]^+$ m/z: 148 (100), 128 (40).

*(R)-4-(2-Amino-3-(5-fluoroindolin-1-yl)-3-oxopropyl)benzonitrile ((R)-**10i**).* Yellow solid, quantitative yield. ^{1}H NMR ($CDCl_3$, 500 MHz) δ: 1.90 (br s, 2H, D_2O exchanged), 2.92 (dd, 1H, J = 6.8 and 13.2 Hz), 2.99−3.05 (m, 1H), 3.11−3.17 (m, 2H), 3.66−3.71 (m, 1H), 3.88 (br t, 1H), 4.10−4.15 (m, 1H), 7.04 (t, 1H, J = 7.3 Hz), 7.17−7.25 (m, 1H), 7.35 (d, 2H, J = 8.3 Hz), 7.57 (d, 2H, J = 8.3 Hz), 8.22 (d, 1H, J = 7.8 Hz). HRMS (ESI$^+$) calcd for $[(C_{18}H_{16}FN_3O) + H]^+$, 310.1350; found, 310.1348. ESI$^+$/MS/MS $[M + H]^+$ m/z: 145 (100).

*(S)-4-(2-Amino-3-(5-fluoroindolin-1-yl)-3-oxopropyl)benzonitrile ((S)-**10i**).* White solid, quantitative yield. ^{1}H NMR ($CDCl_3$, 500 MHz) δ: 1.90 (br s, 2H, D_2O exchanged), 2.92 (dd, 1H, J = 6.8 and 13.2 Hz), 2.99−3.05 (m, 1H), 3.11−3.17 (m, 2H), 3.66−3.71 (m, 1H), 3.88 (br t, 1H), 4.10−4.15 (m, 1H), 7.04 (t, 1H, J = 7.3 Hz), 7.17−7.25 (m, 1H), 7.35 (d, 2H, J = 8.3 Hz), 7.57 (d, 2H, J = 8.3 Hz), 8.22 (d, 1H, J = 7.8 Hz). HRMS (ESI$^+$) calcd for $[(C_{18}H_{16}FN_3O) + H]^+$, 310.1350; found, 310.1348. ESI$^+$/MS/MS $[M + H]^+$ m/z: 145 (100).

*(R)-4-(2-Amino-3-(6-fluoroindolin-1-yl)-3-oxopropyl)benzonitrile ((R)-**10l**).* White solid, 49% yield. ^{1}H NMR ($CDCl_3$, 300 MHz) δ: 1.69 (br s, 2H, D_2O exchanged), 2.86−3.16 (m, 4H), 3.68−3.84 (m, 2H), 4.12−4.21 (m, 1H), 6.73 (td, 1H, J = 2.34 and 8.70 Hz), 7.05−7.10 (m, 1H), 7.34 (d, 2H, J = 8.2 Hz), 7.57 (d, 2H, J = 8.2 Hz), 8.00 (dd, 1H, J = 2.3 and 10.5 Hz). HRMS (ESI$^+$) calcd for $[(C_{18}H_{16}FN_3O) + H]^+$, 310.1350; found, 310.1345. ESI$^+$/MS/MS $[M + H]^+$ m/z: 148 (100), 128 (400).

*(S)-4-(2-Amino-3-(6-fluoroindolin-1-yl)-3-oxopropyl)benzonitrile ((S)-**10l**).* White solid, 97% yield. ^{1}H NMR ($CDCl_3$, 300 MHz) δ: 1.69 (br s, 2H, D_2O exchanged), 2.86−3.16 (m, 4H), 3.68−3.84 (m, 2H), 4.12−4.21 (m, 1H), 6.73 (td, 1H, J = 2.34 and 8.70 Hz), 7.05−7.10 (m, 1H), 7.34 (d, 2H, J = 8.2 Hz), 7.57 (d, 2H, J = 8.2 Hz), 8.00 (dd, 1H, J = 2.3 and 10.5 Hz). HRMS (ESI$^+$) calcd for $[(C_{18}H_{16}FN_3O) + H]^+$, 310.1350; found, 310.1345. ESI$^+$/MS/MS $[M + H]^+$ m/z: 148 (100), 128 (40).

*(R)-4-(2-Amino-3-(2,3-dihydro-1H-pyrrolo[2,3-b]pyridin-1-yl)-3-oxopropyl)benzonitrile ((R)-**10m**).* White solid, 18% yield. ^{1}H NMR ($CDCl_3$, 300 MHz) δ: 1.68 (br s, 2H, D_2O exchanged), 2.68−2.76 (m, 1H), 3.08 (app t, 2H), 3.26 (dd, 1H, J = 4.7 and 13.5 Hz), 4.03−4.16 (m, 2H), 5.20−5.25 (m, 1H), 6.92 (dd, 1H, J = 5.3 and 7.6 Hz), 7.37−7.48 (m, 3H), 7.57 (d, 2H, J = 8.2 Hz), 8.15 (d, 1H, J = 4.7 Hz). HRMS (ESI$^+$) calcd for $[(C_{17}H_{16}N_4O) + H]^+$, 293.1397; found, 293.1393. ESI$^+$/MS/MS $[M + H]^+$ m/z: 121 (100).

*(S)-4-(2-Amino-3-(2,3-dihydro-1H-pyrrolo[2,3-b]pyridin-1-yl)-3-oxopropyl)benzonitrile ((S)-**10m**).* White solid, 28% yield. ^{1}H NMR ($CDCl_3$, 300 MHz) δ: 1.68 (br s, 2H, D_2O exchanged), 2.68−2.76 (m, 1H), 3.08 (app t, 2H), 3.26 (dd, 1H, J = 4.7 and 13.5 Hz), 4.03−4.16 (m, 2H), 5.20−5.25 (m, 1H), 6.92 (dd, 1H, J = 5.3 and 7.6 Hz), 7.37−7.48 (m, 3H), 7.57 (d, 2H, J = 8.2 Hz), 8.15 (d, 1H, J = 4.7 Hz). HRMS (ESI$^+$) calcd for $[(C_{17}H_{16}N_4O) + H]^+$, 293.1397; found, 293.1393. ESI$^+$/MS/MS $[M + H]^+$ m/z: 121 (100).

*(R)-4-(2-Amino-3-(7-fluoro-3,4-dihydroisoquinolin-2(1H)-yl)-3-oxopropyl)benzonitrile ((R)-**10n**).* Yellow oil, 60% yield. ^{1}H NMR ($CDCl_3$, 300 MHz) δ: 1.67 (br s, 2H, D_2O exchanged), 2.47−2.54 (m, 1H), 2.70−2.90 (m, 1H), 2.92−2.98 (m, 1H), 3.05 (dd, 1H, J = 6.44 and 1.2 Hz), 3.35−3.51 (m, 2H), 3.58−3.64 (m, 1H), 3.95−4.07 (m, 2H), 6.83−6.89 (m, 2H), 7.02−7.07 (m, 1H), 7.23−7.29 (m, 1H), 7.31 (d, 1H, J = 8.2 Hz), 7.41 (d, 1H, J = 8.2 Hz), 7.53 (d, 1H, J = 8.2 Hz). HRMS (ESI$^+$) calcd for $[(C_{19}H_{18}FN_3O) + H]^+$, 324.1507; found, 324.1505. ESI$^+$/MS/MS $[M + H]^+$ m/z: 145 (100), 128 (40).

*(S)-4-(2-Amino-3-(7-fluoro-3,4-dihydroisoquinolin-2(1H)-yl)-3-oxopropyl)benzonitrile ((S)-**10n**).* Yellow oil, 83% yield. ^{1}H NMR ($CDCl_3$, 300 MHz) δ: 1.67 (br s, 2H, D_2O exchanged), 2.47−2.54 (m, 1H), 2.70−2.90 (m, 1H), 2.92−2.98 (m, 1H), 3.05 (dd, 1H, J = 6.44 and 1.2 Hz), 3.35−3.51 (m, 2H), 3.58−3.64 (m, 1H), 3.95−4.07 (m, 2H), 6.83−6.89 (m, 2H), 7.02−7.07 (m, 1H), 7.23−7.29 (m, 1H), 7.31 (d, 1H, J = 8.2 Hz), 7.41 (d, 1H, J = 8.2 Hz), 7.53 (d, 1H, J = 8.2 Hz). HRMS (ESI$^+$) calcd for $[(C_{19}H_{18}FN_3O) + H]^+$, 324.1507; found, 324.1505. ESI$^+$/MS/MS $[M + H]^+$ m/z: 145 (100), 128 (40).

*(S)-4-(2-Amino-3-(7-fluoro-4,4-dimethyl-3,4-dihydroisoquinolin-2(1H)-yl)-3-oxopropyl)benzonitrile ((S)-**10o**).* Yellow oil, 68% yield. ^{1}H NMR ($CDCl_3$, 300 MHz) δ: 1.40 (s, 6H), 1.67 (br s, 2H, D_2O exchanged), 3.19−3.23 (m, 1H), 3.38−3.45 (m, 3H), 3.92−4.02 (m, 2H), 4.47 (s, 1H), 6.62−6.69 (m, 1H), 6.92−6.97 (m, 1H), 7.28−7.32 (m, 1H), 7.30 (d, 2H, J = 8.20 Hz), 7.40 (d, 1H, J = 8.20 Hz). HRMS (ESI$^+$) calcd for $[(C_{21}H_{22}FN_3O) + H]^+$, 352.1820; found, 352.1803. ESI$^+$/MS/MS $[M + H]^+$ m/z: 180 (80), 145 (100).

https://doi.org/10.1021/acs.jmedchem.1c02203
J. Med. Chem. XXXX, XXX, XXX−XXX

General Procedure for the Synthesis of the Target Compounds (*R*)- and (*S*)-11a−o. A solution of the appropriate amine (*R*)- and (*S*)-**10a−o** (0.28 mmol) and *F*-phenylisocyanate (0.31 mmol) was stirred overnight at room temperature. Next, the reaction mixture was concentrated in vacuo, and the crude residue was purified on silica gel column as detailed below to obtain the pure target compounds.

*(2R)-3-(4-Cyanophenyl)-2-(3-(4-fluorophenyl)ureido)-N-(2-oxoazepan-3-yl)propenamide ((2R)-**11a**).* Eluted with $CHCl_3$/MeOH, 95:5. White solid, 45% yield. ^{1}H NMR (DMSO-d_6, 500 MHz) δ: 1.14−1.21 (m, 2H), 1.28−1.48 (m, 1H), 1.56−1.66 (m, 1H), 1.71−1.83 (m, 2H), 1.85−1.97 (m, 1H), 2.86−2.94 (m, 1H), 3.03−3.06 (m, 1H), 3.12−3.17 (m, 2H), 4.34−4.36 (m, 1H), 4.58−4.67 (m, 1H), 6.31−6.39 (m, 1H), 7.01 (t, 2H, J = 8.3 Hz), 7.28 (br s, 2H), 7.43 (d, 2H, J = 7.83 Hz), 7.70−7.73 (m, 2H), 7.80−7.82 (m, 1H), 8.14−8.19 (m, 1H), 8.66 (d, 1H, J = 7.8 Hz). HRMS (ESI$^-$) calcd for [($C_{23}H_{24}FN_5O_3$) − H]$^-$, 463.1785; found, 436.1783. ESI$^-$/MS/MS [M − H]$^-$ m/z: 116 (100).

*(2S)-3-(4-Cyanophenyl)-2-(3-(4-fluorophenyl)ureido)-N-(2-oxoazepan-3-yl)propenamide ((2S)-**11a**).* Eluted with $CHCl_3$/MeOH, 95:5. White solid, 52% yield. ^{1}H NMR (DMSO-d_6, 500 MHz) δ: 1.14−1.21 (m, 2H), 1.28−1.48 (m, 1H), 1.56−1.66 (m, 1H), 1.71−1.83 (m, 2H), 1.85−1.97 (m, 1H), 2.86−2.94 (m, 1H), 3.03−3.06 (m, 1H), 3.12−3.17 (m, 1H), 4.34−4.36 (m, 1H), 4.58−4.67 (m, 1H), 6.31−6.39 (m, 1H), 7.01 (t, 2H, J = 8.3 Hz), 7.28 (br s, 2H), 7.43 (d, 2H, J = 7.83 Hz), 7.70−7.73 (m, 2H), 7.80−7.82 (m, 1H), 8.14−8.19 (m, 1H), 8.66 (d, 1H, J = 7.8 Hz). HRMS (ESI$^-$) calcd for [($C_{23}H_{24}FN_5O_3$) − H]$^-$, 463.1785; found, 436.1783. ESI$^-$/MS/MS [M − H]$^-$ m/z: 116 (100).

*(R)-1-(3-(4-Cyanophenyl)-1-oxo-1-(piperidin-1-yl)propan-2-yl)-3-(4-fluorophenyl)urea ((R)-**11b**).* Eluted with $CHCl_3$/EtOAc, 8:2. Colorless solid, 46% yield. ^{1}H NMR ($CDCl_3$, 500 MHz) δ: 1.14 (m, 1H), 1.39−1.44 (m, 1H), 1.53−1.61 (m, 4H), 3.03 (dd, 1H, J = 5.9 and 13.2 Hz), 3.06−3.11 (m, 1H), 3.21−3.24 (m, 1H), 3.37−3.41 (m, 1H), 3.49−3.54 (m, 2H), 5.19 (app t, 1H), 6.97 (t, 2H, J = 8.8 Hz), 7.22−7.24 (m, 2H), 7.31 (d, 2H, J = 7.8 Hz), 7.57 (d, 2H, J = 7.8 Hz). HRMS (ESI$^-$) calcd for [($C_{22}H_{23}FN_4O_2$) − H]$^-$, 393.1727; found, 393.1725. ESI$^-$/MS/MS [M − H]$^-$ m/z: 116 (100).

*(S)-1-(3-(4-Cyanophenyl)-1-oxo-1-(piperidin-1-yl)propan-2-yl)-3-(4-fluorophenyl)urea ((S)-**11b**).* Eluted with $CHCl_3$/EtOAc, 8:2. White solid, 69% yield. ^{1}H NMR ($CDCl_3$, 500 MHz) δ: 1.14 (m, 1H), 1.39−1.44 (m, 1H), 1.53−1.61 (m, 4H), 3.03 (dd, 1H, J = 5.9 and 13.2 Hz), 3.06−3.11 (m, 1H), 3.21−3.24 (m, 1H), 3.37−3.41 (m, 1H), 3.49−3.54 (m, 2H), 5.19 (app t, 1H), 6.97 (t, 2H, J = 8.8 Hz), 7.22−7.24 (m, 2H), 7.31 (d, 2H, J = 7.8 Hz), 7.57 (d, 2H, J = 7.8 Hz). HRMS (ESI$^-$) calcd for [($C_{22}H_{23}FN_4O_2$) − H]$^-$, 393.1727; found, 393.1727. ESI$^-$/MS/MS [M − H]$^-$ m/z: 116 (100).

*(R)-1-(3-(4-Cyanophenyl)-1-oxo-1-(pyrrolidin-1-yl)propan-2-yl)-3-(4-fluorophenyl)urea ((R)-**11c**).* Eluted with $CHCl_3$/EtOAc, 8:2. White solid, 79% yield. ^{1}H NMR (DMSO-d_6, 300 MHz) δ: 1.65−1.82 (m, 4H), 2.90 (dd, 1H, J = 7.0 and 12.9 Hz), 3.02 (dd, 1H, J = 6.4 and 13.5 Hz), 3.15−3.27 (m, 3H), 3.48−3.54 (m, 1H), 4.63−4.70 (m, 1H), 6.51 (d, 1H, J = 8.78 Hz, D_2O exchanged), 7.02 (t, 2H, J = 8.8 Hz), 7.28−7.33 (m, 2H), 7.39 (d, 2H, J = 8.2 Hz), 7.73 (d, 2H, J = 8.2 Hz), 8.66 (s, 1H, D_2O exchanged). HRMS (ESI$^-$) calcd for [($C_{21}H_{21}FN_4O_2$) − H]$^-$, 379.1570; found, 379.1575. ESI$^-$/MS/MS [M − H]$^-$ m/z: 116 (100).

*(S)-1-(3-(4-Cyanophenyl)-1-oxo-1-(pyrrolidin-1-yl)propan-2-yl)-3-(4-fluorophenyl)urea ((S)-**11c**).* Eluted with $CHCl_3$/EtOAc, 8:2. White solid, 72% yield. ^{1}H NMR (DMSO-d_6, 300 MHz) δ: 1.65−1.82 (m, 4H), 2.90 (dd, 1H, J = 7.0 and 12.9 Hz), 3.02 (dd, 1H, J = 6.4 and 13.5 Hz), 3.15−3.27 (m, 3H), 3.48−3.54 (m, 1H), 4.63−4.70 (m, 1H), 6.51 (d, 1H, J = 8.78 Hz, D_2O exchanged), 7.02 (t, 2H, J = 8.8 Hz), 7.28−7.33 (m, 2H), 7.39 (d, 2H, J = 8.2 Hz), 7.73 (d, 2H, J = 8.2 Hz), 8.66 (s, 1H, D_2O exchanged). HRMS (ESI$^-$) calcd for [($C_{21}H_{21}FN_4O_2$) − H]$^-$, 379.1570; found, 379.1570. ESI$^-$/MS/MS [M − H]$^-$ m/z: 116 (100).

*(R)-1-(3-(4-Cyanophenyl)-1-(isoindolin-2-yl)-1-oxopropan-2-yl)-3-(4-fluorophenyl)urea ((R)-**11d**).* Gradient elution from *n*-hexane/EtOAc, 7:3, to *n*-hexane/EtOAc, 1:9. White solid, 38% yield. ^{1}H NMR ($CDCl_3$, 300 MHz) δ: 3.16 (app d, 2H), 4.40 (d, 1H, J = 13.5 Hz), 4.67 (d, 1H, J = 15.8 Hz), 4.87 (d, 1H, J = 15.8 Hz), 5.08−5.18 (m, 2H), 6.93 (t, 2H, J = 8.8 Hz), 7.17−7.23 (m, 4H), 7.27−7.31 (m, 4H, 1H, D_2O exchanged), 7.40 (d, 2H, J = 8.2 Hz), 7.57 (d, 2H, J = 8.2 Hz). HRMS (ESI$^-$) calcd for [($C_{25}H_{21}FN_4O_2$) − H]$^-$, 427.1570; found, 427.1570. ESI$^+$/MS/MS [M − H]$^-$ m/z: 116 (100).

*(S)-1-(3-(4-Cyanophenyl)-1-(isoindolin-2-yl)-1-oxopropan-2-yl)-3-(4-fluorophenyl)urea ((S)-**11d**).* Gradient elution from *n*-hexane/EtOAc, 7:3, to *n*-hexane/EtOAc, 1:9. White solid, 39% yield. ^{1}H NMR ($CDCl_3$, 300 MHz) δ: 3.15 (app d, 2H), 4.40 (d, 1H, J = 13.5 Hz), 4.68 (d, 1H, J = 15.8 Hz), 4.85 (d, 1H, J = 15.8 Hz), 5.10−5.15 (m, 2H), 6.93 (t, 2H, J = 8.8 Hz), 7.17−7.23 (m, 4H), 7.27−7.31 (m, 4H, 1H, D_2O exchanged), 7.40 (d, 2H, J = 8.2 Hz), 7.57 (d, 2H, J = 8.2 Hz). HRMS (ESI$^-$) calcd for [($C_{25}H_{21}FN_4O_2$) − H]$^-$, 427.1570; found, 427.1570. ESI$^+$/MS/MS [M − H]$^-$ m/z: 116 (100).

*(R)-1-(3-(4-Cyanophenyl)-1-(indolin-1-yl)-1-oxopropan-2-yl)-3-(4-fluorophenyl)urea ((R)-**11e**).* Eluted with *n*-hexane/EtOAc, 1:1. Colorless solid, 48% yield. ^{1}H NMR ($CDCl_3$, 300 MHz) δ: 2.99−3.14 (m, 3H), 3.22 (dd, 1H, J = 7.0 and 14.0 Hz), 3.68−3.77 (m, 1H), 4.40−4.49 (m, 1H), 5.08 (t, 1H, J = 7.0 Hz), 6.80 (app t, 2H), 6.99−7.08 (m, 3H), 7.10−7.23 (m, 4H), 7.39 (d, 2H, J = 8.2 Hz), 7.56 (d, 2H, J = 8.2 Hz), 8.12 (br d, 1H). HRMS (ESI$^-$) calcd for [($C_{25}H_{21}FN_4O_2$) − H]$^-$, 427.1570; found, 427.1563. ESI$^-$/MS/MS [M − H]$^-$ m/z: 265 (45), 116 (100).

*(S)-1-(3-(4-Cyanophenyl)-1-(indolin-1-yl)-1-oxopropan-2-yl)-3-(4-fluorophenyl)urea ((S)-**11e**).* Eluted with $CHCl_3$/EtOAc, 8:2. Colorless solid, 49% yield. ^{1}H NMR ($CDCl_3$, 300 MHz) δ: 2.98−3.02 (m, 2H), 3.12−3.15 (m, 2H), 3.68−3.77 (m, 1H), 4.40−4.49 (m, 1H), 4.95−4.98 (m, 1H), 6.80 (app t, 2H), 6.99−7.08 (m, 3H), 7.10−7.23 (m, 4H), 7.39 (d, 2H, J = 8.2 Hz), 7.56 (d, 2H, J = 8.2 Hz), 8.12 (br d, 1H). HRMS (ESI$^-$) calcd for [($C_{25}H_{21}FN_4O_2$) − H]$^-$, 427.1570; found, 427.1560. ESI$^-$/MS/MS [M − H]$^-$ m/z: 265 (45), 116 (100).

*(R)-1-(3-(4-Cyanophenyl)-1-(3,4-dihydroisoquinolin-2(1H)-yl)-1-oxopropan-2-yl)-3-(4-fluorophenyl)urea ((R)-**11f**).* Gradient elution from *n*-hexane/EtOAc, 7:3, to *n*-hexane/EtOAc, 1:9. Colorless solid, 47% yield. ^{1}H NMR (DMSO-d_6, 300 MHz) δ: 2.64−2.69 (m, 2H), 2.93−3.10 (m, 2H), 3.43−3.77 (m, 1H), 3.79−3.85 (m, 1H), 4.46−4.69 (m, 2H), 5.01−5.09 (m, 1H), 6.54 (app t, 1H), 7.00−7.10 (m, 2H), 7.13−7.16 (m, 4H), 7.23−7.41 (m, 4H), 7.55 (d, 1H, J = 7.6 Hz), 7.67 (d, 1H, J = 8.2 Hz), 8.65 (app d, 1H). HRMS (ESI$^-$) calcd for [($C_{26}H_{23}FN_4O_2$) − H]$^-$, 441.1727; found, 441.1727. ESI$^-$/MS/MS [M − H]$^-$ m/z: 213 (13), 116 (100).

*(S)-1-(3-(4-Cyanophenyl)-1-(3,4-dihydroisoquinolin-2(1H)-yl)-1-oxopropan-2-yl)-3-(4-fluorophenyl)urea ((S)-**11f**).* Gradient elution from *n*-hexane/EtOAc, 7:3, to *n*-hexane/EtOAc, 1:9. White solid, 53% yield. ^{1}H NMR (DMSO-d_6, 300 MHz) δ: 2.64−2.69 (m, 2H), 2.93−3.10 (m, 2H), 3.43−3.77 (m, 1H), 3.79−3.85 (m, 1H), 4.46−4.69 (m, 2H), 5.01−5.09 (m, 1H), 6.54 (app t, 1H), 7.00−7.10 (m, 2H), 7.13−7.16 (m, 4H), 7.23−7.41 (m, 4H), 7.55 (d, 1H, J = 7.6 Hz), 7.67 (d, 1H, J = 8.2 Hz), 8.65 (app d, 1H). HRMS (ESI$^-$) calcd for [($C_{26}H_{23}FN_4O_2$) − H]$^-$, 441.1727; found, 441.1723. ESI$^-$/MS/MS [M − H]$^-$ m/z: 213 (13), 116 (100).

*(R)-1-(3-(4-Cyanophenyl)-1-(3,4-dihydroquinolin-1(2H)-yl)-1-oxopropan-2-yl)-3-(4-fluorophenyl)urea ((R)-**11g**).* Eluted with *n*-hexane/EtOAc, 1:1. Yellow oil, 50% yield. ^{1}H NMR ($CDCl_3$, 300 MHz) δ: 1.62−1.72 (m, 2H), 1.76−1.82 (m, 1H), 1.91−1.99 (m, 1H), 2.55−2.62 (m, 1H), 2.82 (dd, 1H, J = 5.9 and 12.0 Hz), 2.92 (dd, 1H, J = 5.9 and 12.0 Hz), 3.14−3.23 (m, 1H), 4.19−4.28 (m, 1H), 5.69 (br d, 1H, D_2O exchanged), 6.38 (m, 1H), 6.92−6.99 (m, 4H), 7.11 (br d, 1H), 7.19−7.22 (m, 2H), 7.29−7.39 (m, 3H), 7.45−7.48 (m, 1H), 7.54 (br s, 1H, D_2O exchanged). HRMS (ESI$^-$) calcd for [($C_{26}H_{23}F_3N_4O_2$) − H]$^-$, 441.1732; found, 441.1715. ESI$^+$/MS/MS [M − H]$^-$ m/z: 116 (100).

*(S)-1-(3-(4-Cyanophenyl)-1-(3,4-dihydroquinolin-1(2H)-yl)-1-oxopropan-2-yl)-3-(4-fluorophenyl)urea ((S)-**11g**).* Eluted with *n*-hexane/EtOAc, 1:1. Colorless oil, 20% yield. ^{1}H NMR ($CDCl_3$, 300 MHz) δ: 1.62−1.72 (m, 2H), 1.76−1.82 (m, 1H), 1.91−1.99 (m, 1H), 2.55−2.62 (m, 1H), 2.82 (dd, 1H, J = 5.9 and 12.0 Hz), 2.92 (dd, 1H, J = 5.9 and 12.0 Hz), 3.14−3.23 (m, 1H), 4.19−4.28 (m, 1H), 5.69 (br d, 1H, D_2O exchanged), 6.38 (m, 1H), 6.92−6.99 (m, 4H), 7.11 (br d, 1H), 7.19−7.22 (m, 2H), 7.29−7.39 (m, 3H), 7.45−7.48 (m, 1H), 7.54

https://doi.org/10.1021/acs.jmedchem.1c02203
J. Med. Chem. XXXX, XXX, XXX−XXX

(br s, 1H, D_2O exchanged). HRMS (ESI^-) calcd for $[(C_{26}H_{23}F_3N_4O_2) - H]^-$, 441.1732; found, 441.1715. ESI^+/MS/MS $[M - H]^-$ *m/z*: 116 (100).

*(R)-1-(3-(4-Cyanophenyl)-1-(4,4-difluoropiperidin-1-yl)-1-oxopropan-2-yl)-3-(4-fluorophenyl)urea ((R)-**11h**).* Eluted in gradient from *n*-hexane/EtOAc, 8:2, to *n*-hexane/EtOAc, 1:1. White solid, 38% yield. ^1H NMR (DMSO-d_6, 500 MHz) δ: 1.98−2.17 (m, 4H), 3.02 (dd, 1H, *J* = 5.9 and 13.2 Hz), 3.09 (dd, 1H, *J* = 7.8 and 13.7 Hz), 3.30−3.34 (m, 1H), 3.44−3.50 (m, 1H), 3.63−3.66 (m, 1H), 3.86−3.90 (m, 1H), 5.17−5.20 (m, 1H), 5.94 (br d, 1H), 6.82 (br s, 1H), 6.95−7.02 (m, 2H), 7.16−7.22 (m, 2H), 7.30 (d, 2H, *J* = 8.3 Hz), 7.59 (d, 2H, *J* = 8.3 Hz). HRMS (ESI^-) calcd for $[(C_{22}H_{21}F_3N_4O_2) - H]^-$, 429.0743; found, 429.0739. ESI^-/MS/MS $[M - H]^-$ *m/z*: 116 (100).

*(S)-1-(3-(4-Cyanophenyl)-1-(4,4-difluoropiperidin-1-yl)-1-oxopropan-2-yl)-3-(4-fluorophenyl)urea ((S)-**11h**).* Gradient elution from *n*-hexane/EtOAc, 7:3, to *n*-hexane/EtOAc, 1:1. White solid, yield 80%. ^1H NMR (DMSO-d_6, 500 MHz) δ: 1.98−2.17 (m, 4H), 3.02 (dd, 1H; *J* = 5.9 and 13.2 Hz), 3.09 (dd, 1H, *J* = 7.8 and 13.7 Hz), 3.30−3.34 (m, 1H), 3.44−3.50 (m, 1H), 3.63−3.66 (m, 1H), 3.86−3.90 (m, 1H), 5.17−5.20 (m, 1H), 5.94 (br d, 1H), 6.82 (br s, 1H), 6.95−7.02 (m, 2H), 7.16−7.22 (m, 2H), 7.30 (d, 2H, *J* = 8.3 Hz), 7.59 (d, 2H, *J* = 8.3 Hz). HRMS (ESI^-) calcd for $[(C_{22}H_{21}F_3N_4O_2) - H]^-$, 429.0743; found, 429.0741. ESI^-/MS/MS $[M - H]^-$ *m/z*: 116 (100).

*(R)-1-(3-(4-Cyanophenyl)-1-(5-fluoroisoindolin-2-yl)-1-oxopropan-2-yl)-3-(4-fluorophenyl)urea ((R)-**11j**).* Gradient elution from *n*-hexane/EtOAc, 7:3, to *n*-hexane/EtOAc, 1:1. Yellow solid, 46% yield. ^1H NMR ($CDCl_3$, 500 MHz) δ: 3.12−3.18 (m, 2H), 4.34−4.40 (m, 1H), 4.60−4.66 (m, 1H), 4.76−4.82 (m, 1H), 5.04−5.15 (m, 2H), 6.41−6.47 (m, 1H), 6.88−7.02 (m, 4H), 7.13−7.29 (m, 4H), 7.34 (d, 2H, *J* = 7.8 Hz), 7.57 (d, 2H, *J* = 7.8 Hz). HRMS (ESI^-) calcd for $[(C_{25}H_{20}F_2N_4O_2) - H]^-$, 445.1476; found, 445.1468. ESI^+/MS/MS $[M - H]^-$ *m/z*: 116 (100).

*(S)-1-(3-(4-Cyanophenyl)-1-(5-fluoroisoindolin-2-yl)-1-oxopropan-2-yl)-3-(4-fluorophenyl)urea ((S)-**11j**).* Eluted with CH_2Cl_2/EtOAc, 8:2. White solid, 66% yield. ^1H NMR ($CDCl_3$, 500 MHz) δ: 3.12−3.18 (m, 2H), 4.34−4.40 (m, 1H), 4.60−4.66 (m, 1H), 4.76−4.82 (m, 1H), 5.04−5.15 (m, 2H), 6.41−6.47 (m, 1H), 6.88−7.02 (m, 4H), 7.13−7.29 (m, 4H), 7.34 (d, 2H, *J* = 7.8 Hz), 7.57 (d, 2H, *J* = 7.8 Hz). HRMS (ESI^-) calcd for $[(C_{25}H_{20}F_2N_4O_2) - H]^-$, 445.1476; found, 445.1468. ESI^+/MS/MS $[M - H]^-$ *m/z*: 116 (100).

*(R)-1-(3-(4-Cyanophenyl)-1-(3,3-dimethylindolin-1-yl)-1-oxopropan-2-yl)-3-(4-fluorophenyl)urea ((R)-**11k**).* Eluted with CH_2Cl_2/EtOAc, 8:2. White solid, 15% yield. ^1H NMR ($CDCl_3$, 300 MHz) δ: 1.14 (s, 3H), 1.31 (s, 3H), 2.93 (dd, 1H, *J* = 7.0 and 13.5 Hz), 3.11 (dd, 1H, *J* = 7.0 and 13.5 Hz), 3.33−3.36 (m, 1H), 3.79−3.86 (m, 2H), 6.61 (br s, 1H), 7.06−7.13 (m, 2H), 7.20−7.25 (m, 3H), 7.16−7.22 (m, 3H), 7.35 (d, 2H, *J* = 8.20 Hz), 7.57 (d, 2H, *J* = 8.20 Hz), 8.13 (d, 1H, *J* = 7.8 Hz). HRMS (ESI^-) calcd for $[(C_{27}H_{25}FN_4O_2) - H]^-$, 455.1889; found, 455.1886. ESI^+/MS/MS $[M - H]^-$ *m/z*: 265 (90), 116 (100).

*(S)-1-(3-(4-Cyanophenyl)-1-(3,3-dimethylindolin-1-yl)-1-oxopropan-2-yl)-3-(4-fluorophenyl)urea ((S)-**11k**).* Eluted with CH_2Cl_2/EtOAc, 8:2. White solid, 37% yield. ^1H NMR ($CDCl_3$, 300 MHz) δ: 1.14 (s, 3H), 1.31 (s, 3H), 2.93 (dd, 1H, *J* = 7.0 and 13.5 Hz), 3.11 (dd, 1H, *J* = 7.0 and 13.5 Hz), 3.33−3.36 (m, 1H), 3.79−3.86 (m, 2H), 6.61 (br s, 1H), 7.06−7.13 (m, 2H), 7.20−7.25 (m, 3H), 7.16−7.22 (m, 3H), 7.35 (d, 2H, *J* = 8.20 Hz), 7.57 (d, 2H, *J* = 8.20 Hz), 8.13 (d, 1H, *J* = 7.8 Hz). HRMS (ESI^-) calcd for $[(C_{27}H_{25}FN_4O_2) - H]^-$, 455.1889; found, 455.1886. ESI^+/MS/MS $[M - H]^-$ *m/z*: 265 (90), 116 (100).

*(R)-1-(3-(4-Cyanophenyl)-1-(5-fluoroindolin-1-yl)-1-oxopropan-2-yl)-3-(4-fluorophenyl)urea ((R)-**11i**).* Gradient elution from *n*-hexane/EtOAc, 7:3, to *n*-hexane/EtOAc, 1:1. White solid, 33% yield. ^1H NMR ($CDCl_3$, 500 MHz) δ: 2.97 (dd, 1H, *J* = 8.3 and 13.7 Hz), 3.10−3.21 (m, 3H), 4.12−4.18 (m, 1H), 4.29−4.35 (m, 1H), 4.77−4.81 (m, 1H), 6.73 (d, 1H, *J* = 4.7 Hz), 6.95−7.03 (m, 3H), 7.10 (dd, 1H, *J* = 2.4 and 8.3 Hz), 7.30−7.32 (m, 2H), 7.47 (d, 2H, *J* = 7.8 Hz), 7.74 (d, 2H, *J* = 8.3 Hz), 8.03 (dd, 1H, *J* = 4.9 and 8.8 Hz), 8.69 (s, 1H). HRMS (ESI^-) calcd for $[(C_{25}H_{20}F_2N_4O_2) - H]^-$, 445.1482; found, 445.1480. ESI^-/MS/MS $[M - H]^-$ *m/z*: 265 (50), 116 (100).

*(S)-1-(3-(4-Cyanophenyl)-1-(6-fluoroindolin-1-yl)-1-oxopropan-2-yl)-3-(4-fluorophenyl)urea ((S)-**11i**).* Gradient elution from *n*-hexane/EtOAc, 7:3, to *n*-hexane/EtOAc, 1:1. White solid, 63% yield. ^1H NMR ($CDCl_3$, 500 MHz) δ: 3.02−3.07 (m, 1H), 3.11 (dd, 1H, *J* = 6.8 and 13.2 Hz), 3.17−3.24 (m, 2H), 3.71−3.76 (m, 1H), 4.41−4.48 (m, 1H), 5.09 (q, 1H, *J* = 7.3 Hz), 6.59 (br d, 1H, NH), 6.81−6.84 (m, 2H), 7.05−7.12 (m, 2H), 7.16−7.25 (m, 3H), 7.37 (d, 2H, *J* = 7.8 Hz), 7.54 (d, 2H, *J* = 7.8 Hz), 8.13 (d, 1H, *J* = 7.83 Hz). HRMS (ESI^-) calcd for $[(C_{25}H_{20}F_2N_4O_2) - H]^-$, 445.1482; found, 445.1480. ESI^-/MS/MS $[M - H]^-$ *m/z*: 265 (50), 116 (100).

*(R)-1-(3-(4-Cyanophenyl)-1-(6-fluoroindolin-1-yl)-1-oxopropan-2-yl)-3-(4-fluorophenyl)urea ((R)-**11l**).* Gradient elution from *n*-hexane/EtOAc, 8:2, to *n*-hexane/EtOAc, 10:0. White solid, 84% yield. ^1H NMR (DMSO-d_6, 300 MHz) δ: 2.85−3.05 (m, 1H), 3.07−3.22 (m, 3H), 4.13−4.22 (m, 1H), 4.31−4.40 (m, 1H), 4.75−4.82 (m, 1H), 6.31 (d, 1H, *J* = 8.2 Hz), 6.74−6.81 (m, 1H), 6.99 (t, 2H, *J* = 8.8 Hz), 7.19−7.23 (m, 1H), 7.26−7.32 (m, 2H), 7.49 (d, 2H, *J* = 8.2 Hz), 7.72 (d, 2H, *J* = 8.2 Hz), 7.80 (dd, 1H, *J* = 2.3 and 10.5 Hz), 8.65 (s, 1H). HRMS (ESI^-) calcd for $[(C_{25}H_{20}F_2N_4O_2) - H]^-$, 445.1482; found, 445.1472. ESI^+/MS/MS $[M - H]^-$ *m/z*: 116 (100).

*(S)-1-(3-(4-Cyanophenyl)-1-(6-fluoroindolin-1-yl)-1-oxopropan-2-yl)-3-(4-fluorophenyl)urea ((S)-**11l**).* Eluted with CH_2Cl_2/EtOAc, 8:2. White solid, 57% yield. ^1H NMR (DMSO-d_6, 300 MHz) δ: 2.85−3.05 (m, 1H), 3.07−3.22 (m, 3H), 4.13−4.22 (m, 1H), 4.31−4.40 (m, 1H), 4.75−4.82 (m, 1H), 6.31 (d, 1H, *J* = 8.2 Hz), 6.74−6.81 (m, 1H), 6.99 (t, 2H, *J* = 8.8 Hz), 7.19−7.23 (m, 1H), 7.26−7.32 (m, 2H), 7.49 (d, 2H, *J* = 8.2 Hz), 7.72 (d, 2H, *J* = 8.2 Hz), 7.80 (dd, 1H, *J* = 2.3 and 10.5 Hz), 8.65 (s, 1H). HRMS (ESI^-) calcd for $[(C_{25}H_{20}F_2N_4O_2) - H]^-$, 445.1482; found, 445.1472. ESI^+/MS/MS $[M - H]^-$ *m/z*: 116 (100).

*(R)-1-(3-(4-Cyanophenyl)-1-(2,3-dihydro-1H-pyrrolo[2,3-b]-pyridin-1-yl)-1-oxopropan-2-yl)-3-(4-fluorophenyl)urea ((R)-**11m**).* Gradient elution from *n*-hexane/EtOAc, 7:3, to *n*-hexane/EtOAc, 3:7. Colorless oil, 53% yield. ^1H NMR ($CDCl_3$, 300 MHz) δ: 2.81−2.88 (m, 1H), 3.02−3.19 (m, 2H), 3.37 (dd, 1H, *J* = 4.2 and 14.1 Hz), 4.01−4.22 (m, 3H), 6.27 (d, 1H, *J* = 8.8 Hz), 6.49−6.53 (m, 1H), 6.86 (t, 2H, *J* = 8.8 Hz), 6.92−7.01 (m, 1H), 7.07−7.11 (m, 3H), 7.45 (d, 2H, *J* = 8.2 Hz), 7.58 (d, 2H, *J* = 7.6 Hz), 8.23 (d, 1H, *J* = 4.7 Hz). HRMS (ESI^-) calcd for $[(C_{24}H_{20}F_2N_5O_2) - H]^-$, 428.1528; found, 428.1520. ESI^+/MS/MS $[M - H]^-$ *m/z*: 116 (96), 110 (100).

*(S)-1-(3-(4-Cyanophenyl)-1-(2,3-dihydro-1H-pyrrolo[2,3-b]-pyridin-1-yl)-1-oxopropan-2-yl)-3-(4-fluorophenyl)urea ((S)-**11m**).* Gradient elution from *n*-hexane/EtOAc, 8:2, to *n*-hexane/EtOAc, 0:10. White solid, 84% yield. ^1H NMR ($CDCl_3$, 300 MHz) δ: 2.81−2.88 (m, 1H), 3.02−3.19 (m, 2H), 3.37 (dd, 1H, *J* = 4.2 and 14.1 Hz), 4.01−4.22 (m, 3H), 6.27 (d, 1H, *J* = 8.8 Hz), 6.49−6.53 (m, 1H), 6.86 (t, 2H, *J* = 8.8 Hz), 6.92−7.01 (m, 1H), 7.07−7.11 (m, 3H), 7.45 (d, 2H, *J* = 8.2 Hz), 7.58 (d, 2H, *J* = 7.6 Hz), 8.23 (d, 1H, *J* = 4.7 Hz). HRMS (ESI^-) calcd for $[(C_{24}H_{20}F_2N_5O_2) - H]^-$, 428.1528; found, 428.1520. ESI^+/MS/MS $[M - H]^-$ *m/z*: 116 (96), 110 (100).

*(R)-1-(3-(4-Cyanophenyl)-1-(7-fluoro-3,4-dihydroisoquinolin-2(1H)-yl)-1-oxopropan-2-yl)-3-(4-fluorophenyl)urea ((R)-**11n**).* Eluted with $CHCl_3$/EtOAc, 7:3. White solid, 36% yield. ^1H NMR ($CDCl_3$, 300 MHz) δ: 2.39−2.48 (m, 1H), 2.73−2.98 (m, 1H), 3.10−3.14 (m, 2H), 3.35−3.51 (m, 1H), 3.71−3.80 (m, 1H), 4.30−4.36 (m, 1H), 4.57−4.62 (m, 1H), 5.22−5.33 (m, 1H), 6.40 (m, 1H), 6.88−6.94 (m, 3H), 6.95−7.07 (m, 1H), 7.20−7.28 (m, 5H), 7.33 (d, 1H, *J* = 8.2 Hz), 7.42−7.45 (m, 2H). HRMS (ESI^-) calcd for $[(C_{26}H_{22}F_2N_4O_2) - H]^-$, 459.1638; found, 459.1632. ESI^+/MS/MS $[M - H]^-$ *m/z*: 116 (100).

*(S)-1-(3-(4-Cyanophenyl)-1-(7-fluoro-3,4-dihydroisoquinolin-2(1H)-yl)-1-oxopropan-2-yl)-3-(4-fluorophenyl)urea ((S)-**11n**).* Eluted with CH_2Cl_2/EtOAc, 8:2. Yellow solid, 30% yield. ^1H NMR ($CDCl_3$, 300 MHz) δ: 2.39−2.48 (m, 1H), 2.73−2.98 (m, 1H), 3.10−3.14 (m, 2H), 3.35−3.51 (m, 1H), 3.71−3.80 (m, 1H), 4.30−4.36 (m, 1H), 4.57−4.62 (m, 1H), 5.22−5.33 (m, 1H), 6.40 (m, 1H), 6.88−6.94 (m, 3H), 6.95−7.07 (m, 1H), 7.20−7.28 (m, 5H), 7.33 (d, 1H, *J* = 8.2 Hz), 7.42−7.45 (m, 2H). HRMS (ESI^-) calcd for $[(C_{26}H_{22}F_2N_4O_2) - H]^-$, 459.1638; found, 459.1632. ESI^+/MS/MS $[M - H]^-$ *m/z*: 116 (100).

*(S)-1-(3-(4-Cyanophenyl)-1-(7-fluoro-4,4-dimethyl-3,4-dihydroisoquinolin-2(1H)-yl)-1-oxopropan-2-yl)-3-(4-fluorophenyl)urea ((S)-**11o**).* Eluted with CH_2Cl_2/EtOAc, 8:2. Yellow solid, 6% yield. ^1H

https://doi.org/10.1021/acs.jmedchem.1c02203
J. Med. Chem. XXXX, XXX, XXX−XXX

NMR ($CDCl_3$, 300 MHz) δ: 1.40 (s, 6H), 3.12−3.23 (m, 2H), 3.39−3.45 (m, 2H), 4.34−4.40 (m, 2H), 4.76−4.82 (m, 1H), 5.04−5.15 (m, 2H), 6.41−6.47 (m, 2H), 6.88−7.02 (m, 3H), 7.13−7.29 (m, 2H), 7.34 (d, 2H, J = 7.8 Hz), 7.57 (d, 2H, J = 7.8 Hz). HRMS (ESI^-) calcd for $[(C_{28}H_{26}F_2N_4O_2) - H]^-$, 487.1951; found, 487.1942. ESI^+/MS/MS $[M - H]^-$ m/z: 116 (100).

Molecular Modeling Methods. The compounds' molecular skeletons were built in both the (*R*) and (*S*) configurations by converting the relative SMILES strings to three-dimensional structures within the Maestro software package[54] and performing thereafter with Open Babel[55] a 10,000 steps of Steepest Descent minimization using the Universal Force Field. The FPR2 X-ray-solved sequence (chain A from the PDB code 6OMM) was prepared with the Protein Preparation Wizard interface of Maestro by removing the ligand and water molecules, adding hydrogen atoms, optimizing their position, and assigning the ionization states of acid and basic residues according to PROPKA prediction at pH 7.0. Electrostatic charges for protein atoms were loaded according to the AMBER UNITED force field,[56] while the *molcharge* complement of QUACPAC[57] was used in order to achieve Marsili−Gasteiger charges for the inhibitors. Affinity maps were first calculated on a 0.375 Å-spaced 90 × 70 × 70 $Å^3$ rectangular box having the barycenter on residues Leu81, Glu89, His102, Val105, Asp106, Phe110, Phe178, Arg201, Arg205, Trp254, Phe257, Ser288, and Phe292, and accessibility of the binding site was exploited throughout 1000 runs of Lamarckian Genetic Algorithm (LGA) implemented in AUTODOCK 4.2.6[58] using the GPU-OpenCL algorithm version.[59] Explicit water contribution was considered according to the hydration force field,[60] and the population size and the number of energy evaluation figures were set to 300 and 10,000,000, respectively. Among all the plausible ones, the best free energy of pose, ranked by the AUTODOCK scoring functions, was selected as representative of ligand binding mode, and the matching of this conformation with the best FEB pose was obtained for the docking of compound **43** according to the shape matching algorithm ROCS.[61]

Stability Assays in Rat Liver Microsomes. Test compounds were pre-incubated at 37 °C with rat liver microsomes (Tebu-Bio, Milan, Italy) (1.0 mg/mL microsomal protein) at a 10 μM final concentration in 100 mM potassium phosphate buffer (pH 7.4) for 10 min. Metabolic reactions were initiated by the addition of the NADPH regenerating system (containing 10 mM NADP, 50 mM glucose-6-phosphate, and 10 unit/mL glucose-6-phosphate dehydrogenase; final glucose-6-phosphate dehydrogenase concentration, 1 unit/mL). Aliquots were removed at specific time end points and immediately mixed with an equal volume of cold acetonitrile containing the internal standard. To assess the in vitro half-life ($t_{1/2}$), the aliquots were removed at 0, 5, 15, 30, 60, and 120 min. Test compounds incubated with microsomes without the NADPH regenerating system were included. Quenched samples were centrifuged at 4500 rpm for 15 min, and the supernatants were injected for quantification analysis. Samples (100 μL) were analyzed using an Agilent 1260 Infinity Binary LC system equipped with a diode array detector (Open Lab software was used to analyze the chromatographic data) and a Phenomenex Gemini C-18 column (250 × 4.6 mm, 5 μm particle size). The samples were eluted using CH_3CN/20 mM ammonium formate (pH 5.5, 70:30, v/v) as the eluent (1 mL/min). Concentrations were quantified by measuring the area under the peak. The percentage of the parent compound remaining after a 30 min incubation was calculated according to the following equation:

$$\%\text{of parent compound remaining after 30 min} = C_{parent}/C_{control}\cdot 100$$

where $C_{paren}t$ is the test compound concentration after incubation with the microsome fraction and NADPH regenerating system and $C_{control}$ is the test compound concentration after incubation with the microsome fraction only.

The *in vitro* half-life ($t_{1/2}$) was calculated using the expression $t_{1/2} = 0.693/b$, where b is the slope found in the linear fit of the natural logarithm of the fraction remaining of the parent compound vs incubation time.[62] The *in vitro* half-life was then used to calculate the intrinsic plasma clearance (CL_{int}) according to the following equation:

$$CL_{int} = \frac{0.693}{\text{in vitro } t_{1/2}} \cdot \frac{1}{\text{mg/mL microsomal protien}}$$

Biological Methods. *Cell Culture.* Murine microglial cells N9 were purchased from Neuro-Zone, Bresso, Italy. N9 cells were grown in Iscove's modified Dulbecco's medium containing 25 mM HEPES and L-glutamine, supplemented with 5% fetal bovine serum (FBS), 100 IU/mL penicillin, and 100 μg/mL streptomycin, in a humidified 5% CO_2 atmosphere at 37 °C. Cells were plated at a final density of 2×10^4 cells/well in 96-well plates.

In all experiments, cells were pre-treated for 30 min with various concentrations of FPR2 agonists and then stimulated for 24 h with the lipopolysaccharide (LPS; 100 ng/mL) (*Escherichia coli* O111:B4, Sigma). In experiments where the secretion of cytokines was measured, the FPR2 antagonist WRW4 (Tocris, USA) was added 30 min before agonists.

Ca^{2+} Mobilization Assay. Changes in intracellular Ca^{2+} were measured with a FlexStation II scanning fluorometer (Molecular Devices, Sunnyvale, CA, USA). The cells, suspended in Hank's balanced salt solution without Ca^{2+} and Mg^{2+} but with 10 mM HEPES ($HBSS^-$), were loaded with 1.25 μg/mL Fluo-4 AM dye and incubated for 30 min in the dark at 37 °C. After dye loading, the cells were washed with $HBSS^-$ containing 10 mM HEPES, resuspended in $HBSS^+$ containing Ca^{2+}, Mg^{2+}, and 10 mM HEPES ($HBSS^+$), and aliquoted into the wells of flat-bottom, half-area-well black microtiter plates (2×10^5 cells/well). For the evaluation of direct agonist activity, compounds were added from a source plate containing dilutions of the test compounds in HBSS+, and changes in fluorescence were monitored (λ_{ex} = 485 nm, λ_{em} = 538 nm) every 5 s for 240 s at room temperature after the automated addition of compounds. The maximum change in fluorescence during the first 3 min, expressed in arbitrary units over baseline, was used to determine a response. Responses for FPR1 agonists were normalized to the response induced by 5 nM *f*MLF for FPR1-HL60 cells, or 5 nM WKYMVM for FPR2-HL60 cells, which were assigned a value of 100%. To evaluate inhibitory effects of the compounds on FPR1/FPR2-dependent Ca^{2+} flux, the compounds were added to the wells (the final concentration of DMSO was 1%) with FPR1/FPR2 HL60 cells. The samples were pre-incubated for 10 min followed by addition of 5 nM *f*MLF (for FPR1-HL60 cells) or 5 nM WKYMVM (for FPR2-HL60 cells). The maximum change in fluorescence, expressed in arbitrary units over baseline, was used to determine the agonist response. Curve fitting (at least five or six points) and calculations of median effective concentration values (EC_{50} or IC_{50}) were performed by nonlinear regression analysis of the dose−response curves (four-parameter logistic curve fitting) generated using Prism 8 (GraphPad Software, Inc., San Diego, CA, USA). Efficacy was determined by comparing individual responses activated by the test compounds to that induced by a positive control (5 nM *f*MLF for FPR1-HL60 cells or 5 nM WKYMVM for FPR2-HL60 cells), which was assigned a value of 100%.

Cell Viability. Determination of cell viability was performed on N9 cells using the MTT assay at 48 h.[63] On day 1, 25,000 cells/well were seeded into 96-well plates in a volume of 100 μL. On day 2, the various drug concentrations (1−100 μM) were added. In all the experiments, the drug solvent (DMSO) was added in each control to evaluate possible solvent cytotoxicity. After the established incubation time with drugs (48 h), MTT (0.5 mg/mL) was added to each well, and after 3−4 h of incubation at 37 °C, the supernatant was removed. The formazan crystals were solubilized using 100 μL of DMSO/EtOH (1:1), and the absorbance values at 570 and 630 nm were determined on the microplate reader Victor 3 (PerkinElmer Life Sciences). Data were analyzed by applying the one-way repeated measures analysis of variance, and Bonferroni's multiple comparison test followed as a post hoc test. Results are reported as mean ± SD of at least two to three independent experiments, performed in triplicate. Statistical significance was accepted at $P < 0.05$.

Lactate Dehydrogenase (LDH) Test. Cells (2×10^4 cells/well) were seeded into 96-well plates in 200 μL of medium. After 3−4 h, LPS (100 ng/mL), alone or in combination with the test compounds (0.5 or 5 μM), was added to the cells. The plates were incubated at 37 °C for 24

https://doi.org/10.1021/acs.jmedchem.1c02203
J. Med. Chem. XXXX, XXX, XXX−XXX

h. To quantify the cell integrity, the level of LDH release from the damaged cells into the culture media was measured 24 h after the treatment. Cell culture supernatants were collected from each well of the 96-well plates and were incubated with the appropriate reagent mixture according to the supplier's instructions (Cytotoxicity Detection Kit, Roche, Germany) at room temperature for 30 min. Absorbance of the samples was measured at λ = 490 nm (Infinite 200 PRO Detector, TECAN, Switzerland) and the reference wavelength of 630 nm. The data were normalized to the activity of LDH released from untreated cells (100%) and expressed as a percentage of the control ± SEM.

Enzyme-Linked Immunosorbent Assay (ELISA). N9 cells were seeded in 24-well plates, and after 3−4 h, LPS (100 ng/mL), alone or in combination with the test compounds (0.05, 0.1, 0.5, 1, and 5 μM), was added to the cells. The plates were incubated at 37 °C for 24 h. The culture supernatants were collected, and the levels of IL1β and TNFα in the culture medium were assayed using Mouse IL1β and Mouse TNFα Quantikine ELISA kits (R&D Systems, Minneapolis, MN, USA) according to the manufacturer's instructions. The absorbance at 450 nm was recorded using a microplate reader.

Rat Primary Microglial Cell Cultures. Animals. Sprague−Dawley rats (weight of 200−250 g, Charles River, Sulzfeld, Germany) were kept under standard conditions (temperature of 23 °C, light/dark cycle of 12/12 h, and lights on at 8.00 a.m.) with food and water available ad libitum. To determine the phase of the estrous cycle, vaginal smears were taken daily from the female rats. On the proestrus day, females were placed with males for 12 h, and the presence of sperm in vaginal smears was checked. Pregnant females were left undisturbed in their home cages. The experiments were approved by the Local Ethics Committee, Kraków, Poland (approval no. 204/2018, 28.06.2018).

Cell Culture. Primary microglial cell cultures were prepared from the cortices of 1−2 day-old Sprague−Dawley rat pups according to the procedure described by Zawadzka and Kaminska[64] and with slight modifications, as described previously.[65,66] Briefly, after decapitation, the brains were removed, and the cerebral cortices were cut into small pieces. The minced tissue was incubated in Hanks' balanced salt solution (HBSS, Gibco, New York, USA) containing glucose, bovine serum albumin (BSA), and HEPES with 0.025% trypsin at 37 °C for 20 min. The trypsinization process was stopped by adding the trypsin inhibitor *Glycine max* (soy-bean) (Sigma-Aldrich, St. Louis, MO, USA). A completely dissociated suspension of the tissue was prepared by mild trituration. Next, the cells were plated at a density of 3×10^5 cells/cm^2 in a culture medium consisting of Dulbecco's modified Eagle's medium (DMEM) with GlutaMax and high glucose (4.5 g/L) supplemented with heat-inactivated 10% fetal bovine serum (FBS), 100 U/mL penicillin, and 0.1 mg/mL streptomycin (all reagents are obtained from Gibco, New York, USA) in poly-L-lysine-coated 75 cm^2 culture flasks. On the 9th day *in vitro* (37 °C, 5% CO_2), the flasks were agitated on a horizontal shaker (1 h, 37 °C, 80 rpm). After centrifugation, the cells were resuspended in the culture medium and seeded at a final density of 1.25×10^6 cells/well in 6-well plates, 2×10^5 cells/well in 24-well plates, or 4×10^4 cells/well in 96-well plates. The purity of microglial cell cultures was assessed using a specific microglia marker anti-Iba-1 antibody (ab5076, Abcam, Cambridge, U.K.). Images were captured using a confocal microscope (Leica Microsystems CMS GmbH, Mannheim, Germany). We obtained a highly homogeneous microglia population (greater than 95% of cells were stained with Iba-1 positively). Two days after plating, the cells were used for experiments. One hour before the cell treatment, the culture medium was changed to a medium with 1% FBS.

Cell Treatment. In all experiments, the cells were pretreated for 30 min with the FPR2 antagonist WRW4 (10 μM; Alomone Labs, Israel). After that, (*S*)-**11e** (0.1 μM) or (*S*)-**11l** (0.1 μM) was added for 1 h, and then the cells were stimulated for 24 h with LPS (100 ng/mL; *Escherichia coli* 0111:B4; Sigma-Aldrich, St. Louis, MO, USA). Control cultures were treated with the appropriate vehicle. Stock solutions of the examined compounds were prepared as follows: (*S*)-**11e** and (*S*)-**11l** (1 mM DMSO), WRW4 (1 mM distilled water), and LPS (1 mg/mL phosphate buffer saline). The final solutions of the tested compounds were prepared in distilled water. Each experimental set of the control cultures was supplemented with the appropriate vehicles, and the solvent was present in cultures at a final concentration of 0.1% (v/v).

Nitric Oxide (NO) Release Assay. The Greiss reaction was used to assess the production of NO from LPS-treated microglial cells, as we previously described.[66] Twenty-four hours after treatment, equal volume of the cell culture medium and Griess reagents (Griess A: 0.1% *N*-1-naphthylethylenediamine dihydrochloride and Griess B: 1% sulfanilamide in 5% phosphoric acid) were mixed in a 96-well plate and incubated for 10 min at room temperature. Absorbance was measured at 540 nm in an Infinite M200PRO microplate reader (TECAN, Mä;nnedorf, Switzerland). The data were normalized to NO released from vehicle-treated cells (100%) and expressed as a percentage of the control ± SEM.

Lactate Dehydrogenase (LDH) Release Assay. To estimate cell damage 24 h after LPS treatment, LDH release was measured as previously described.[25] Cell culture supernatants were incubated with the reagent mixture according to the supplier's instructions (Cytotoxicity Detection kit, Roche, Germany). The intensity of the red color formed in the assay is proportional to the LDH activity and to the number of damaged cells. Absorbance was measured at 540 nm in an Infinite M200PRO microplate reader (TECAN, Mä;nnedorf, Switzerland). The data were normalized to the activity of LDH released from vehicle-treated cells (100%) and expressed as a percentage of the control ± SEM.

Mitochondrial Membrane Potential ($\Delta\psi$m) Assay. JC-1 (5,5′,6,6′-tetrachloro-1,1′,3,3′-tetraethylbenzimidazolylcarbocyanine iodide, Cayman Chemical Company, Ann Arbor, USA) is a positively charged cationic dye that exhibits membrane potential-dependent accumulation in mitochondria. It was used to study the change in the mitochondrial membrane potential of microglial cells as previously described.[67] Briefly, the cells were seeded into 96-well black plates, and 24 h after LPS treatment (100 ng/mL), the cells were stained with JC-1 for 30 min at 37 °C. In healthy cells with high mitochondrial potential, JC-1 forms complexes with intense red fluorescence (535 nm excitation and 595 nm emissions), but in apoptotic or unhealthy cells with low potential, JC-1 remains in the monomeric form, showing green fluorescence (485 nm excitation and 535 nm emissions). Fluorescence intensities were measured using an Infinite M200PRO microplate reader (TECAN, Switzerland), and the ratio of fluorescence intensity was used as an indicator of cell health. A decrease in the red/green fluorescence intensity ratio was interpreted as a loss of $\Delta\psi$m, whereas an increase in the ratio was interpreted as a gain in $\Delta\psi$m.

Caspase-3 Activity. Caspase-3 activity was detected using a caspase-3 colorimetric assay kit (BioVision, CA, USA). Primary microglial cells 24 h after LPS treatment were lysed with cell lysis buffer (Bio-Vision, CA, USA), incubated on ice for 10 min, and centrifuged (1 min, 4 °C, 14,000 rpm). The supernatant was incubated with reaction buffer containing dithiothreitol (DTT, 10 mM) and a DEVD-*p*-nitroaniline substrate (DEVD-pNA, 200 μM) for 2 h at 37 °C. The chromophore pNA light emission was quantified using an Infinite M200PRO microplate reader (TECAN, Switzerland) at a wavelength of 405 nm. The data (expressed as the mean relative fluorescence units, RFU) were normalized to the protein level (measured by the BCA method), calculated as a percent of control cultures, and presented as the mean ± SEM.

Enzyme-Linked Immunosorbent Assay (ELISA). The medium of microglial cells for IL-1β, TNF-α, IL-6, and IL-10 measurements was collected 24 h after LPS treatment. The protein levels of the cytokines TNF (rat TNF-alpha uncoated ELISA kit, Thermo Fisher, Waltham, MA, USA), IL-1β (rat interleukin 1-beta), IL-6 (rat interleukin 6 ELISA kit), and IL-10 (rat interleukin 10 ELISA kit; all obtained from Bioassay Technology Laboratory, Shanghai, China) were measured using commercially available enzyme-linked immunosorbent assay kits according to the manufacturers' instructions. The detection limits were as follows: TNF-α, 16 pg/mL; IL-1β, 10.27 pg/mL; IL-6, 0.052 ng/L; and IL-10, 1.51 pg/mL. The interassay precision was as follows: TNF-α < 8.8%, IL-1β < 10%, IL-6 < 10%, and IL-10 < 10%; the intra-assay precision was as follows: TNF-α < 2.1%, IL-1β < 8%, IL-6 < 8%, and IL-10 < 8%.

https://doi.org/10.1021/acs.jmedchem.1c02203
J. Med. Chem. XXXX, XXX, XXX−XXX

Statistical Analysis. The results presented in this study were derived from three independent microglia cultures, and "*n*" for each culture was 2−5. The results of the NO/LDH release, mitochondrial membrane potential, and caspase-3 activity are presented as the mean ± SEM percentage of the control (vehicle-treated cells). The data obtained in the ELISA study are presented as the mean ± SEM percentage of the control (vehicle-treated cells). All groups were compared by factorial analysis of variance (ANOVA) followed by Duncan's post hoc test to assess the differences between the treatment groups. A *p*-value less than or equal to 0.05 was considered statistically significant: $^{*}p < 0.05$ vs control, $^{\#}p < 0.05$ vs LPS group, and $^{\wedge}p < 0.05$ vs FPR2 ligand + LPS.

***In Vivo* Pharmacokinetic Studies.** Male CD-1 mice (25−30 g) were administered with compound (*S*)-**11l** (1 mg/kp i.v.; 10 mg/kg i.p., dissolved in 5% DMSO, 10% solutol HS 15, and 85% sterile water). For i.v. pharmacokinetic profiles, blood samples ($n = 3$) were collected after 0.083, 0.25, 0.50, 1, 2, 4, and 8 h from administration in animals anesthetized by isofluorane, by cardiac puncture. For i.p. profiles, blood samples were collected after 0.25, 0.50, 1, 2, 4, 8, and 24 h from administration in animals anesthetized by isofluorane, by cardiac puncture; K_2EDTA was used as an anticoagulant and stored in wet ice. Within 30 min from withdrawal, blood samples were centrifuged (3000*g*, 10 min, 4 °C), and 10 μL of plasma was transferred into micronic tubes containing 40 μL of HEPES (0.1 N). The samples were stored at −20 °C up to the day of analysis. Brain samples were collected after 2, 8, and 24 h after decapitation of anesthetized animals and removal from skull. The samples were stored at −20 °C up to the day of analysis. After defrosting, each brain was weighted and diluted with four volumes of HEPES (0.1 N) and homogenized with Precellys 24 homogenizer (Bertin Instruments). The samples were prepared by protein precipitation (two volumes of acetonitrile with 20 ng/mL Rolipram used as the internal standard) and vortex-mixed for 5 min. After centrifugation (3000*g*, 10 min, 4 °C), the supernatants were transferred and diluted (1:1.8) with water using a Hamilton Microlab STARlet.

Chromatography was performed by UPLC (ACQUITY UPLC I-Class System-Waters) on an Acquity UPLC BEH C18 1.7 μm column (2.1 × 30 mm) using a fast chromatography gradient (1.5 min; phase A: 0.1% of formic acid in water, phase B: 0.1% of formic acid in acetonitrile; the gradient is from 95 to 5% A). The mass spectrometer was an AB Sciex triple quadrupole, API4000. The analytes were monitored in multiple reaction monitoring (MRM) using 350.2/160.2 and 276.1/208.2 as quantifier channels for (*S*)-**11l** and IS, respectively.

■ ASSOCIATED CONTENT

Supporting Information

The Supporting Information is available free of charge at https://pubs.acs.org/doi/10.1021/acs.jmedchem.1c02203.

Elemental analysis of target compounds; yields and spectroscopic data of amines **3j−i,l,m**; docking poses of compounds (*R*)- and (*S*)-**11e,f,l**; intramolecular distances between pharmacophore terminals; RMSD of a receptor−ligand complex during MD; HPLC traces of selected compounds (PDF)

The molecular formula strings file of the target compounds (CSV)

PDB of the receptor−ligand complex of compounds (*R*)- and (*S*)-**11e,f,l** and "compound 43" (ZIP)

■ AUTHOR INFORMATION

Corresponding Author

Enza Lacivita − *Dipartimento di Farmacia−Scienze del Farmaco, Università degli Studi di Bari Aldo Moro, 70125 Bari, Italy;* orcid.org/0000-0003-2443-1174; Email: enza.lacivita@uniba.it

Authors

Margherita Mastromarino − *Dipartimento di Farmacia−Scienze del Farmaco, Università degli Studi di Bari Aldo Moro, 70125 Bari, Italy*

Maria Favia − *Dipartimento di Farmacia−Scienze del Farmaco, Università degli Studi di Bari Aldo Moro, 70125 Bari, Italy*

Igor A. Schepetkin − *Department of Microbiology and Cell Biology, Montana State University, Bozeman, Montana 59717, United States*

Lylia N. Kirpotina − *Department of Microbiology and Cell Biology, Montana State University, Bozeman, Montana 59717, United States*

Ewa Trojan − *Laboratory of Immunoendocrinology, Department of Experimental Neuroendocrinology, Maj Institute of Pharmacology, 31-343 Kraków, Poland*

Mauro Niso − *Dipartimento di Farmacia−Scienze del Farmaco, Università degli Studi di Bari Aldo Moro, 70125 Bari, Italy*

Antonio Carrieri − *Dipartimento di Farmacia−Scienze del Farmaco, Università degli Studi di Bari Aldo Moro, 70125 Bari, Italy;* orcid.org/0000-0002-7725-6667

Monika Leśkiewicz − *Laboratory of Immunoendocrinology, Department of Experimental Neuroendocrinology, Maj Institute of Pharmacology, 31-343 Kraków, Poland*

Magdalena Regulska − *Laboratory of Immunoendocrinology, Department of Experimental Neuroendocrinology, Maj Institute of Pharmacology, 31-343 Kraków, Poland*

Massimiliano Darida − *Aptuit Srl, an Evotec Company, 37135 Verona, Italy*

Francesco Rossignolo − *Aptuit Srl, an Evotec Company, 37135 Verona, Italy*

Stefano Fontana − *Aptuit Srl, an Evotec Company, 37135 Verona, Italy*

Mark T. Quinn − *Department of Microbiology and Cell Biology, Montana State University, Bozeman, Montana 59717, United States;* orcid.org/0000-0001-8114-5073

Agnieszka Basta-Kaim − *Laboratory of Immunoendocrinology, Department of Experimental Neuroendocrinology, Maj Institute of Pharmacology, 31-343 Kraków, Poland*

Marcello Leopoldo − *Dipartimento di Farmacia−Scienze del Farmaco, Università degli Studi di Bari Aldo Moro, 70125 Bari, Italy;* orcid.org/0000-0001-8401-2815

Complete contact information is available at: https://pubs.acs.org/10.1021/acs.jmedchem.1c02203

Author Contributions

The manuscript was written through contributions of all authors. All authors have given approval to the final version of the manuscript.

Notes

The authors declare no competing financial interest.

■ ACKNOWLEDGMENTS

This work was supported by a grant from the Alzheimer's Association (AARG-NTF-18−565227), grant no. 2017/26/M/NZ7/01048 (HARMONIA) from the National Science Centre, Poland, the National Institutes of Health IDeA Program Grants GM115371 and GM103474, the USDA National Institute of Food and Agriculture Hatch project 1009546, and the Montana State University Agricultural Experiment Station.

ABBREVIATIONS USED

CNS, central nervous system; COPD, chronic obstructive pulmonary disease; ERK1/2, extracellular signal-regulated kinase 1/2; LXA_4, lipoxin A_4; MAPK, mitogen-activated protein kinase; MD, molecular dynamics; NLRP3, NOD-, LRR-, and pyrin domain-containing protein 3; SPMs, specialized pro-resolving mediators

REFERENCES

(1) Serhan, C. N.; Brain, S. D.; Buckley, C. D.; Gilroy, D. W.; Haslett, C.; O'Neill, L. A.; Perretti, M.; Rossi, A. G.; Wallace, J. L. Resolution of inflammation: state of the art, definitions and terms. *FASEB J.* **2007**, *21*, 325−332.

(2) Nathan, C.; Ding, A. Nonresolving inflammation. *Cell* **2010**, *140*, 871−882.

(3) Levy, B. D.; Clish, C. B.; Schmidt, K.; Gronert, K.; Serhan, C. N. Lipid mediator class switching during acute inflammation: signal in resolutions. *Nat. Immunol.* **2001**, *2*, 612−619.

(4) Serhan, C. N.; Chiang, N.; Van Dyke, T. E. Resolving inflammation: dual anti-inflammatory and pro-resolution lipid mediators. *Nat. Rev. Immunol.* **2008**, *8*, 349−361.

(5) Serhan, C. N. Novel pro-resolving lipid mediators in inflammation are leads for resolution physiology. *Nature* **2014**, *510*, 92−101.

(6) Dalli, J.; Serhan, C. N. Identification and structure elucidation of the pro-resolving mediators provides novel leads for resolution pharmacology. *Br. J. Pharmacol.* **2019**, *176*, 1024−1037.

(7) Perretti, M.; Godson, C. Formyl peptide receptor type 2 agonists to kick-start resolution pharmacology. *Br. J. Pharmacol.* **2020**, *177*, 4595−4600.

(8) Perretti, M.; Leroy, X.; Bland, E. J.; Montero-Melendez, T. Resolution pharmacology: Opportunities for therapeutic innovation in inflammation. *Trends Pharmacol. Sci.* **2015**, *36*, 737−755.

(9) Corminboeuf, O.; Leroy, X. FPR2/ALXR agonists and the resolution of inflammation. *J. Med. Chem.* **2015**, *58*, 537−559.

(10) Capó, X.; Martorell, M.; Busquets-Cortés, C.; Tejada, S.; Tur, J. A.; Pons, A.; Sureda, A. Resolvins as proresolving inflammatory mediators in cardiovascular disease. *Eur. J. Med. Chem.* **2018**, *153*, 123−130.

(11) Maciuszek, M.; Cacace, A.; Brennan, E.; Godson, C.; Chapman, T. M. Recent advances in the design and development of formyl peptide receptor 2 (FPR2/ALX) agonists as pro-resolving agents with diverse therapeutic potential. *Eur. J. Med. Chem.* **2021**, *213*, 113167.

(12) Derada Troletti, C.; Enzmann, G.; Chiurchiù, V.; Kamermans, A.; Tietz, S. M.; Norris, P. C.; Jahromi, N. H.; Leuti, A.; van der Pol, S. M. A.; Schouten, M.; Serhan, C. N.; de Vries, H. E.; Engelhardt, B.; Kooij, G. Pro-resolving lipid mediator lipoxin A4 attenuates neuro-inflammation by modulating T cell responses and modifies the spinal cord lipidome. *Cell Rep.* **2021**, *35*, 109201.

(13) Mastromarino, M.; Lacivita, E.; Colabufo, N. A.; Leopoldo, M. G-Protein coupled receptors involved in the resolution of inflammation: ligands and therapeutic perspectives. *Mini-Rev. Med. Chem.* **2020**, *20*, 2090−2103.

(14) Ye, R. D.; Boulay, F.; Wang, J. M.; Dahlgren, C.; Gerard, C.; Parmentier, M.; Serhan, C. N.; Murphy, P. M. International union of basic and clinical pharmacology. LXXIII. Nomenclature for the formyl peptide receptor (FPR) family. *Pharmacol. Rev.* **2009**, *61*, 119−161.

(15) Perretti, M.; Chiang, N.; La, M.; Fierro, I. M.; Marullo, S.; Getting, S. J.; Solito, E.; Serhan, C. N. Endogenous lipid- and peptide-derived anti-inflammatory pathways generated with glucocorticoid and aspirin treatment activate the lipoxin A4 receptor. *Nat. Med.* **2002**, *8*, 1296−1302.

(16) Cattaneo, F.; Parisi, M.; Ammendola, R. Distinct signaling cascades elicited by different formyl peptide receptor 2 (FPR2) agonists. *Int. J. Mol. Sci.* **2013**, *4*, 7193−7230.

(17) Forsman, H.; Önnheim, K.; Andreasson, E.; Dahlgren, C. What formyl peptide receptors, if any, are triggered by compound 43 and lipoxin A4? *Scand. J. Immunol.* **2011**, *74*, 227−234.

(18) Hanson, J.; Ferreirós, N.; Pirotte, B.; Geisslinger, G.; Offermanns, S. Heterologously expressed formyl peptide receptor 2 (FPR2/ALX) does not respond to lipoxin A_4. *Biochem. Pharmacol.* **2013**, *85*, 1795−1802.

(19) Chen, T.; Xiong, M.; Zong, X.; Ge, Y.; Zhang, H.; Wang, M.; Han, G. W.; Yi, C.; Ma, L.; Ye, R. D.; Xy, Y.; Zhao, Q.; Wu, B. Structural basis of ligand binding modes at the human formyl peptide receptor 2. *Nat. Commun.* **2020**, *11*, 1208.

(20) Inoue, A.; Raimondi, F.; Kadji, F. M. N.; Singh, G.; Kishi, T.; Uwamizu, A.; Ono, Y.; Shinjo, Y.; Ishida, S.; Arang, N.; Kawakami, K.; Gutkind, J. S.; Aoki, J.; Russell, R. B. Illuminating G-protein-coupling selectivity of GPCRs. *Cell* **2019**, *177*, 1933−1947.e25.

(21) Qin, C. X.; May, L. T.; Li, R.; Cao, N.; Rosli, S.; Deo, M.; Alexander, A. E.; Horlock, D.; Bourke, J. E.; Yang, Y. H.; Stewart, A. G.; Kaye, D. M.; Du, X. J.; Sexton, P. M.; Christopoulos, A.; Gao, X. M.; Ritchie, R. H. Small-molecule-biased formyl peptide receptor agonist compound 17b protects against myocardial ischaemia-reperfusion injury in mice. *Nat. Commun.* **2017**, *8*, 14232.

(22) Deora, G. S.; Qin, C. X.; Vecchio, E. A.; Debono, A. J.; Priebbenow, D. L.; Brady, R. M.; Beveridge, J.; Teguh, S. C.; Deo, M.; May, L. T.; Krippner, G.; Ritchie, R. H.; Baell, J. B. Substituted pyridazin-3(2*H*)-ones as highly potent and biased formyl peptide receptor agonists. *J. Med. Chem.* **2019**, *62*, 5242−5248.

(23) Asahina, Y.; Wurtz, N. R.; Arakawa, K.; Carson, N.; Fujii, K.; Fukuchi, K.; Garcia, R.; Hsu, M. Y.; Ishiyama, J.; Ito, B.; Kick, E.; Lupisella, J.; Matsushima, S.; Ohata, K.; Ostrowski, J.; Saito, Y.; Tsuda, K.; Villarreal, F.; Yamada, H.; Yamaoka, T.; Wexler, R.; Gordon, D.; Kohno, Y. Discovery of BMS-986235/LAR-1219: a potent Formyl Peptide Receptor 2 (FPR2) selective agonist for the prevention of heart failure. *J. Med. Chem.* **2020**, *63*, 9003−9019.

(24) Maciuszek, M.; Ortega-Gomez, A.; Maas, S. L.; Perretti, M.; Merritt, A.; Soehnlein, O.; Chapman, T. M. Synthesis and evaluation of novel cyclopentane urea FPR2 agonists and their potential application in the treatment of cardiovascular inflammation. *Eur. J. Med. Chem.* **2021**, *214*, 113194.

(25) Stama, M. L.; Ślusarczyk, J.; Lacivita, E.; Kirpotina, L. N.; Schepetkin, I. A.; Chamera, K.; Riganti, C.; Perrone, R.; Quinn, M. T.; Basta-Kaim, A.; Leopoldo, M. Novel ureidopropanamide based N-formyl peptide receptor 2 (FPR2) agonists with potential application for central nervous system disorders characterized by neuroinflammation. *Eur. J. Med. Chem.* **2017**, *141*, 703−720.

(26) Tylek, K.; Trojan, E.; Leśkiewicz, M.; Regulska, M.; Bryniarska, N.; Curzytek, K.; Lacivita, E.; Leopoldo, M.; Basta-Kaim, A. Time-dependent protective and pro-resolving effects of FPR2 agonists on lipopolysaccharide-exposed microglia cells involve inhibition of NF-κB and MAPKs pathways. *Cell* **2021**, *10*, 2373.

(27) Trojan, E.; Tylek, K.; Leśkiewicz, M.; Lasoń, W.; Brandenburg, L. O.; Leopoldo, M.; Lacivita, E.; Basta-Kaim, A. The N-Formyl Peptide Receptor 2 (FPR2) agonist MR-39 exhibits anti-inflammatory activity in LPS-stimulated organotypic hippocampal cultures. *Cell* **2021**, *10*, 1524.

(28) Trojan, E.; Tylek, K.; Schröder, N.; Kahl, I.; Brandenburg, L. O.; Mastromarino, M.; Leopoldo, M.; Basta-Kaim, A.; Lacivita, E. The N-Formyl Peptide Receptor 2 (FPR2) agonist MR-39 improves ex vivo and in vivo amyloid beta (1-42)-induced neuroinflammation in mouse models of Alzheimer's Disease. *Mol. Neurobiol.* **2021**, *58*, 6203−6221.

(29) Schepetkin, I. A.; Kirpotina, L. N.; Khlebnikov, A. I.; Jutila, M. A.; Quinn, M. T. Gastrin-releasing peptide/neuromedin B receptor antagonists PD176252, PD168368, and related analogs are potent agonists of human formyl-peptide receptors. *Mol. Pharmacol.* **2011**, *79*, 77−90.

(30) Stama, M. L.; Lacivita, E.; Kirpotina, L. N.; Niso, M.; Perrone, R.; Schepetkin, I. A.; Quinn, M. T.; Leopoldo, M. Functional N-Formyl Peptide Receptor 2 (FPR2) antagonists based on the ureidopropanamide scaffold have potential to protect against inflammation-associated oxidative stress. *ChemMedChem* **2017**, *12*, 1839−1847.

(31) Lacivita, E.; Niso, M.; Mastromarino, M.; Garcia Silva, A.; Resch, C.; Zeug, A.; Loza, M. I.; Castro, M.; Ponimaskin, E.; Leopoldo, M. Knowledge-based design of long-chain arylpiperazine derivatives

https://doi.org/10.1021/acs.jmedchem.1c02203
J. Med. Chem. XXXX, XXX, XXX−XXX

targeting multiple serotonin receptors as potential candidates for treatment of autism spectrum disorder. *ACS Chem. Neurosci.* **2021**, *12*, 1313−1327.
(32) Houston, J. B. Utility of in vitro drug metabolism data in predicting in vivo metabolic clearance. *Biochem. Pharmacol.* **1994**, *47*, 1469−1479.
(33) Di, L.; Kerns, E. H.; Ma, X. J.; Huang, Y.; Carter, G. T. Applications of high throughput microsomal stability assay in drug discovery. *Comb. Chem. High Throughput Screening* **2008**, *11*, 469e476.
(34) Zhuang, Y.; Liu, H.; Edward Zhou, X.; Kumar Verma, R.; de Waal, P. W.; Jang, W.; Xu, T. H.; Wang, L.; Meng, X.; Zhao, G.; Kang, Y.; Melcher, K.; Fan, H.; Lambert, N. A.; Eric Xu, H.; Zhang, C. Structure of formylpeptide receptor 2-Gi complex reveals insights into ligand recognition and signaling. *Nat. Commun.* **2020**, *11*, 885.
(35) Mills, J. S.; Miettinen, H. M.; Cummings, D.; Jesaitis, A. J. Characterization of the binding site on the formyl peptide receptor using three receptor mutants and analogs of Met-Leu-Phe and Met-Met-Trp-Leu-Le. *J. Biol. Chem.* **2000**, *275*, 39012−39017.
(36) Prossnitz, E. R.; Schreiber, R. E.; Bokoch, G. M.; Ye, R. D. Binding of low affinity N-formyl peptide receptors to G protein. Characterization of a novel inactive receptor intermediate. *J. Biol. Chem.* **1995**, *270*, 10686−10694.
(37) Cai, H. Y.; Xu, Z. J.; Tang, J.; Sun, Y.; Chen, K. X.; Wang, H. Y.; Zhu, W. L. The essential role for aromatic cluster in the β3 adrenergic receptor. *Acta Pharmacol. Sin.* **2012**, *33*, 1062−1068.
(38) Molteni, M.; Gemma, S.; Rossetti, C. The role of Toll-Like receptor 4 in infectious and noninfectious inflammation. *Mediators Inflammation* **2016**, *2016*, 6978936.
(39) Kettenmann, H.; Hanisch, U. K.; Noda, M.; Verkhratsky, A. Physiology of microglia. *Physiol. Rev.* **2011**, *91*, 461−553.
(40) Slusarczyk, J.; Trojan, E.; Glombik, K.; Piotrowska, A.; Budziszewska, B.; Kubera, M.; Popiolek-Barczyk, K.; Lason, W.; Mika, J.; Basta-Kaim, A. Anti-inflammatory properties of tianeptine on lipopolysaccharide-induced changes in microglial cells involve toll-like receptor-related pathways. *J. Neurochem.* **2016**, *136*, 958−970.
(41) Tiffany, H. L.; Lavigne, M. C.; Cui, Y. H.; Wang, J. M.; Leto, T. L.; Gao, J. L.; Murphy, P. M. Amyloid-b induces chemotaxis and oxidant stress by acting at Formylpeptide receptor 2, a G protein-coupled receptor expressed in phagocytes and brain. *J. Biol. Chem.* **2001**, *276*, 23645.
(42) Marin, I.; Kipnis, J. Learning and memory and the immune system. *Learn. Mem.* **2013**, *20*, 601−606.
(43) Džoljić, E.; Grbatinić, I.; Kostić, V. Why is nitric oxide important for our brain? *Funct. Neurol.* **2015**, *30*, 159−163.
(44) Jung, T. W.; Park, H. S.; Choi, G. H.; Kim, D.; Ahn, S. H.; Kim, D. S.; Lee, T.; Jeong, J. H. Maresin 1 attenuates pro-inflammatory reactions and ER stress in HUVECs via PPARα-mediated pathway. *Mol. Cell. Biochem.* **2018**, *448*, 335−347.
(45) Yang, Y.; Zhu, Y.; Xiao, J.; Tian, Y.; Ma, M.; Li, X.; Li, L.; Zhang, P.; Li, M.; Wang, J.; Jin, S. Maresin conjiugates in tissue regeneration 1 prevents lipopolysaccharide-induced cardiac dysfuntion through improvement of mitochondrial biogenesis and function. *Biochem. Pharmacol.* **2020**, *177*, 114005.
(46) El Kebir, D.; József, L.; Khreiss, T.; Pan, W.; Petasis, N. A.; Serhan, C. N.; Filep, J. G. Aspirin-triggered lipoxins override the apoptosis-delaying action of serum amyloid A in human neutrophils: a novel mechanism for resolution of inflammation. *J. Immunol.* **2007**, *179*, 616−622.
(47) Jin, W.; Jia, Y.; Huang, L.; Wang, T.; Wang, H.; Dong, Y.; Zhang, H.; Fan, M.; Lv, P. Lipoxin A4 methyl ester ameliorates cognitive deficits induced by chronic cerebral hypoperfusion through activating ERK/Nrf2 signaling pathway in rats. *Pharmacol. Biochem. Behav.* **2014**, *124*, 145−152.
(48) Van Goethem, S.; Van der Veken, P.; Dubois, V.; Soroka, A.; Lambeir, A. M.; Chen, X.; Haemers, A.; Scharpé, S.; De Meester, I.; Augustyns, K. Inhibitors of dipeptidyl peptidase 8 and dipeptidyl peptidase 9. Part 2: isoindoline containing inhibitors. *Bioorg. Med. Chem. Lett.* **2008**, *18*, 4159−4162.
(49) Gottschling, D.; Dahmann, G.; Doods, H.; Heimann, A.; Mueller, S. G.; Rudolf, K.; Schaenzle, G. G.; Stenkamp, K. Novel Compounds, 2011, US201195954.
(50) Aubry, C.; Wilson, A. J.; Emmerson, D.; Murphy, E.; Chan, Y. Y.; Dickens, M. P.; García, M. D.; Jenkins, P. R.; Mahale, S.; Chaudhuri, B. Fascaplysin-inspired diindolyls as selective inhibitors of CDK4/cyclin D1. *Bioorg. Med. Chem.* **2009**, *17*, 6073−6084.
(51) Sato, K.; Sugimoto, H.; Rikimaru, K.; Imoto, H.; Kamaura, M.; Negoro, N.; Tsujihata, Y.; Miyashita, H.; Odani, T.; Murata, T. Discovery of a novel series of indoline carbamate and indolinylpyrimidine derivatives as potent GPR119 agonists. *Bioorg. Med. Chem.* **2014**, *22*, 1649−1666.
(52) Huang, H.; Yu, M.; Su, X.; Guo, P.; Zhao, J.; Zhou, J.; Li, Y. Sustainable radical cascades to synthesize difluoroalkylated pyrrolo-[1,2-a]indoles. *J. Org. Chem.* **2018**, *83*, 2425−2437.
(53) Ananthan, S.; Augelli-Szafran, C.; Bennett, R. P; Smith, H. C.; Venukadasula, P. Triazolophthalazine compounds, use as anti-human immunodeficiency virus inhibitors of HIV VIF-dependent degradation of APOBEC3. 2019, WO2019133666.
(54) *Schrödinger Release* 2021−1, Maestro, Schrödinger, LLC, New York, NY, 2021.
(55) O'Boyle, N. M.; Banck, M.; James, C. A.; Morley, C.; Vandermeersch, T.; Hutchison, G. R. Open Babel: An open chemical toolbox. *Aust. J. Chem.* **2011**, *3*, 33.
(56) Cornell, W. D.; Cieplak, P.; Bayly, C. I.; Gould, I. R.; Merz, K. M.; Ferguson, D. M.; Spellmeyer, D. C.; Fox, T.; Caldwell, J. W.; Kollman, P. A. A second generation force field for the simulation of proteins, nucleic acids, and organic molecules. *J. Am. Chem. Soc.* **1995**, *117*, 5179−5197.
(57) QUACPAC 2.1.0.4: OpenEye Scientific Software, Santa Fe, NM.
(58) Morris, G. M.; Goodsell, D. S.; Halliday, R. S.; Huey, R.; Hart, W. E.; Belew, R. K.; Olson, A. J. Automated docking using a Lamarckian genetic algorithm and empirical binding free energy function. *J. Comput. Chem.* **1998**, *19*, 1639−1662.
(59) El Khoury, L.; Santos-Martins, D.; Sasmal, S.; Eberhardt, J.; Bianco, G.; Ambrosio, F. A.; Solis-Vasquez, L.; Koch, A.; Forli, S.; Mobley, D. L. Comparison of affinity ranking using AutoDock-GPU and MM-GBSA scores for BACE-1 inhibitors in the D3R Grand Challenge 4. *J. Comput.-Aided Mol. Des.* **2019**, *33*, 1011−1020.
(60) Forli, S.; Olson, A. J. A force field with discrete displaceable waters and desolvation entropy for hydrated ligand docking. *J. Med. Chem.* **2012**, *55*, 623−638.
(61) ROCS 3.4.0.4: OpenEye Scientific Software, Santa Fe, NM.
(62) Obach, R. S.; Baxter, J. G.; Liston, T. E.; Silber, B. M.; Jones, B. C.; MacIntyre, F.; Rance, D. J.; Wastall, P. The prediction of human pharmacokinetic parameters from preclinical and in vitro metabolism data. *J. Pharmacol. Exp. Ther.* **1997**, *283*, 46−58.
(63) Pati, M. L.; Hornick, J. R.; Niso, M.; Berardi, F.; Spitzer, D.; Abate, C.; Hawkins, W. Sigma-2 receptor agonist derivatives of 1-cyclohexyl-4-[3-(5-methoxy-1,2,3,4-tetrahydronaphthalen-1-yl)-propyl]piperazine (PB28) induce cell death via mitochon-drial superoxide production and caspase activation in pancreatic cancer. *BMC Cancer* **2017**, *17*, 51.
(64) Zawadzka, M.; Kaminska, B. A novel mechanism of FK506-mediated neuroprotection: Downregulation of cytokine expression in glial cells. *Glia* **2005**, *49*, 36−51.
(65) Ślusarczyk, J.; Trojan, E.; Głombik, K.; Budziszewska, B.; Kubera, M.; Lasoń, W.; Popiołek-Barczyk, K.; Mika, J.; Wędzony, K.; Basta-Kaim, A. Prenatal stress is a vulnerability factor for altered morphology and biological activity of microglia cells. *Front. Cell. Neurosci.* **2015**, *9*, 1−14.
(66) Ślusarczyk, J.; Trojan, E.; Głombik, K.; Piotrowska, A.; Budziszewska, B.; Kubera, M.; Popiołek-Barczyk, K.; Lasoń, W.; Mika, J.; Basta-Kaim, A. Targeting the NLRP3 inflammasome-related pathways via tianeptine treatment-suppressed microglia polarization to the M1 phenotype in lipopolysaccharide-stimulated cultures. *Int. J. Mol. Sci.* **2018**, *19*, 1−23.
(67) Leskiewicz, M.; Regulska, M.; Budziszewska, B.; Jantas, D.; Jaworska-Feil, L.; Basta-Kaim, A.; Kubera, M.; Jagla, G.; Nowak, W.;

https://doi.org/10.1021/acs.jmedchem.1c02203
J. Med. Chem. XXXX, XXX, XXX−XXX

2244 Lason, W. Effects of neurosteroids on hydrogen peroxide- and
2245 staurosporine-induced damage of human neuroblastoma SH-SY5Y
2246 cells. *J. Neurosci. Res.* **2008**, *86*, 1361−1370.

https://doi.org/10.1021/acs.jmedchem.1c02203
J. Med. Chem. XXXX, XXX, XXX−XXX